1971

The Interaction Between A Streaming Plasma And A Transverse Magnetic Field

Murray Dennis Kucherawy

Recommended Citation

Kucherawy, Murray Dennis, "The Interaction Between A Streaming Plasma And A Transverse Magnetic Field" (1971). *Digitized Theses*. 506.
https://ir.lib.uwo.ca/digitizedtheses/506

NATIONAL LIBRARY
OF CANADA

CANADIAN THESES

ON MICROFILM

CANADA

BIBLIOTHÈQUE
NATIONALE
DU CANADA

THÈSES CANADIENNES

SUR MICROFILM

No. 7218

THE INTERACTION BETWEEN A STREAMING PLASMA

AND

A TRANSVERSE MAGNETIC FIELD

by

Murray Dennis Kucherawy

Department of Physics

Submitted in Partial Fulfillment

of the requirements for the degree of

Doctor of Philosophy

Faculty of Graduate Studies

University of Western Ontario

London, Canada

August 1970

ABSTRACT

The discovery of the existence of the magnetosphere
has stimulated laboratory studies of the interaction
between streaming plasmas and magnetic fields. The project
described herein was undertaken particularly to study
the boundary layer established in such an interaction
and the transfer of plasma across this boundary.

To simplify the geometry, a special solenoid was
designed with a turns distribution such that the resulting
external magnetic field was cylindrically symmetrical.
Field calculations were carried out by computer. The
experiments were performed in an evacuated chamber where
copper plasma generated in a plasma discharge gun was
directed perpendicular to the axis of the solenoid.
Velocity probes and a triple probe were used to measure
the plasma parameters - streaming velocity, electron
density and electron temperature. Magnetic probes
recorded perturbations of the magnetic field by the
streaming plasma and various cameras recorded the
interaction photographically.

The results showed the existence of a _magnetic_
boundary layer and measurements of the thickness of this
boundary layer showed general agreement with the value
predicted using the Rosenbluth sheath model. Furthermore,

the parameters of the interaction were found to satisfy a simple relationship equating magnetic energy density and plasma kinetic pressure. However, it was observed that the boundary did not represent a "contact surface" - i.e. plasma was able to flow across the boundary. In addition, a magnetic perturbation was observed to develop into a field-dependent asymmetry after the main interaction. A corresponding visual asymmetry was recorded by the high-speed camera.

An hypothesis, supported by computer calculations, is proposed to explain the observed phenomena.

ACKNOWLEDGEMENTS

The author would like to express his appreciation to Dr. Graham S. Rose for his advice and encouragement throughout this work.

The author would also like to thank Dr. Peter A. Fraser for many helpful and stimulating discussions, not only concerning the thesis problem but physics in general.

Special thanks are due to Mrs. Cheryl O'Meara for her unflagging efforts to complete the typing of this thesis.

Financial assistance in the form of a National Research Council Post-Graduate Fellowship and a Province of Ontario Graduate Fellowship is gratefully acknowledged.

The author is especially indebted to his family for their patience over the past few years and, in particular, dedicates this work to his wife, Mary Ann.

TABLE OF CONTENTS

LIST OF FIGURES

CHAPTER 1

INTRODUCTION

This thesis is concerned with the fundamental study of the interaction between a streaming plasma and a transverse magnetic field.

A survey of the evolution of laboratory experimentation and theoretical work is presented in Chapter 1 as well as an outline of the thesis objectives. A description of the experimental apparatus and diagnostic techniques used in this project is presented in Chapter 2 while the experimental results appear in Chapter 3. A model of the interaction is proposed in Chapter 4 followed by the theoretical analysis of the problem based on this model. Chapter 5 discusses the results of the theoretical analysis - particularly the mechanism by which plasma penetrates the boundary. Various appendices conclude the presentation.

1-1 EARLY INVESTIGATIONS

Laboratory experiments in plasma physics were initiated by Birkeland (1901) for the purpose of explaining auroral phenomena. In his experiments, an electron beam was directed

towards a magnetized sphere (terrella) which simulated
the dipole magnetic field of the earth. Excitation and
ionization of the background gas rendered the electron
trajectories visible and they were observed to impinge
preferentially on the polar regions of the terrella. This
led Birkeland to the conclusion that the sun was a source
of cathode rays and was responsible for the phenomena
known as aurora borealis.

Impressed by Birkeland's work, Stormer undertook an
analytic investigation of the problem and produced a
monumental study of high energy particle trajectories in
a dipole magnetic field (1955). Results of this work seemed
to verify Birkeland's conclusions and Bennett (1959)
further enlarged on Birkeland's and Stormer's investigations
using the "Stormertron" apparatus. Though his results
were essentially photographic, Bennett's work did indeed
verify Stormer's results and seemed to realistically
simulate the aurora. However, both qualitative and
quantitative problems arose and, though vigorously defended
by Bennett, the work faded in importance with respect
to auroral phenomena though it remains important in the
study of cosmic rays.

1-2   MODERN INVESTIGATIONS

Interest in laboratory simulation experiments lagged

until the advent of artificial earth satellites, one of which (Lunik 2, 1961) measured properties of the solar wind thereby confirming its existence which had been predicted experimentally by Biermann (1951) from the study of comet tails and theoretically by Parker (1958) in a study of the hydrodynamic expansion of the solar corona. Subsequent satellite investigations revealed the existence and extent of the magnetosphere and the existence of the Van Allen radiation belts (see figure 1-1) and several research groups began studies of these phenomena on a laboratory scale, (for example, Alfven et al. 1963, Bostick et al. 1963, Osborne et al. 1964, Sellen and Bernstein, 1964).

Difficulties in scaling interaction parameters from geophysical dimensions to laboratory scale have imposed constricting limitations on the value of this work and much care must be taken in forming general conclusions from simulation experiments. For example, electric fields due to charge separation are a result of inertial effects and, since particle masses cannot be scaled down, charge separation phenomena cannot be properly represented in the laboratory. Such difficulties are detailed in articles by Block (1967) and Gore (1969).

Unlike experimental endeavours, theoretical work continued in the years following the Birkeland experiments — the most notable work being Chapman and Ferraro's discussion of "magnetic storms" (1931, 1932, 1933).

FIG. 1-1   4

A VIEW OF THE EARTH FROM OUTER SPACE SHOWING THE TOROIDAL VAN ALLEN BELTS (ARTIST'S CONCEPTION)
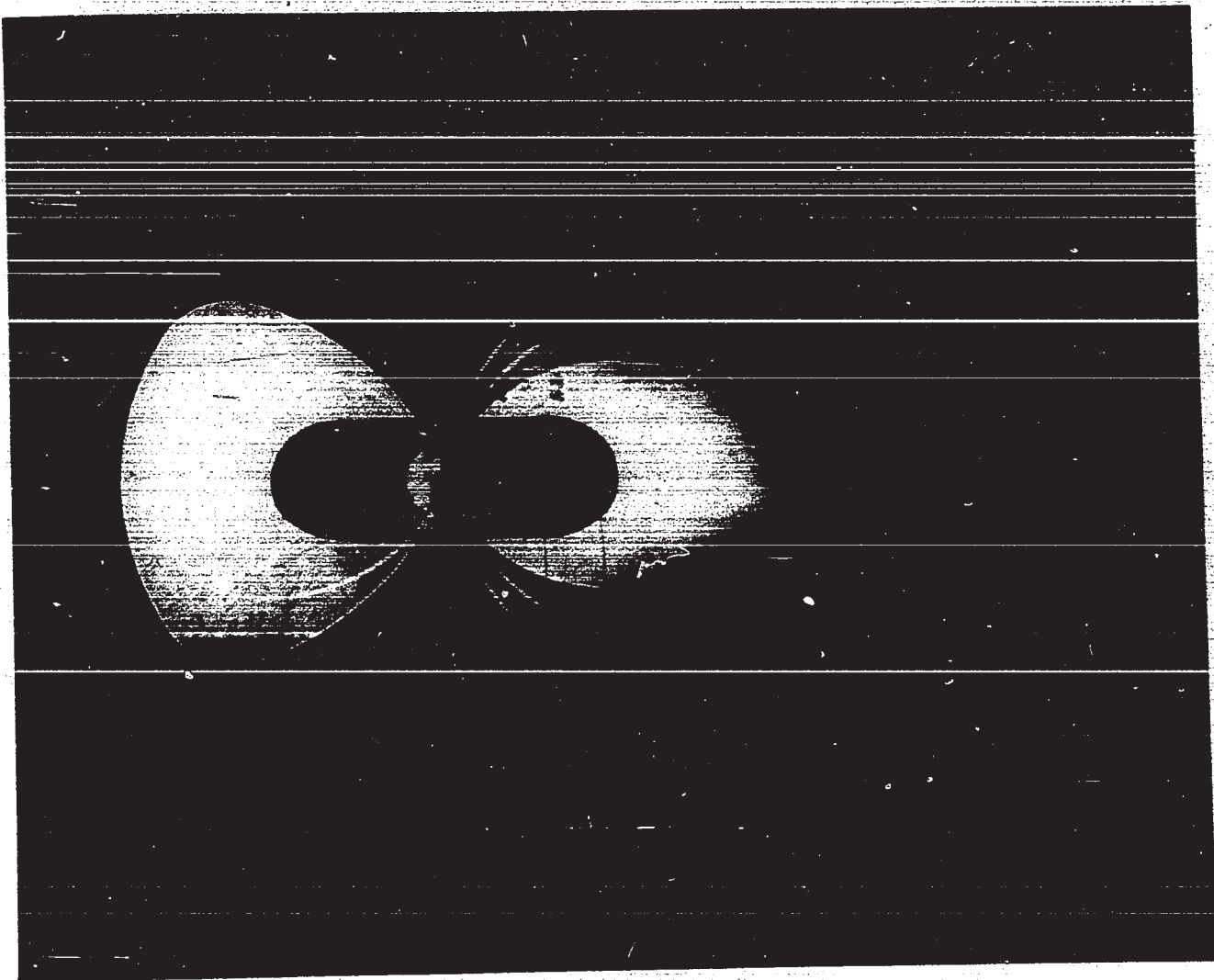
In an undisturbed condition, the earth's magnetic field is usually depicted as the familiar dipole configuration. However, under the influence of the solar wind (arrows), the magnetic field lines (light-coloured lines) are compressed and distorted with the result that the geomagnetic field is confined to a teardrop-shaped cavity with an elongated tail. This cavity is called the magnetosphere, the cavity boundary is termed the magnetopause, and leakage of particles across this boundary (by mechanisms yet to be explained) is responsible for the presence of the Van Allen belts.

Hampered by insufficient data concerning the corpuscular
radiation emanating from the sun, they nevertheless
developed a remarkably sound theory, consistent with current
data. Noting that the geomagnetic field was affected by
solar flare activity, Chapman and Ferraro postulated that
the agent of this perturbation was an electrically neutral
cloud of protons and electrons (a plasma) ejected by the
sun during the course of a solar flare. As this cloud
encountered the earth's magnetic field, current systems
were induced which cancelled the geomagnetic field in the
cloud and strengthened the field between the cloud and the
earth. The cloud continued to advance until its forward
momentum was expended in compressing the geomagnetic field.
Subsequent satellite investigations clarified many
uncertainties concerning the magnetosphere and new models
of interaction appeared. In particular, interest has
focussed on the magnetopause (boundary layer of the
magnetosphere) and possible mechanisms by which plasma
could be transferred across this boundary. The transition
layer between a plasma and a magnetic field was first
examined by Rosenbluth (1954) who determined the behaviour
of the internal electric and magnetic fields for a plane
interface. This work was expanded by Shkarofsky and
Johnston (1961) who calculated the particle trajectories
inside the boundary and deduced fine structure such as charge
distribution and the ion-overshoot layer. Other important

aspects of boundary theory have been discussed by Grad (1961), Bernstein et al. (1964), and Sestero (1965).

Determination of the shape and position of the boundary between a magnetic field and a streaming plasma is a cyclic problem. In the most common approach, it is defined by a surface on which kinetic energy density of the incident plasma equals the magnetic energy density. To determine the magnetic field on the boundary requires a knowledge of the electrical currents flowing on the boundary. These currents are determined by the shape of the boundary which, in turn, depends on the magnetic field on the boundary and the problem has gone full circle.

Hurley (1961) approached a two-dimensional version of this problem in a unique way. Setting up a dipole field in a complex plane, he surrounded it with a circular boundary. Using a conformal transformation, this surface was deformed in a manner consistent with Maxwell's equations, a pressure balance equation, and behaviour of the field at the origin. The result was an exact solution of the boundary problem as well as detailed knowledge of the deformation of the magnetic field. Unfortunately, as Hurley notes, "The solution of the three-dimensional problem appears to be quite hopeless.". Several independent methods of approximation have been used to calculate the boundary in three dimensions – a multipole expansion by Midgeley and Davis (1962), a free surface

method by Slutz (1962), and the **self-consistent field**
method by Beard (1964).

1-3 THESIS PROBLEM

In an earlier survey of the literature (1966), the
author was impressed by two **characteristics** of laboratory
plasma research –

a) the fundamental difficulties **of simulating** geophysical
phenomena in the laboratory,

b) the lack of correlation **between theoretical** and
experimental work.

As a result, it was proposed that the thesis experiment
have the following objectives:

1) The investigation would be carried out in an attempt
to understand the basic physical principles involved in
the plasma-magnetic field interface rather than to simulate
geophysical phenomena,

2) A serious attempt would be made to simplify the experiment
so that a meaningful analytical study could be carried out.

Most laboratory experiments have been carried out
using a dipole magnetic field. It was recognized that
this configuration had a complicating feature by virtue
of its three-dimensional curvature and so this complication
was removed by adopting a specially-wound solenoid as

the magnetic field source rather than the conventional "flux ball*". With proper baffling of the incident plasma stream, the experiment becomes essentially two-dimensional, thereby simplifying analysis.

The experimental configuration is depicted in figure 2-1. The plasma stream is generated by the pulsed discharge of a coaxial plasma gun with a copper-centre electrode. The electromagnetic forces associated with the high discharge current propel the plasma away from the gun and into the main interaction chamber towards the solenoid which is energized by a capacitor bank. Since the lifetime of the plasma stream (about 40 microseconds) is short compared with the time variation of the solenoid magnetic field (about 3 milliseconds), the plasma encounters an essentially unchanging magnetic field (neglecting plasma-induced perturbations). Before reaching the solenoid, the plasma encounters a baffle which prevents the stream from "spilling" over the sides of the solenoid thereby ensuring the two-dimensional nature of the experiment. Two side ports of the interaction chamber were available for photographic and magnetic studies of the interaction.

* a spherically-wound coil which sets up a dipole magnetic field when energized.

CHAPTER 2

DESCRIPTION OF EXPERIMENTAL APPARATUS

The experimental configuration is shown in figure 2-1.

2-1 INTERACTION CHAMBER

The plasma-magnetic field interaction was studied inside a spherical thick-walled glass vacuum chamber approximately 60 cm. in diameter, with six ports (four 15 cm. and two 22 cm. in diameter) situated in mutually perpendicular positions over its surface. This chamber was evacuated using a six-inch oil-diffusion pump and rotary mechanical fore pump with a water-cooled baffle to minimize backstreaming of oil vapour. A base pressure of less than 10^{-6} mm. of mercury was readily obtained in the interaction region. A vacuum thermocouple gauge and an ionization gauge were mounted on the rear port for the purpose of monitoring the system pressure. Diametrically opposite this port was a 22 cm. port leading to the plasma gun. A 30 cm. length of glass cylinder was attached to this port and the plasma gun was mounted at the other end of the cylinder. The other ports were used for pumping, for optical recording, for supporting the magnetic field solenoid,

Magnetic Field Bank
and Thyratron Switch

40 µ fd.
10 kv.

Vacuum
Gauge
Port

Solenoid

Magnetic
Probe

Vacuum Pump System

Baffle

Plasma
Flow

Photographic
Recording
Port

Coaxial
Plasma
Gun

Gun Capacitor
Bank

60 µ fd.
1.0 kv.

Button
Gun
(trigger)

Trigger Bank
and Thyratron

2 µ fd.

5C22
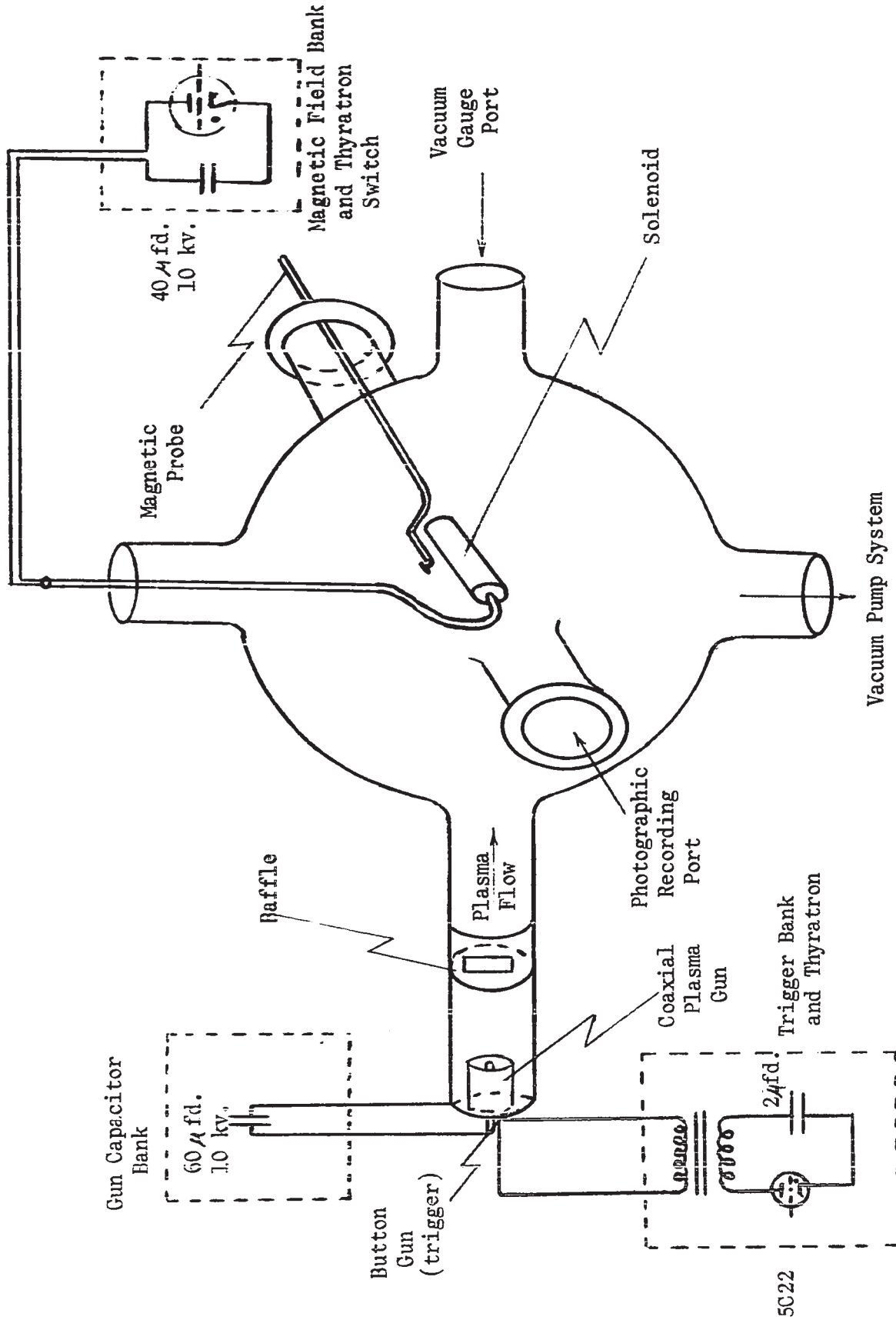
FIG. 2-1 EXPERIMENTAL CONFIGURATION

and for insertion of the magnetic diagnostic probes into
the interaction region as shown in figure 2-1. In order
to minimize reflections when making photographic
observations, the chamber was painted internally with
matte-finish glyptal cement and externally with a matte-
finish black non-conducting paint.

2-2 PLASMA GUN

A plasma "gust" of approximately 30 microseconds
duration was generated using a coaxial plasma gun (see
figure 2-2a) which was operated as follows:

A 60 microfarad capacitor bank across the electrodes
was charged to the desired voltage (maximum 10 kilovolts).
The main discharge was then triggered by a small amount
of ionized material ejected from a thyratron-controlled
button gun producing main discharge currents of the order
of 60 kiloamperes. The circuit containing the gun and
capacitor bank also contained a length of manganin ribbon
(resistance 0.12 ohms) effectively establishing a critically-
damped LCR circuit and ensuring only one gust of plasma.
Current waveforms were observed using a Rogowski coil
and a typical example is shown in figure 2-2b.

Since the plasma is essentially material eroded from
the central electrode (anode), tests were carried out using
various materials for this electrode to obtain suitable
values for interaction parameters such as particle density,
ion mass, light intensity, and boundary position. As a
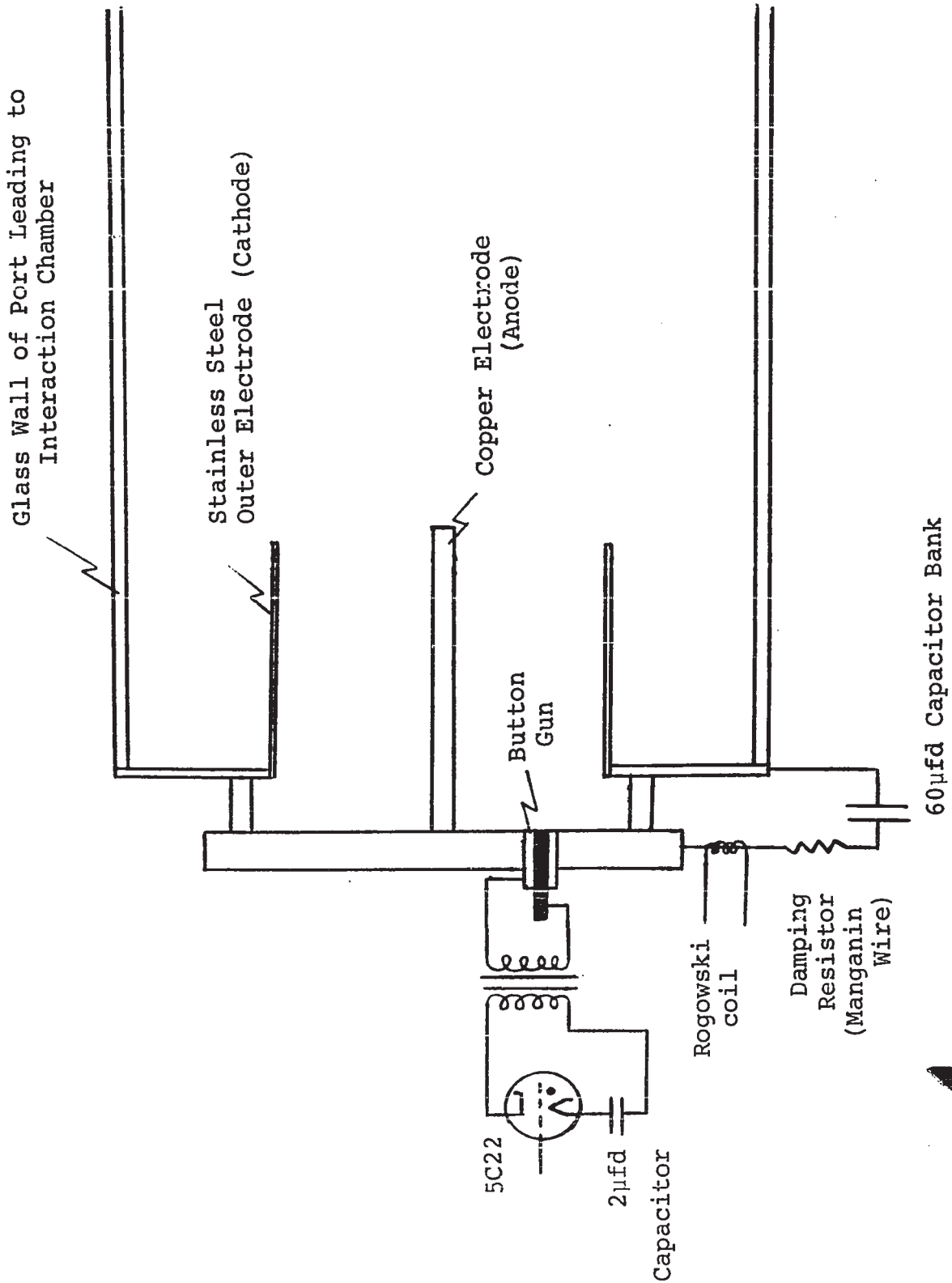
FIG. 2-2a CROSS-SECTION of COAXIAL PLASMA GUN
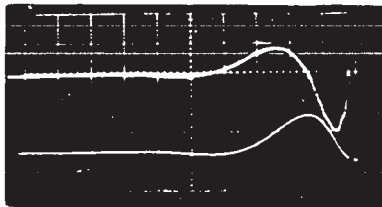
FIG. 2-2b ROGOWSKI COIL
WAVE FORM (upper trace)

The lower trace represents the integral of the upper

trace and shows that the discharge circuit is effectively

critically damped and hence only one gust of plasma is

ejected.

        vertical sensitivity
            upper trace - 20 volts/cm.
            lower trace - 0.5 volts/cm.

        horizontal sensitivity
            5 microseconds/cm.

result of these tests, a copper electrode was adopted
for use throughout the experiment. The outer cylindrical
electrode was made of stainless steel.

While the operation of the gun was quite straight-
forward, great difficulty was experienced in obtaining
a reproducible plasma. All diagnostic techniques employed
in this work showed wide variations in results obtained,
even in consecutive shots with unchanged experimental
configurations.

2-3   SOLENOID

A transverse magnetic field must, by definition, have
a zero component in a direction parallel to the flowing
plasma. In practice, in a system of finite size, this
requirement can only be approximated over a limited volume
of space. Several configurations were considered but a
specially-wound solenoid was chosen because of its
simplicity and convenience. The windings of a conventional
solenoid were supplemented by end windings in order to
minimize the curvature of the magnetic field lines in the
median plane at a pre-determined radial distance, namely,
that of the expected plasma-magnetic field boundary.

The design calculations were based on mutual inductance
formulae first derived by Jones (1898) and adapted for
use in magnetic field calculations by Fraser and
Romanowski (1955). Details of these calculations are

given in Appendix A.

The final design was as follows:

Wire Used: copper, gauge #22   (nytherm insulation)

Core: plexiglass, diameter 5 cm., length 15 cm.

Basic Windings: 4 layers over entire length of core

End Windings: 6 end layers, one inch in length,

                    at each end of the solenoid.

Experience with initial models demonstrated the
inadequacy of the nytherm insulation of the coil wire
with respect to prevention of electrical breakdown between
adjacent solenoid layers. To supplement this original
insulation, during the winding of the final design, a
condom was installed over each layer of winding. This
device had been tested previously and found to be capable
of withstanding a potential difference of 14 kilovolts.
The entire solenoid was finally "potted" in a cylinder
of epoxy to add mechanical strength and mounted on the
end of a curved brass tube inside the interaction chamber.
Radial and axial field components for this design
are given in figures 2-3a and 2-3b while a pictorial
representation of the field lines is shown in figure 2-3c.
The solenoid was energized by the discharge of a
40 microfarad capacitor bank, triggered by a 5C22 hydrogen
thyratron switch. By controlling the voltage to which
the capacitor bank was charged, a peak current of

16
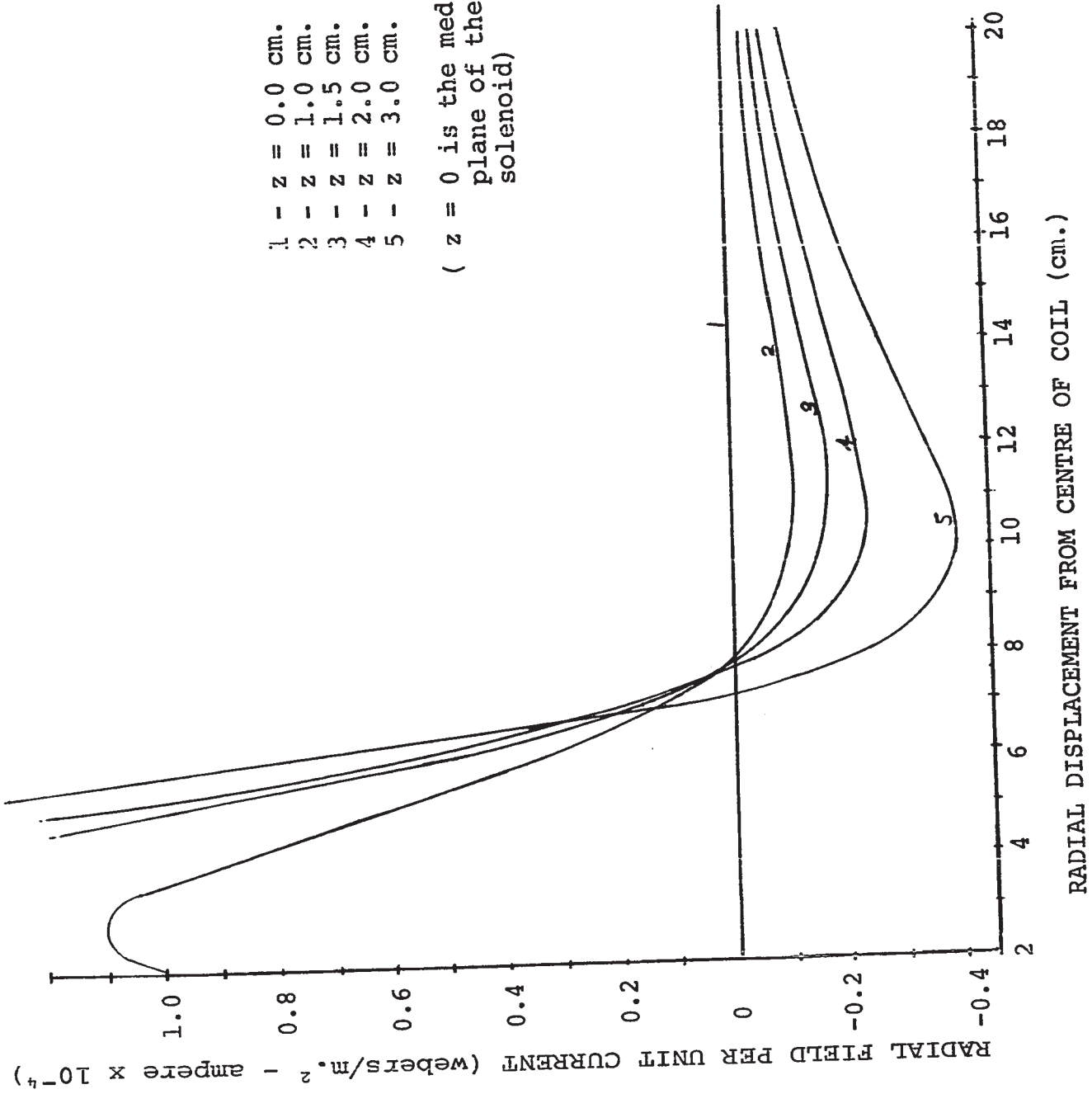
FIG. 2-3a   VARIATION OF RADIAL FIELD
            WITH RADIAL DISPLACEMENT
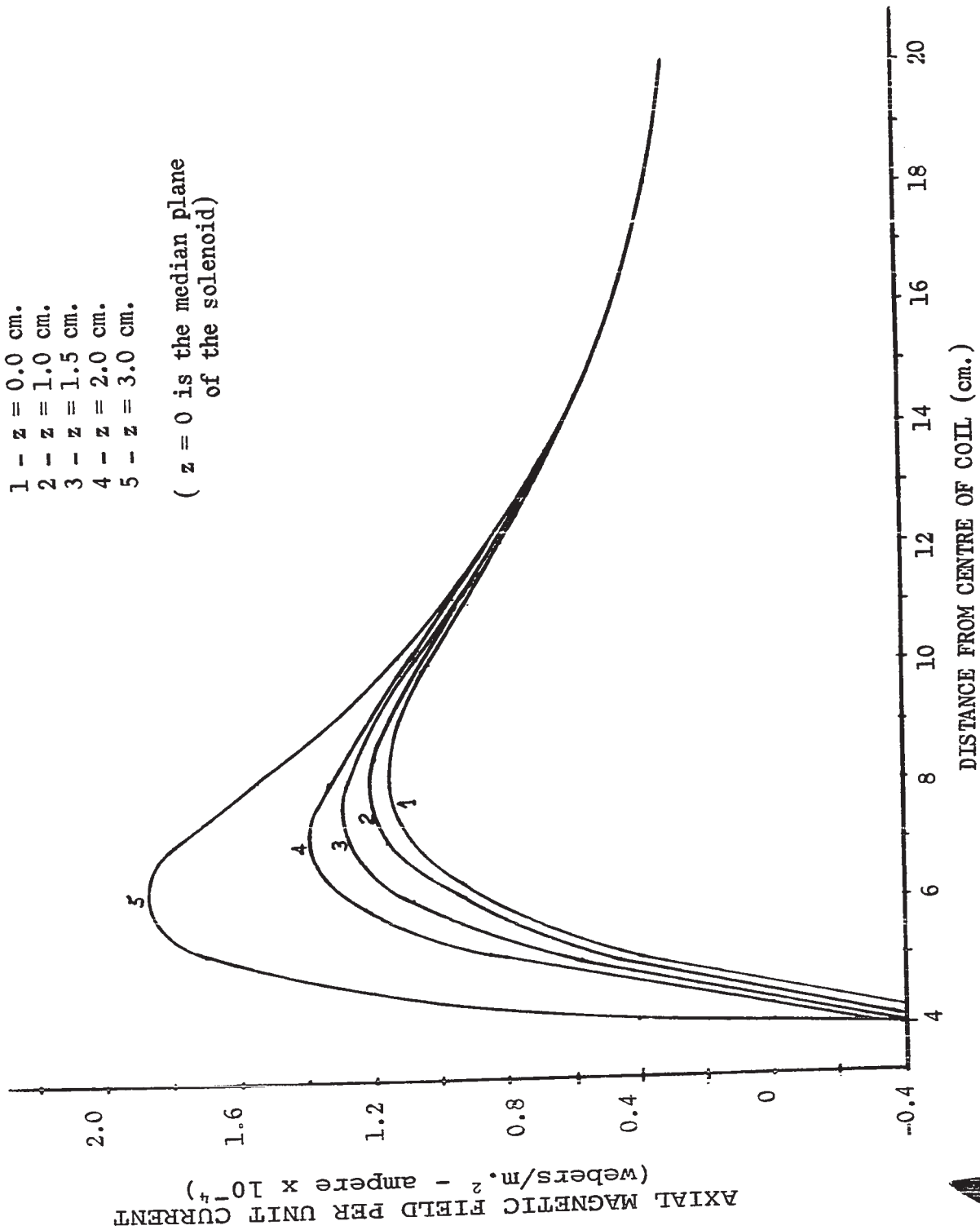
FIG. 2-3b VARIATION OF AXIAL MAGNETIC FIELD
WITH RADIAL DISPLACEMENT
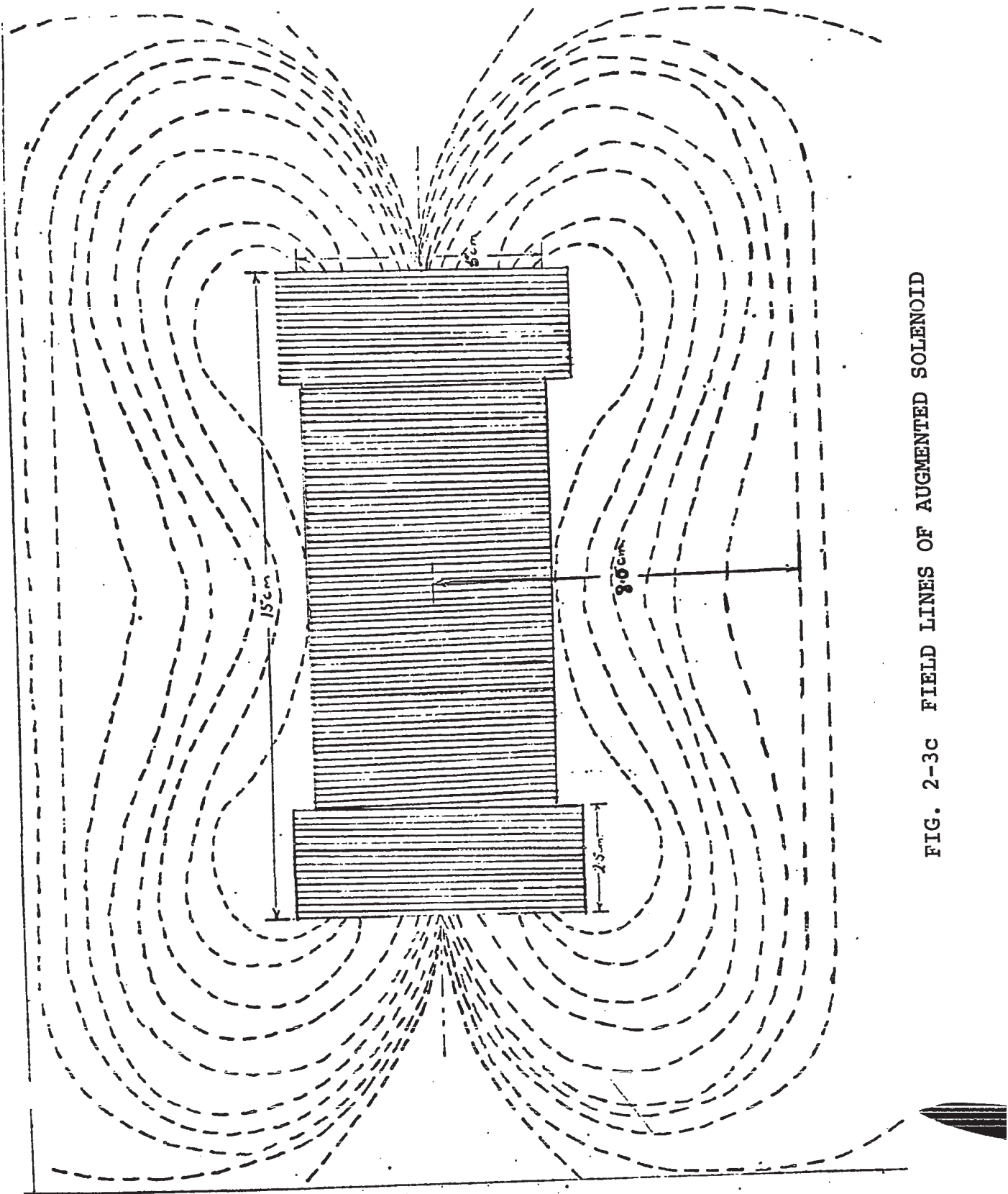
FIG. 2-3c FIELD LINES OF AUGMENTED SOLENOID

approximately 200 amperes was easily obtained.

A delay unit linked both gun and solenoid circuits so
that the sequence of events during a firing occurred as
follows:

With both gun and solenoid capacitor banks charged
to the desired levels, the thyratron of the solenoid circuit
was fired. The solenoid circuit (being an LCR circuit with
solenoid inductance = 23 millihenries) had a period of 6
milliseconds and thus reached maximum solenoid current
(and therefore maximum field) at 1.5 milliseconds after
firing. At this point, the plasma gun was fired with a
time duration of about 30 microseconds. The solenoid current
was essentially unchanged during this time interval and
hence the plasma was streaming into an essentially constant
magnetic field.

As mentioned previously, the field lines could be
straightened only over a limited volume of space and, as
can be seen from figures 2-3a, b, and c, this was achieved
over a length of approximately 5 cm. parallel to the field
lines at a radial distance of about 8 cm. To prevent plasma
from spilling over the edges of the solenoid and encountering
compound field curvature, the plasma stream was baffled
(see figure 2-1) to confine flow to the desired region
of interaction.

A non-inductive current loop was also inserted into
the solenoid circuit to measure solenoid current as a

function of capacitor bank voltage. Results of these
measurements are shown in the following chapter while
the principles of operation of a non-inductive current
loop are discussed in Appendix B.

2-4 TRIPLE PROBE

During the past two decades, electrostatic probes
have been widely used as diagnostic tools for the
determination of electron temperature, energy distribution,
and density of plasmas. In the case of transient plasmas,
such measurements using conventional single (Langmuir,1924)
and double (Johnson & Malter,1950) probes require the
determination of a current-voltage characteristic for
the probe and this procedure requires that the probe voltage
be swept in a time which is short compared with the duration
of the plasma. An alternative method, useful for transient
plasmas whose parameters can be faithfully reproduced,
consists of gathering data for the probe characteristic
curve from a sequence of separate plasmas. Unfortunately,
probe observations of the plasma ejected from the gun
used in this experiment indicated a wide variation from
one shot to another and it was therefore decided to use
a symmetrical triple probe as described by Chen & Sekiguchi
(1965). See also Appendix C.

The triple probe was first used with a voltage sweep circuit to determine the energy distribution of electrons in transient plasmas (Aisenberg,1964). However, Chen and Sekiguchi showed that removal of the voltage sweep function allowed very convenient determinations of electron density and temperature with a reduced response time, limited only by the time of formation of the plasma sheath around the probe electrodes. In addition, the system gives a direct display of electron temperature values and a semi-direct display of electron density values on a dual-beam oscilloscope. It is, therefore, particularly suitable for observing single-shot, rapidly varying, time-dependent plasmas.

The probe consisted of three parallel tungsten electrodes - 0.065 mm. in diameter and 0.5 cm. long. They were mounted at three corners of a square of side 2 mm. (see figure 2-4a) inside a porcelain thermocouple spacer and the assembly was sealed into a long glass tube (7 mm. diameter) using epoxy cement. Connections to the electrodes were made by spot welding #28 enameled copper wire. The leads were then intertwined to minimize inductive pick-up, threaded through spaghetti insulation and finally enclosed in shielding braid. The probe could then be inserted into the interaction chamber via a side port using a vacuum quick-coupling which sealed onto the glass tube.

A schematic of the probe circuit is shown in figure 2-4b. Electrode #2 is allowed to "float" freely at some potential
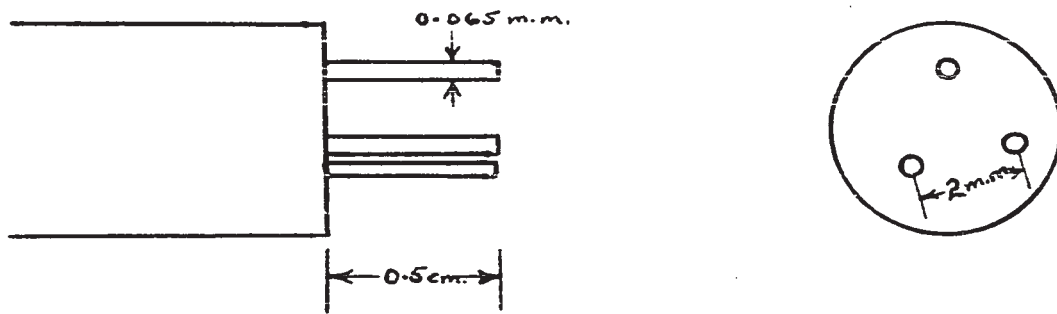
FIG. 2-4a GEOMETRY OF TRIPLE PROBE

R = 250 KΩ

C = 20 μfd.
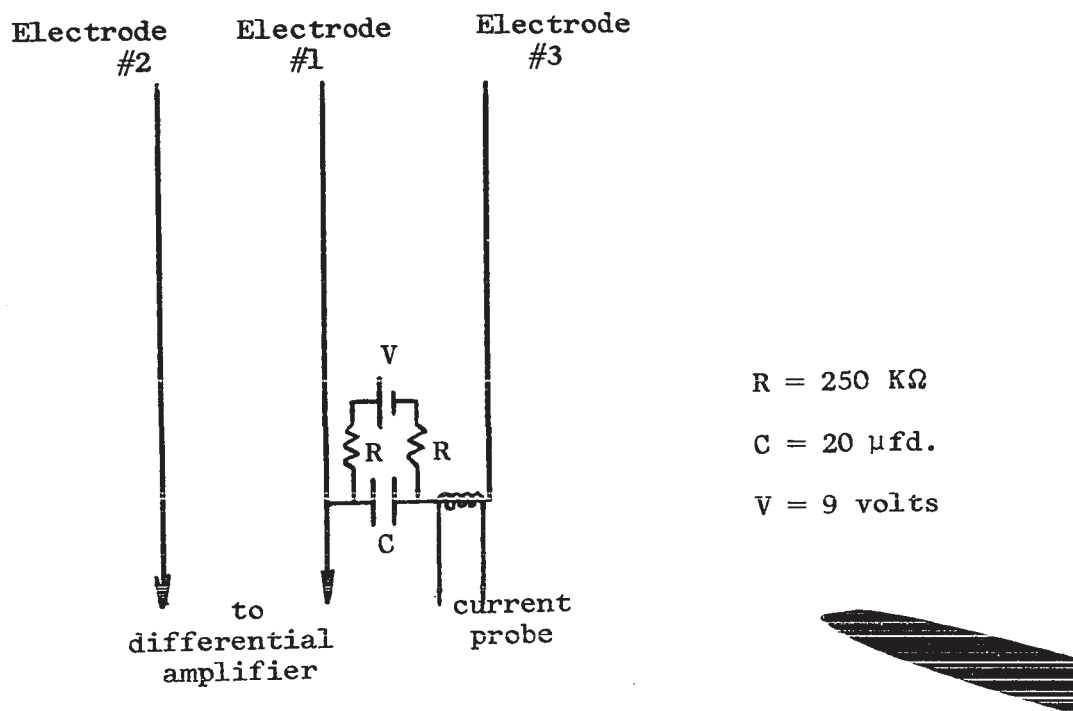
V = 9 volts

FIG. 2-4b SCHEMATIC OF TRIPLE PROBE CIRCUIT

below that of the plasma while a fixed d.c. potential
of 9 volts is maintained between electrodes #1 and #3.
From the theory developed in Appendix C, it is clear that
the electron temperature, T_e, is obtained directly from
the voltage between electrodes #1 and #2. This voltage
was measured using a Tektronix 1A5 high-impedance
differential amplifier which eliminated spurious ambient
fluctuations of plasma potential. Values of electron
density could then be calculated from the electron
temperature and the current flowing from electrodes #1
to #3. This current was measured directly using a Tektronix
current probe (Type 134).

2-5 MAGNETIC SEARCH COIL

Magnetic field perturbations were measured using a
probe comprised of a simple search coil which generated
an output voltage proportional to the rate of change of
magnetic field with time, i.e. to dB/dt. This output was
then integrated electronically to give a signal proportional
to B. In these experiments, the magnetic probe was used to
record changes in magnetic intensity with time at any
given location during the interaction.

Two opposing criteria had to be compromised in the
design of the search coil. Firstly, the coil had to be
physically small so that it did not itself introduce
significant perturbations. Conversely, a smaller coil

gives a reduced output which is further attenuated by
the integrating circuit - particularly at low frequencies -
thereby reducing the overall accuracy of the measurements.
Details of these considerations are given in Appendix D.

Several coils of various sizes were wound and tested.
In the final design, 607 turns of #40 copper wire were
wound on a form 0.24 cm. in diameter and 1.27 cm. long. This
coil was mounted on the end of a thin glass tube, potted
in epoxy cement, and inserted into the interaction chamber
(see figure 2-1). By means of a specially-designed probe
holder (shown in figure 2-5a), the coil could easily be
moved throughout the interaction area and its position
accurately determined.

The output of this probe was amplified by a factor
of 100 and electronically integrated using a Tektronix
Type "O" operational amplifier with integration parameters -
R = 0.2 megohms, C = 0.1 microfarads - chosen to give
accurate integration down to 350 Hz. The resulting signal
was observed on a Tektronix 555 dual-beam oscilloscope
triggered by the firing of the plasma gun. However, by
operating time base "B" in the delayed trigger mode, it
was possible to display the magnetic field perturbations
on a more sensitive vertical scale.

2-6 PHOTOGRAPHIC TECHNIQUES

1) Time Integrated Photographs
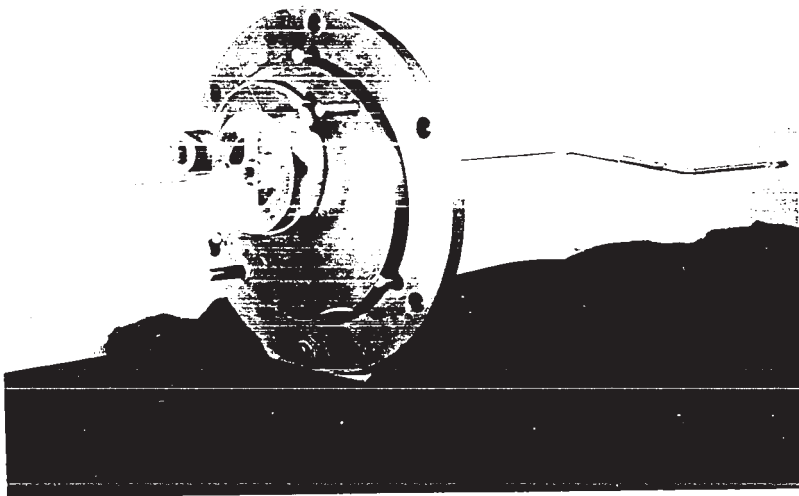
FIG. 2-5a   MAGNETIC PROBE MOUNTED IN
ADJUSTABLE HOLDER

The time integrated photographs were obtained simply
by aiming a tripod-mounted Polaroid Land camera (model # 120)
through the side port of the interaction chamber and
holding the shutter open while the interaction took place.
The camera was focussed on the median plane of the solenoid
with a portrait lens installed to obtain the desired field
of view. Typical film speeds and stop numbers are 10,000
ASA - f64 and 200 ASA - f5.6.

Colour photographs were also taken using 35 mm.
Ektacolor Professional S film (100 ASA - f4).

2) High Speed Photographs

A high speed camera (modified Abtronics model #2HS),
capable of exposure times of 1, 0.1, and 0.01 microseconds,
was also used to record the interaction. An added feature
of this unit was a delayed shutter mechanism which allowed
the interaction to be photographed at any stage of its
development. The film used in these studies was Polaroid
10,000 ASA.

Since recombination of plasma electrons and ions
normally emits radiation in the visible region, photographic
records can therefore be used as a qualitative indication
of the macroscopic behaviour of a plasma and are of
considerable value in observing the dynamics of a plasma
interacting with a magnetic field.

2-7   TIME OF FLIGHT MEASUREMENTS

1) Conductivity Probe Method

Plasma velocities were deduced from time of flight measurements carried out using two double (conductivity) probes separated by a known distance in the flight path of the plasma (see figure 2-7a).

Each double probe consisted of two tantalum wires - 1.5 cm. long and 0.075 mm. in diameter - mounted parallel to each other and separated by a distance of 2 mm. on the end of a long, 7 mm. diameter, glass tube. A potential difference of 225 volts was maintained between them by charging a 20 microfarad capacitor connected between them as shown in figure 2-7b.

When the probe was immersed in a conducting plasma, the circuit was completed, thus allowing current to flow. This current was impulsive in nature and hence produced a voltage pulse across the primary of the pulse transformer (inserted to provide electrical d.c. isolation of the plasma). The pulse was reflected into the secondary producing a voltage across termination resistance R_2. The large resistors serve to isolate the battery supply from the probe circuit during the short time of the plasma flow. Thus the large capacitor effectively establishes a low-impedance constant-voltage power supply.

Pulses from each probe were observed and recorded simultaneously on the two beams of a Tektronix 555 dual-

Probe #1   Probe #2

Plasma Gun

28·9 cm.

Probe #1
Probe #2

Position A

Position B

NOTE: Position B was
viewed through
a side port.

AB = 35 cm.

To
Pumps
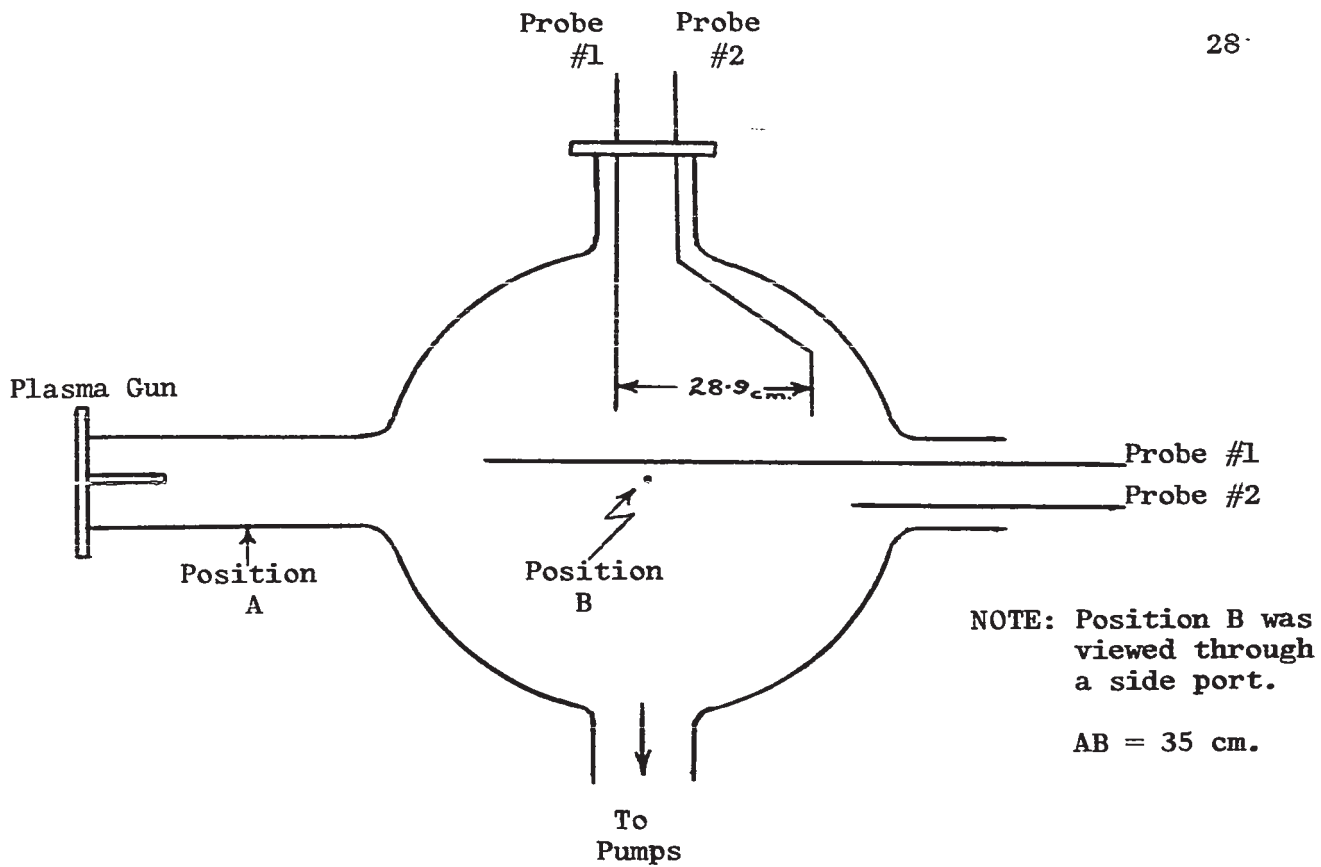
FIG. 2-7a VARIOUS PROBE CONFIGURATIONS
USED IN THIS EXPERIMENT

T   R₁

to probe electrodes   to oscilloscope
                                           R₂

C

R   R

V

C = 20 μ fd., 500 v.
R = 250 KΩ
V = 225 volts
T = 1:1 turns ratio
     pulse transformer
R₁ = 470 ohms

R₂ = 47 ohms
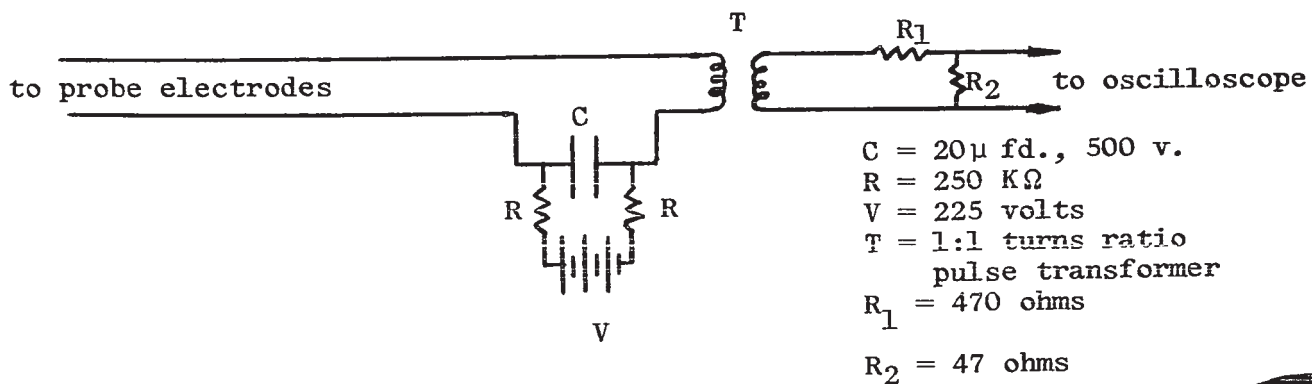
FIG. 2-7b CONDUCTIVITY PROBE CIRCUIT

beam oscilloscope, using both beams on the same time base, triggered by the firing of the plasma gun. The elapsed time between the two pulses was then determined and since the distance between the probes was known, a value of plasma velocity could be calculated.

2) Photodiode Method

Many experimenters have used two photodiodes to record passage of plasma over a known distance for the purpose of determining plasma velocities. This method was attempted in the present work using RCA 929 vacuum photodiodes mounted in positions A and B as shown in figure 2-7a. The photodiode circuit is shown in figure 2-7c and a sample trace recorded at position A is illustrated in figure 2-7d. This shows a well-defined plasma stream of duration 30 microseconds. However, no such trace was obtainable at larger distances from the gun, for example, at position B. The light intensity had been greatly reduced, presumably by dispersion and recombination processes. Further studies using a conductivity probe located at position B showed that the signals from the probe and the photodiode were not simultaneous, with the probe signal always preceding. This suggested that the forward portion of the plasma stream contained substantially more ionized material than the slower portion where, apparently, recombination processes were occurring at a more rapid rate and thereby emitting visible radiation.

225 volts

RCA 929
Vacuum
Photodiode

to
oscilloscope

5.6 KΩ
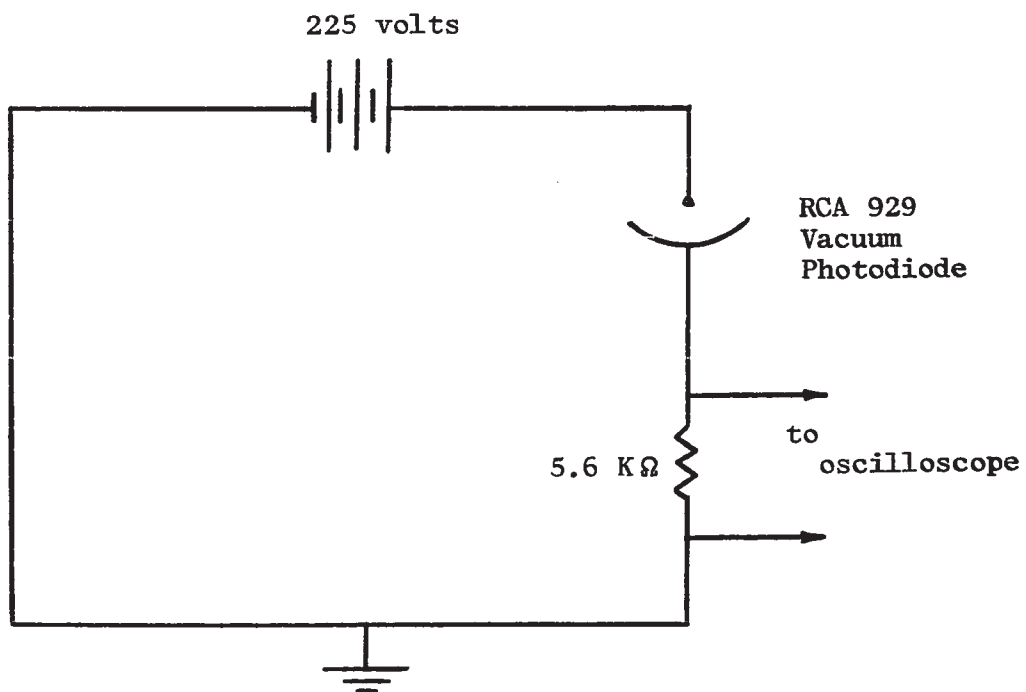
FIG. 2-7c PHOTODIODE CIRCUIT
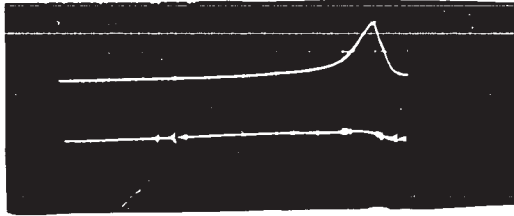
FIG. 2-7d PHOTODIODE TRACES

The upper trace is the signal obtained from the photodiode at position A and the lower trace is the signal obtained from the photodiode at position B.

vertical sensitivity
    upper trace - 0.2 volts/cm.
    lower trace - 0.005 volts/cm.

horizontal sensitivity
        10 microseconds/cm.

Since the ionized material was of interest in this experiment, further investigations using photodiodes were not attempted.

CHAPTER 3

EXPERIMENTAL RESULTS

Uncertainties in the experimental measurements of this chapter are indicated in the form of error bars whose significance is described on the various graphs. A more significant source of uncertainty is the non-reproducible nature of the plasma gun as described previously and since this behaviour is practically unpredictable, a quantitative estimate of its effects is impossible.

3-1 SOLENOID CURRENT MEASUREMENTS

The field capacitor was charged to initial voltages ranging from 1 to 8 kilovolts and then discharged through the solenoid and non-inductive current loop. A plot of initial field-capacitor voltage versus solenoid current was thus obtained as shown in figure 3-1a. The computer calculations of solenoid magnetic field were programmed in units of magnetic induction per unit current and thus, the magnetic induction could be determined for any value of field capacitor voltage.

3-2 TIME OF FLIGHT MEASUREMENTS

The only sensible measurements of plasma velocity were

33

34

Error bars represent possible
experimental error

SOLENOID CURRENT (AMPERES) →

260 240 220 200 180 160 140 120 100 80 60 40 20 0

1 2 3 4 5 6 7 8 9

DISCHARGE VOLTAGE (KILOVOLTS) →
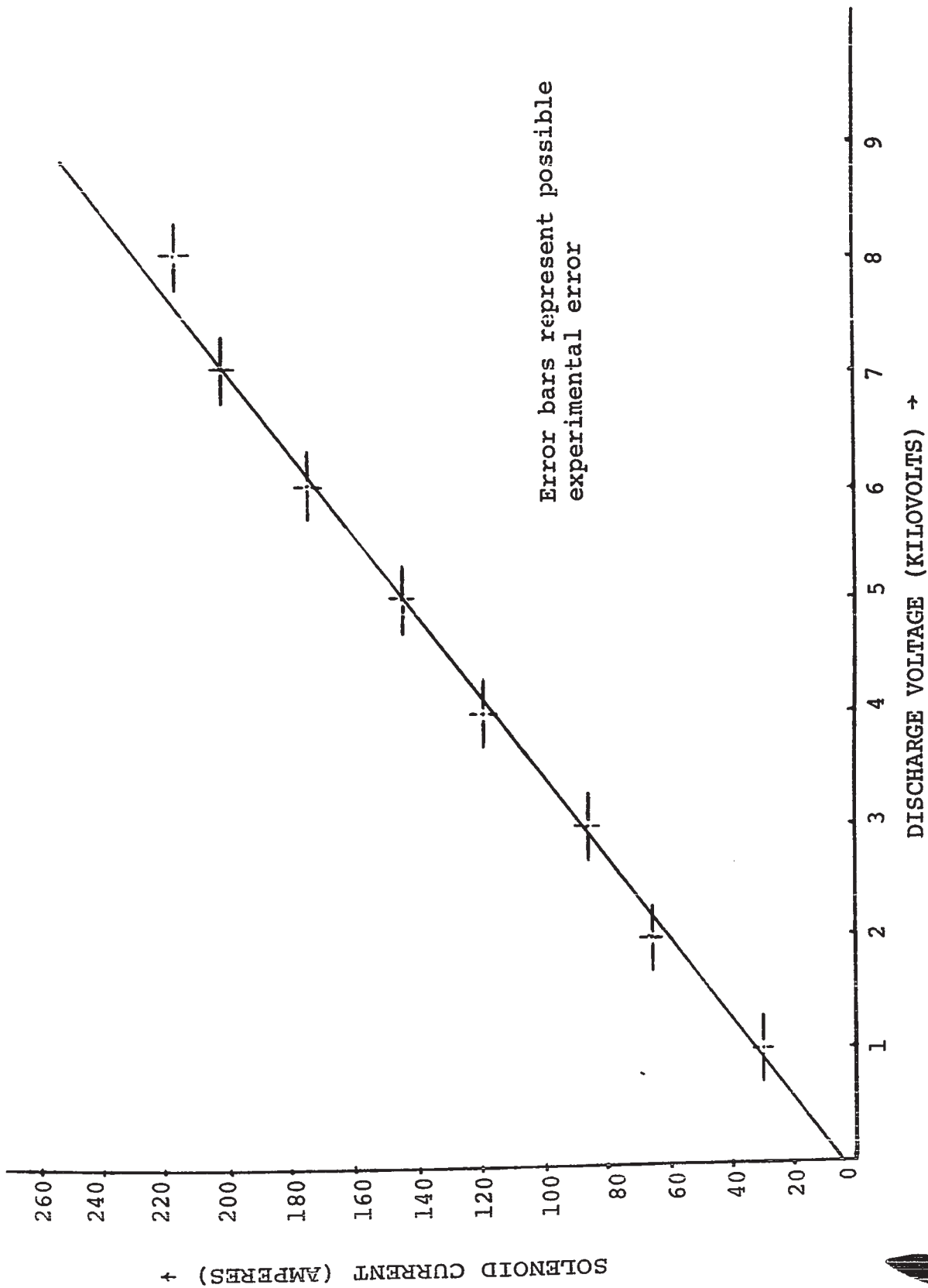
FIG. 3-1a   VARIATION OF SOLENOID CURRENT WITH INITIAL CAPACITOR BANK VOLTAGE

obtained using the conductivity probes described previously.
Typical oscilloscope traces are shown in figure 3-2a and
the variation of plasma velocity with gun-capacitor bank
voltage is depicted in figure 3-2b. It should be noted that
the results showed wide variation, due presumably to the
non-reproducible operation of the plasma gun. However, a
study of the results over a large number of shots indicated
that for a given gun voltage, no particular experimental
value differed from the average velocity (shown on the
graph) by more than a factor of 2.

3-3   TRIPLE PROBE MEASUREMENTS

Typical oscilloscope traces obtained from the triple
probe are shown in figure 3-3a and the effect of gun voltage
upon electron density and temperature - deduced from these
results are depicted in figures 3-3b and 3-3c. Once again,
the experimental results showed a measure of non-reproduci-
bility attributable to the plasma gun operation. A further
problem seems to have been probe contamination giving rise
to unrealistic results. While most laboratory plasmas have
electron temperatures of the order of 30,000°K, the triple
probe, at times, indicated electron temperatures of the
order of 200,000°K and higher. Also, experimental values of
electron density appeared high compared with values
calculated from theoretical expressions relating the plasma-
magnetic field parameters. Furthermore, on successive
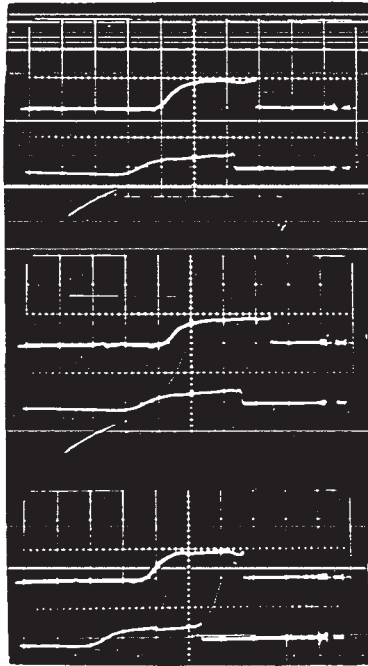
FIG. 3-2a   CONDUCTIVITY PROBE TRACES

Three separate shots are illustrated, the top trace in each case representing the probe nearest the gun (see FIG. 2-7a).

Horizontal sensitivity   5 microseconds/cm.

Vertical sensitivity   20 volts/cm.
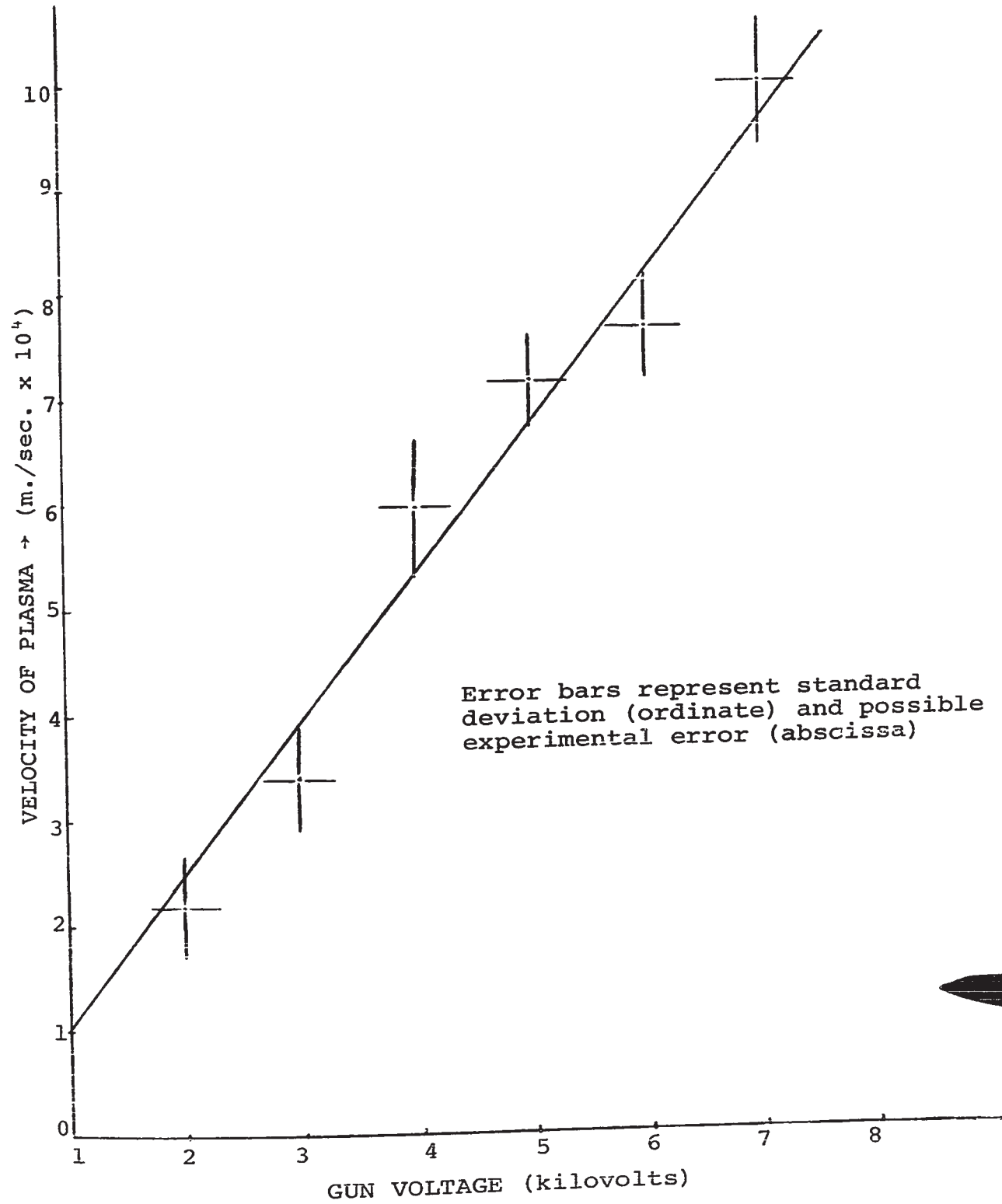
FIG. 3-2b   VELOCITY OF PLASMA MEASURED VIA CONDUCTIVITY PROBES
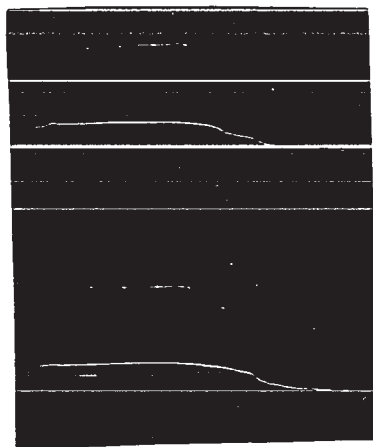
FIG. 3-3a TRIPLE PROBE TRACES

Upper trace is signal from current probe (vertical
sensitivity 1 milliamp./cm.) and lower trace is signal
from differential amplifier (vertical sensitivity 5 volts/
cm.). The horizontal sensitivity is 5 microseconds/cm..

Two separate shots are shown to illustrate the non-
reproducible nature of the gun.

Error bars represent possible experimental error.

ELECTRON DENSITY (x 10^{12}/cm^3.)

GUN VOLTAGE (kilovolts)
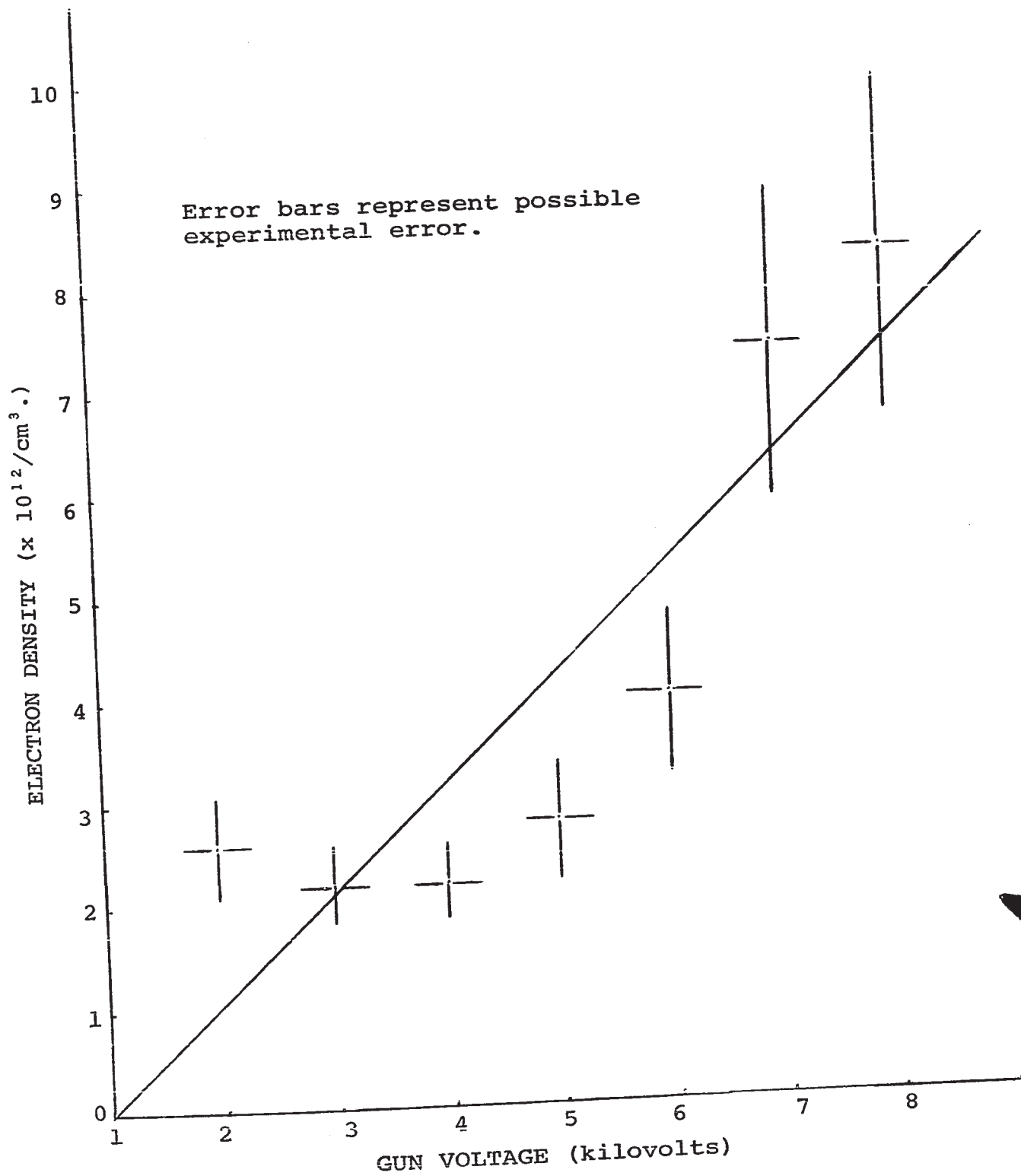
FIG. 3-3b TRIPLE PROBE MEASUREMENTS OF ELECTRON DENSITY

Error bars represent possible experimental error.
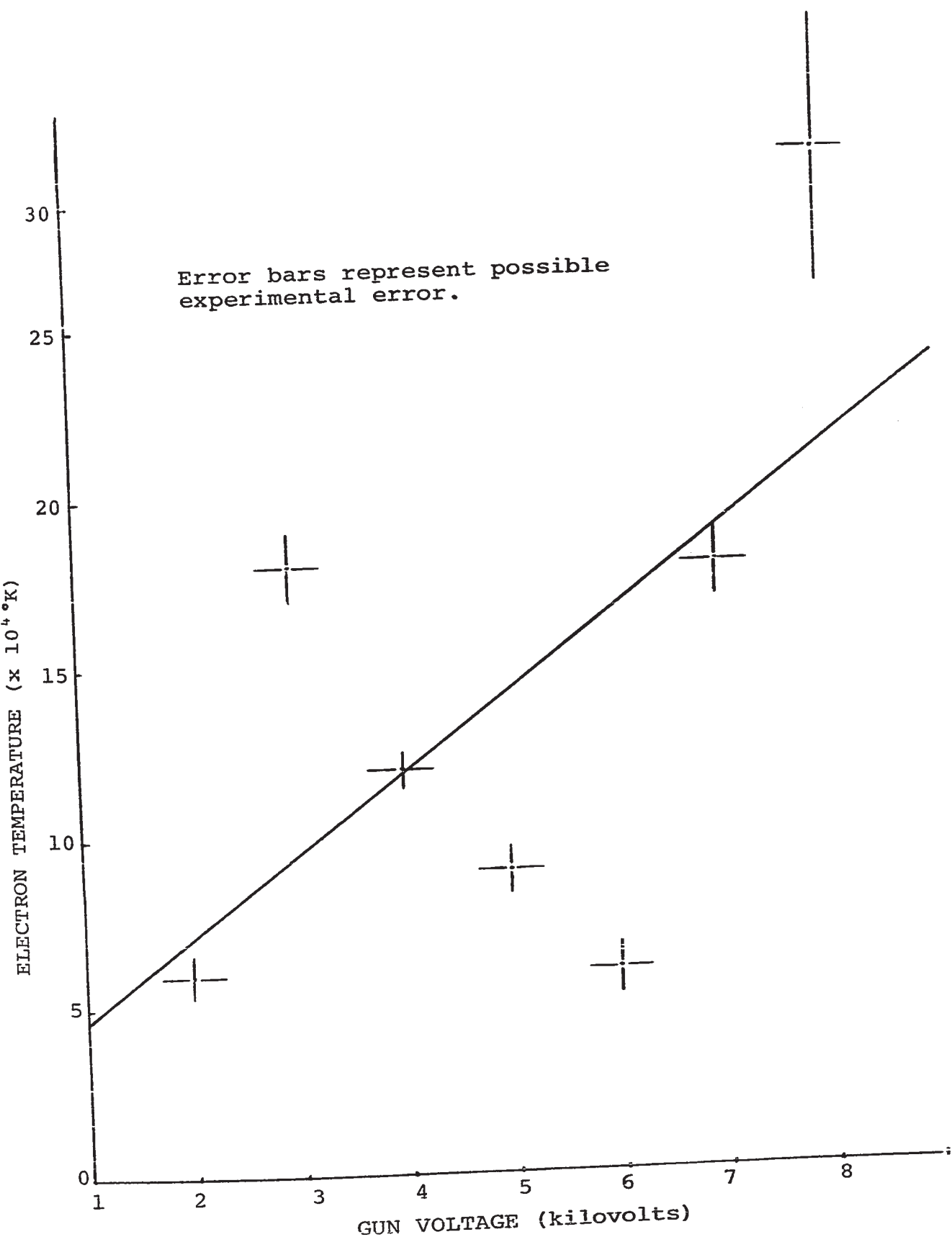
FIG. 3-3c   TRIPLE PROBE MEASUREMENTS OF ELECTRON TEMPERATURE

experimental runs, the electron density values continued
to increase rather than return to the initial value - a
fact which strongly suggested progressively worsening
probe contamination. Examination of the probe electrodes
showed the effects of particle bombardment which presumably
contributed to the deterioration of the epoxy separating
the electrodes. Preceding the final experimental run, the
probe was carefully cleaned to minimize these difficulties.

3-4 MAGNETIC PROBE RESULTS

The entire area forward from the solenoid to a radial
distance of about 20 cm. was magnetically probed and a
magnetic field boundary was found to exist. This boundary
was roughly defined by an enhanced field area on the solenoid
side and a diminished field area on the plasma side. Typical
oscilloscope traces from both areas are shown in figures
3-4a and 3-4b. From the data collected, field contour maps
depicting the evolution of the interaction were compiled
for both directions of magnetic field - ordinary and reversed
as defined on the diagrams. These are shown in figures 3-4c
to f and reveal the development in time of a magnetic field
asymmetry dependent on field direction.

_____ unperturbed field
        level
_____ zero magnetic
        field

FIG. 3-4a MAGNETIC PROBE TRACE
           (exterior to the magnetic boundary)

Magnetic field decreases to essentially zero.

_____ unperturbed field
        level

FIG. 3-4b MAGNETIC PROBE TRACE
           (interior of the magnetic boundary)

Magnetic field increases under the distorting effects
of plasma flow.

Field out of paper
(ordinary orientation)

B = perturbed value
    of field

B_0 = unperturbed value
    of field
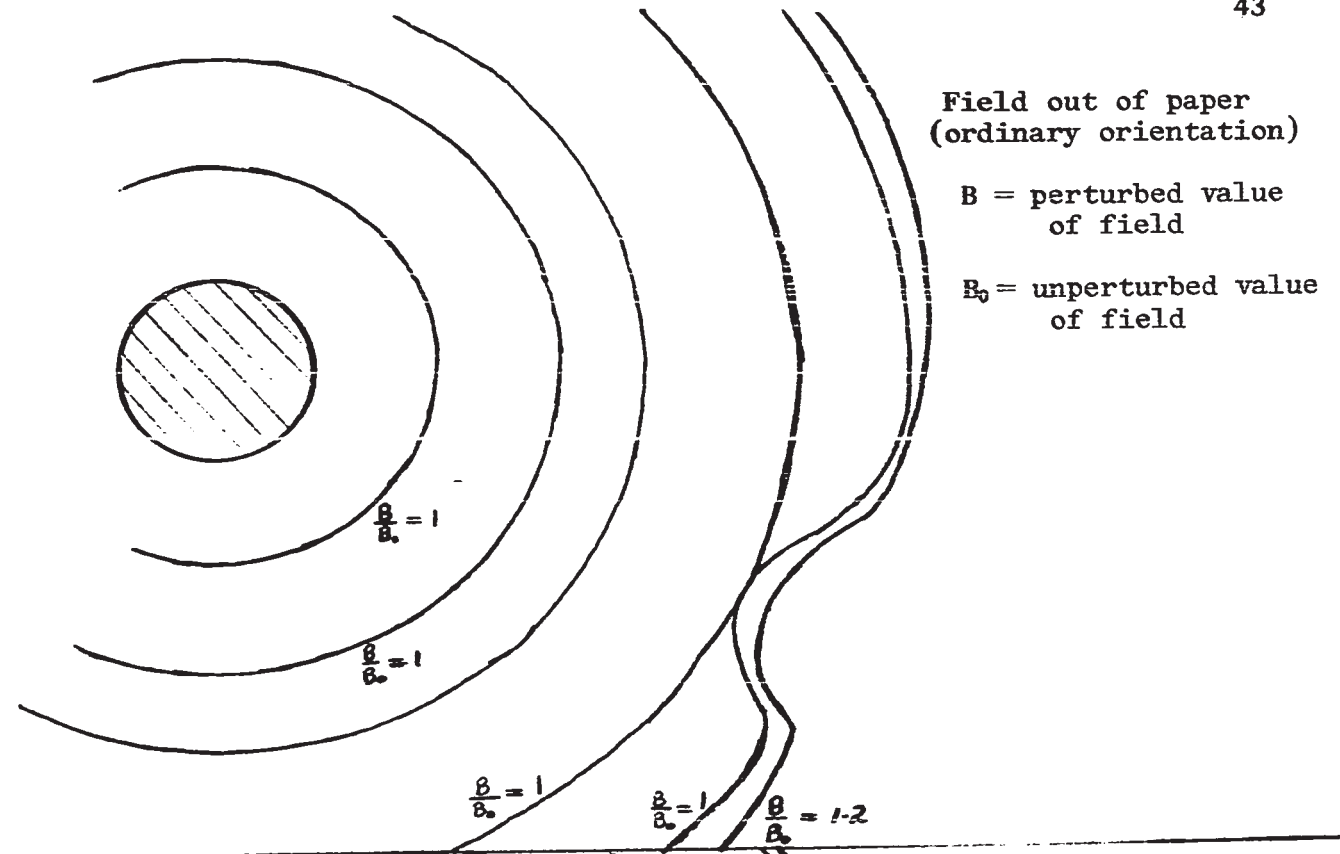
Field into paper
(reversed orientation)
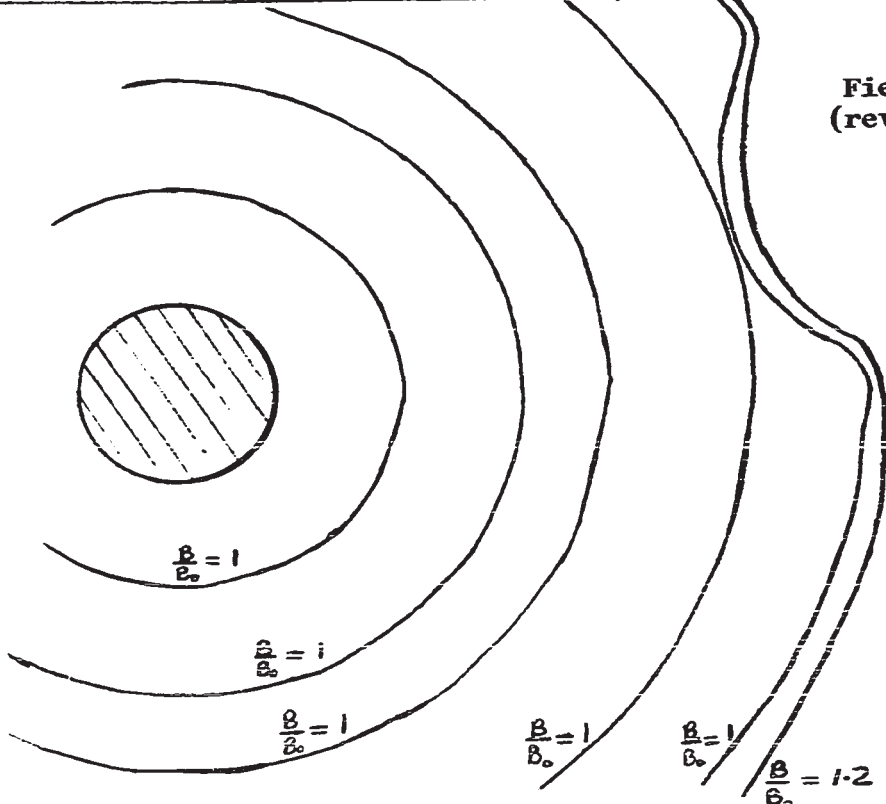
FIG. 3-4c MAGNETIC FIELD CONTOURS
(5 microseconds after firing of plasma gun)

Field out of paper

$\frac{B}{B_o} = 1.3$

$\frac{B}{B_o} = 1$

$\frac{B}{B_o} = 1$

$\frac{B}{B_o} = 1.2$

$\frac{B}{B_o} = 0.5$

$\frac{B}{B_o} = 0.6$

$B = 0$

Field into paper

$\frac{B}{B_c} = 1$

$\frac{B}{B_o} = 1$

$\frac{B}{B_o} = 1.1$

$\frac{B}{B_o} = 0.7$

$\frac{B}{B_o} = 0.6$

$B = 0$
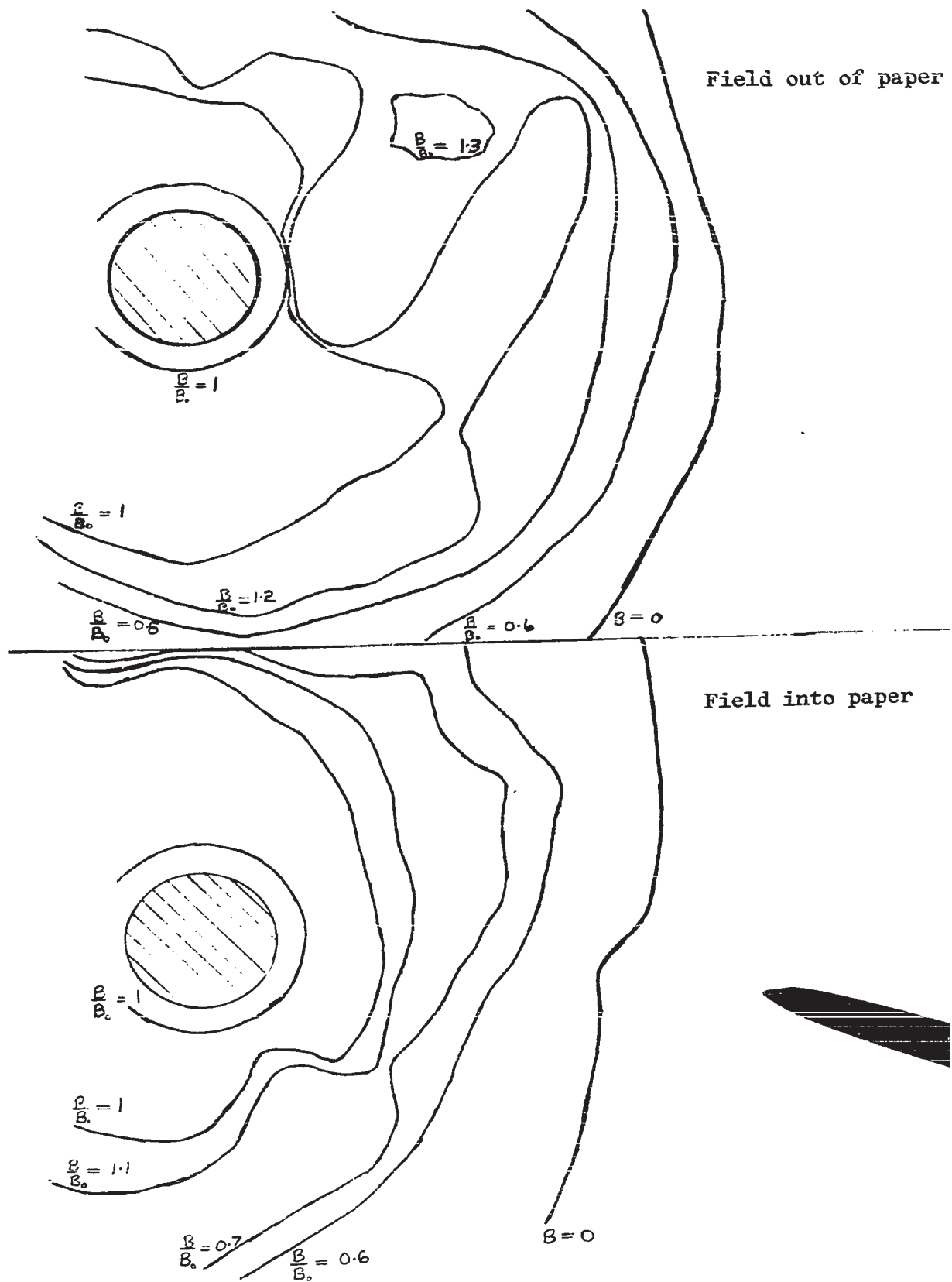
FIG. 3-4d MAGNETIC FIELD CONTOURS
(20 microseconds after firing of plasma gun)

$\frac{B}{B_0} = 1.2$

$\frac{B}{B_0} = 1.2$

Field out of paper

$\frac{B}{B_0} = 1$

$\frac{B}{B_0} = 1$

$\frac{B}{B_0} = 0.8$

$\frac{B}{B_0} = 0.6$

$\frac{B}{B_0} = 0.2$

$B = 0$

Field into paper

$\frac{B}{B_0} = 1$

$\frac{B}{B_0} = 0.8$

$\frac{B}{B_0} = 1.3$

$\frac{B}{B_0} = 0.6$

$B = 0$
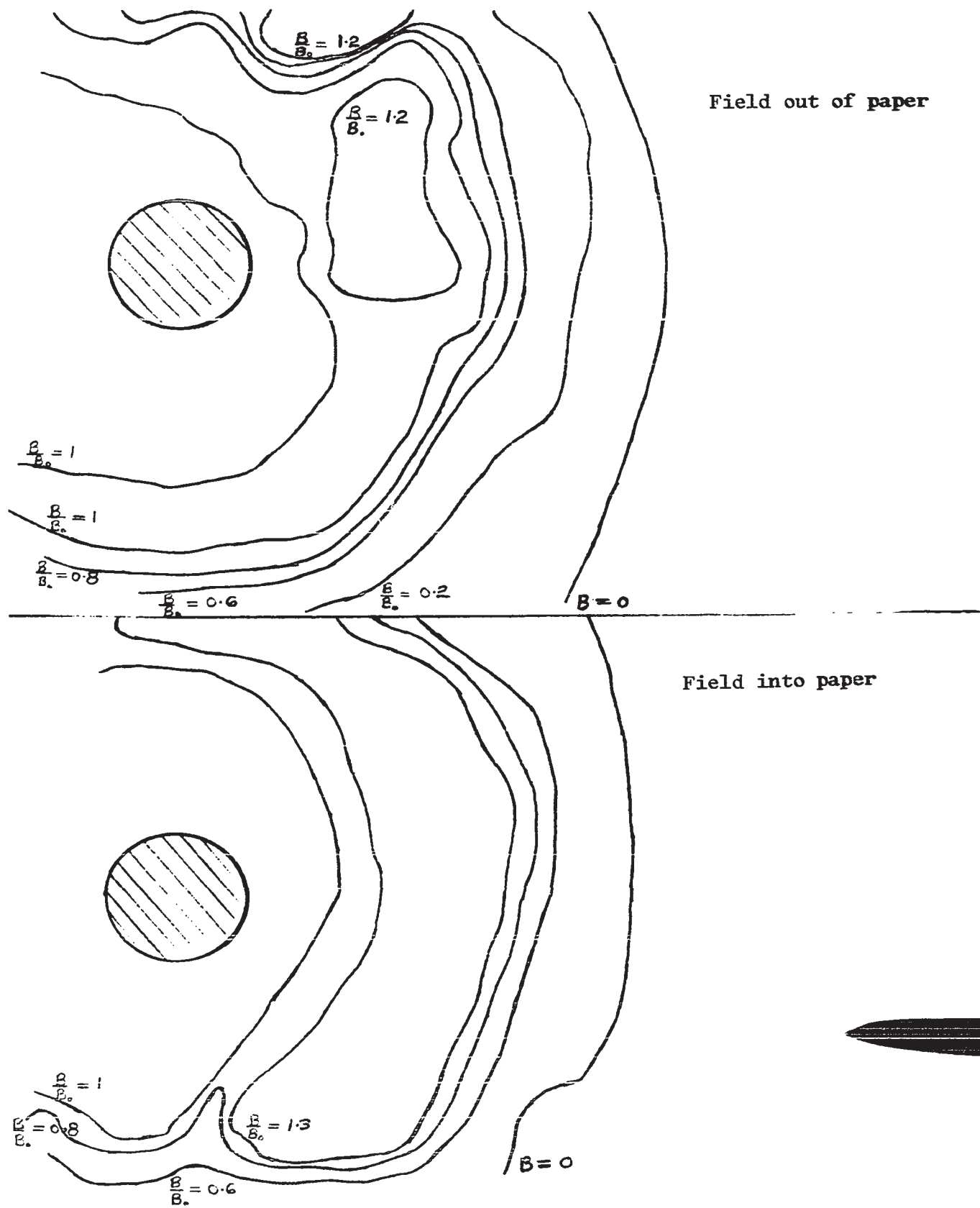
FIG. 3-4e MAGNETIC FIELD CONTOURS
(35 microseconds after firing of plasma gun)

$\frac{B}{B_o} = 1.2$

magnetic
depression

$\frac{B}{B_o} = 1.2$

Field out of paper

$\frac{B}{B_o} = 1$

$\frac{B}{B_o} = 1$

$\frac{B}{B_o} = 0.8$

$\frac{B}{B_o} = 0.6$

$\frac{B}{B_o} = 0.4$

$\frac{B}{B_o} = 1$

$\frac{B}{B_o} = 0.8$

$\frac{B}{B_o} = 0.5$

$\frac{B}{B_o} = 1$

Field into paper

$\frac{B}{B_o} = 1.2$

$\frac{B}{B_o} = 1.4$

magnetic
depression

$\frac{B}{B_o} = 0.4$
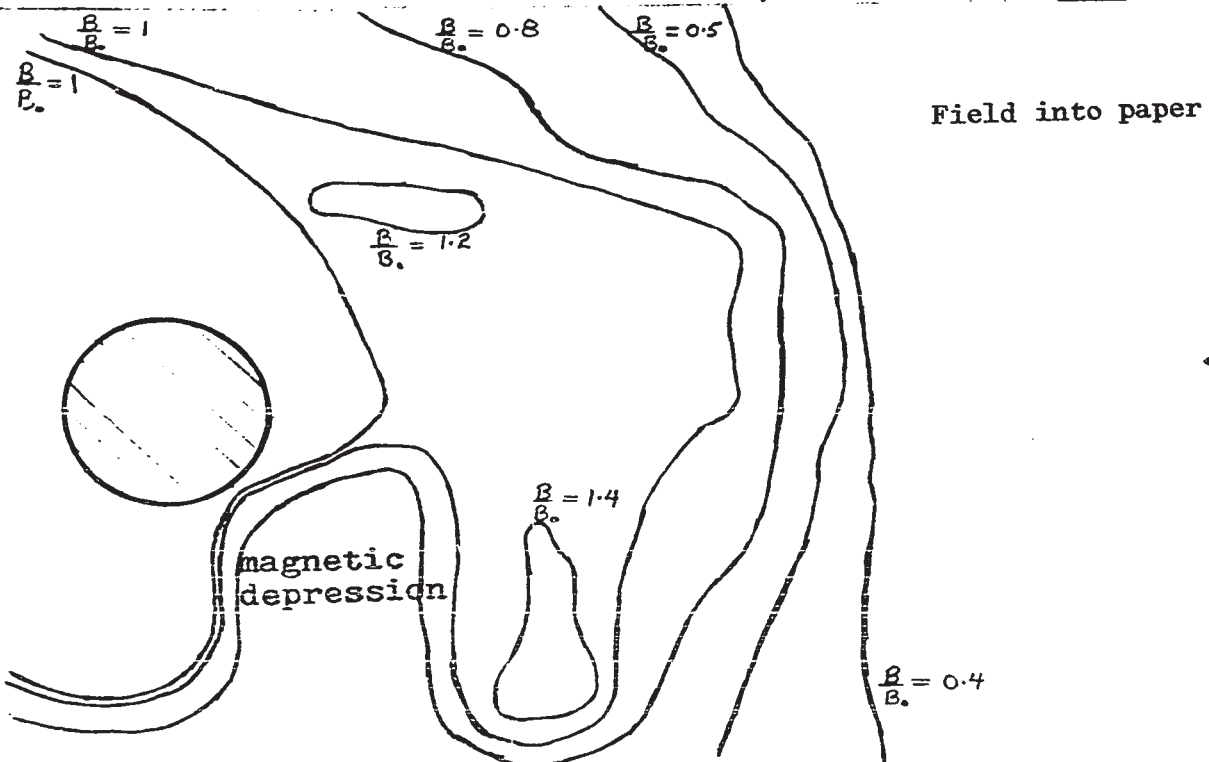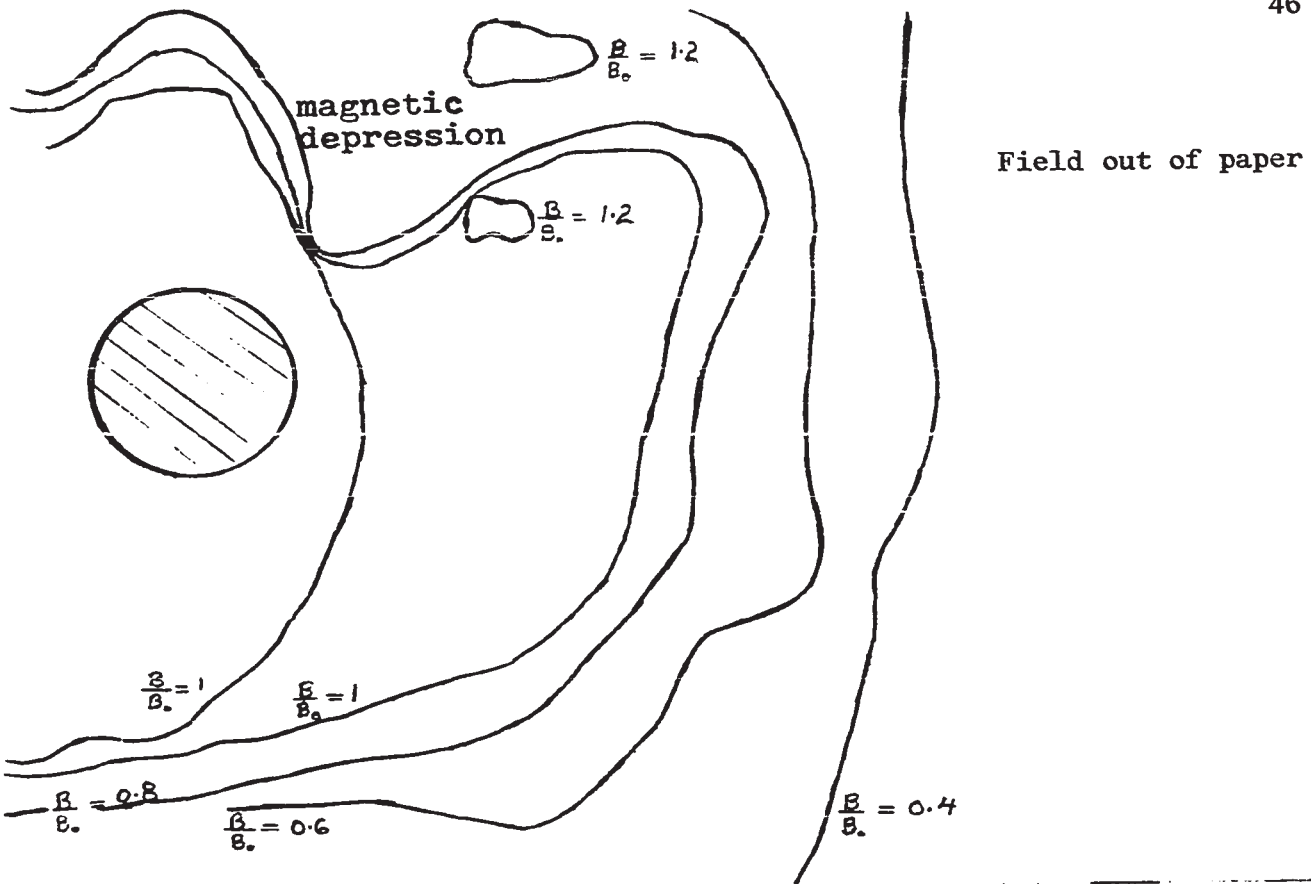
FIG. 3-4f MAGNETIC FIELD CONTOURS
(50 microseconds after firing of plasma gun)

3-5 PHOTOGRAPHIC RESULTS

a) Time Integrated Photographs

Typical examples of time integrated photographs are shown in figures 3-5a, b, and c. These indicate that some plasma does penetrate the boundary since light given off by recombination of ions and electrons is visible on the solenoid. However, there is also evidence of a plasma stand-off in the vicinity of the magnetic boundary as well as a "filament" structure showing plasma penetration across the magnetic field towards the solenoid.

The colour photographs particularly show a definite asymmetry in the interaction (figures 3-5d, e, and f).

b) High Speed Photographs

In order to obtain observable records even on Polaroid ASA 10,000 film, it was necessary to use the longest exposure time of the high speed camera. This was nominally 1 microsecond and was measured electronically to be 1.4 microseconds. Photographs were taken every 5 microseconds during the interaction and typical examples are shown in figures 3-5g to k.

Particularly interesting are the exposures taken at 35 microseconds after the firing of the plasma gun or approximately midway through the interaction. These records illustrate very clearly a strong field-dependent asymmetry.

They also show a direct correlation between the presence
of plasma and the local decrease of the field indicated
in the magnetic field contour maps.

49

FIG. 3-5a TIME INTEGRATED PHOTOGRAPH
(magnetic field into paper)

direction
of
plasma
flow
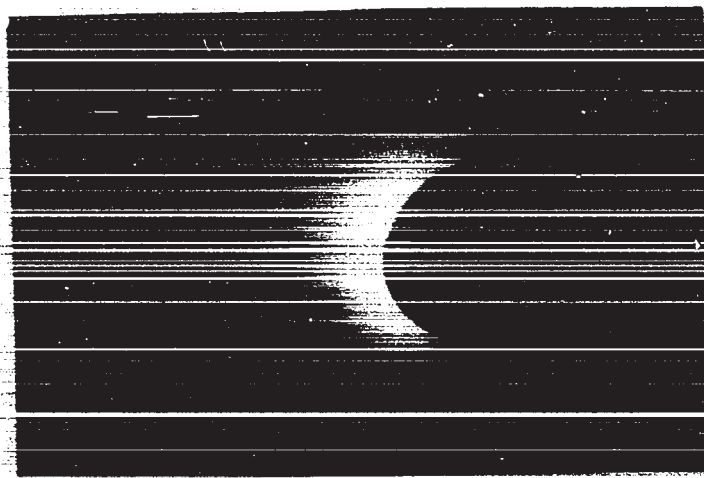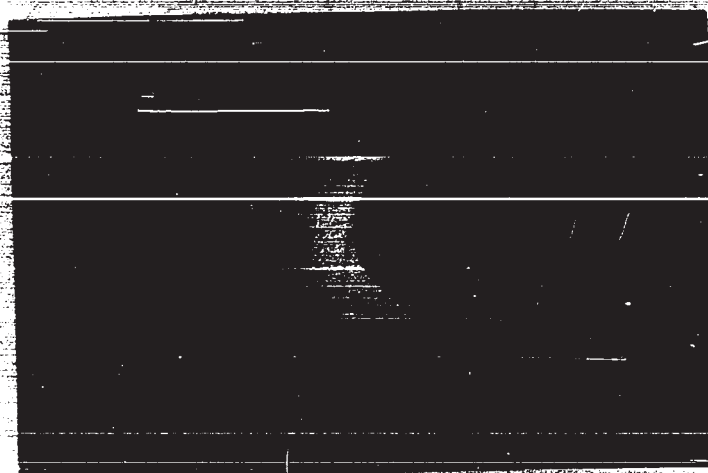
FIG. 3-5b TIME INTEGRATED PHOTOGRAPH
(magnetic field out of paper)

FIG. 3-5c TIME INTEGRATED PHOTOGRAPH
(zero magnetic field)
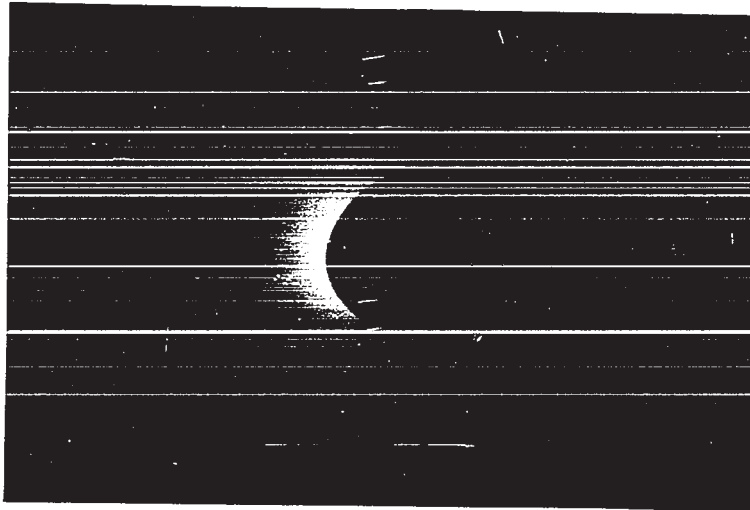
FIG. 3-5d   TIME INTEGRATED PHOTOGRAPH
            (magnetic field into paper)
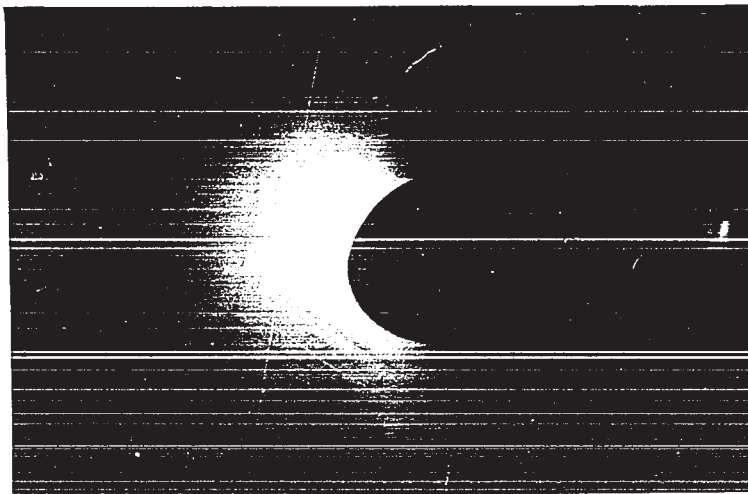
FIG. 3-5e   TIME INTEGRATED PHOTOGRAPH
            (magnetic field out of paper)
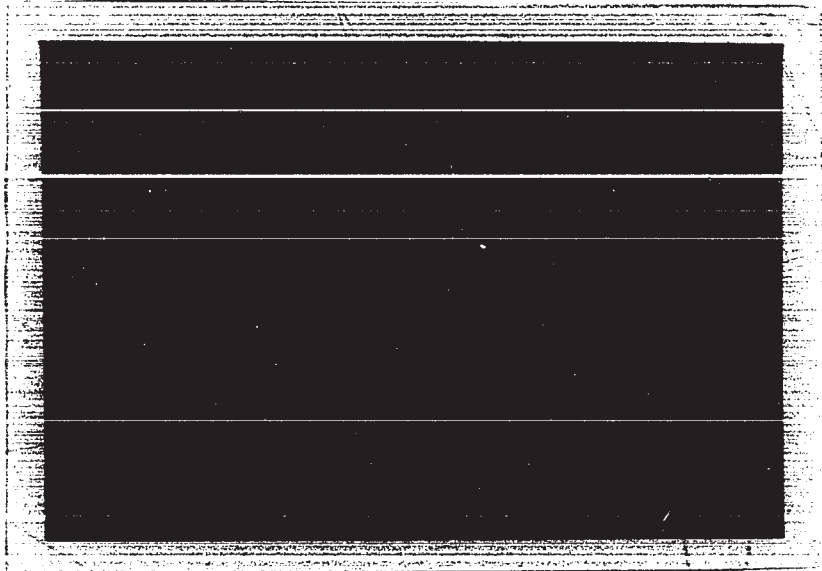
FIG. 3-5f   TIME INTEGRATED PHOTOGRAPH
(zero magnetic field)
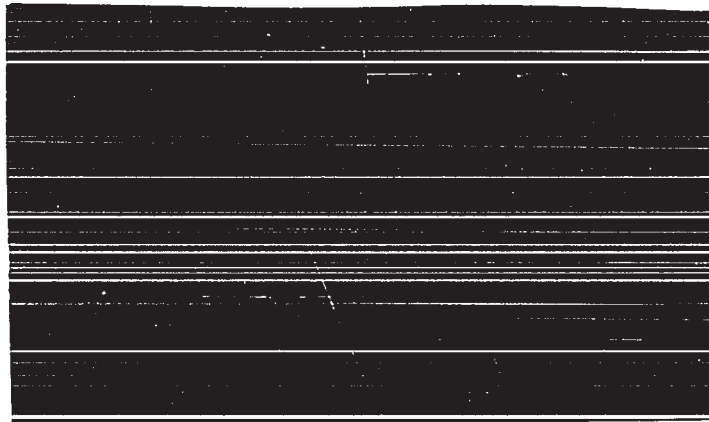
magnetic field
into paper

direction
of
plasma
flow
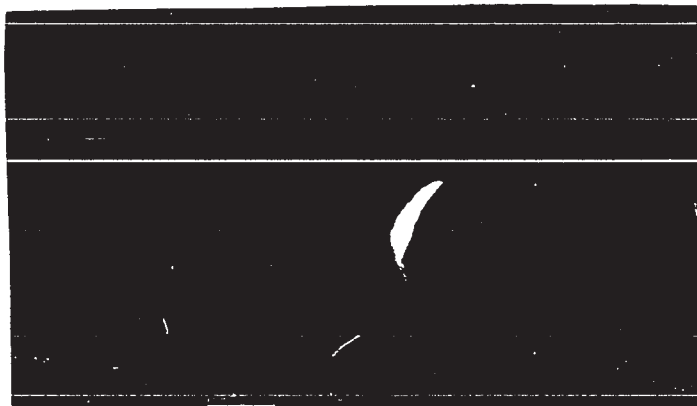
magnetic field
out of paper
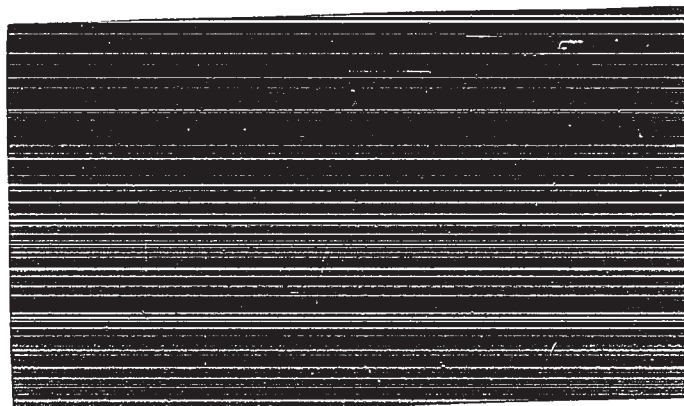
zero magnetic
field

FIG. 3-5g HIGH SPEED PHOTOGRAPHS
(taken 10 microseconds after firing of plasma gun)
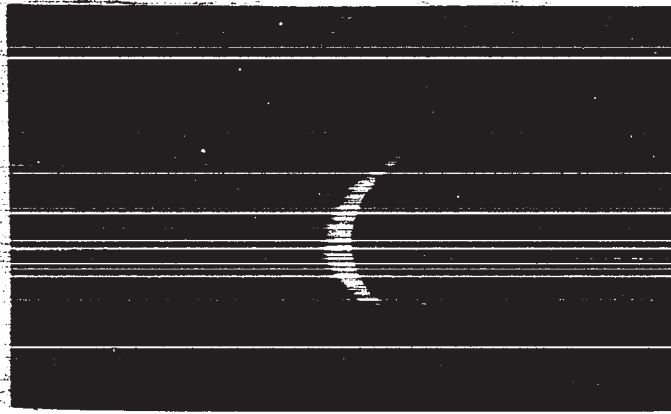
magnetic field
into paper

direction
of
plasma
flow
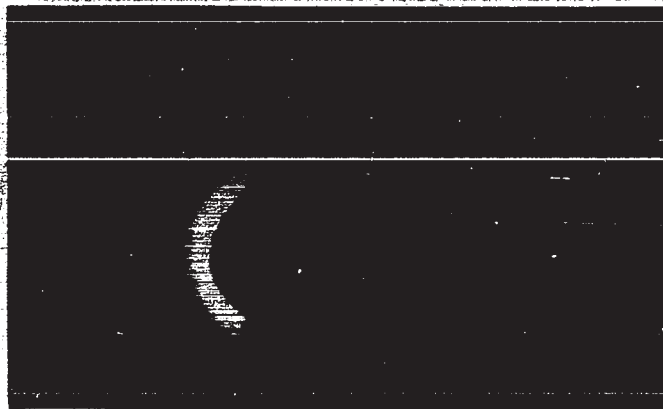
magnetic field
out of paper

zero magnetic
field

FIG. 3-5h   HIGH SPEED PHOTOGRAPHS
(taken 20 microseconds after firing of plasma gun)
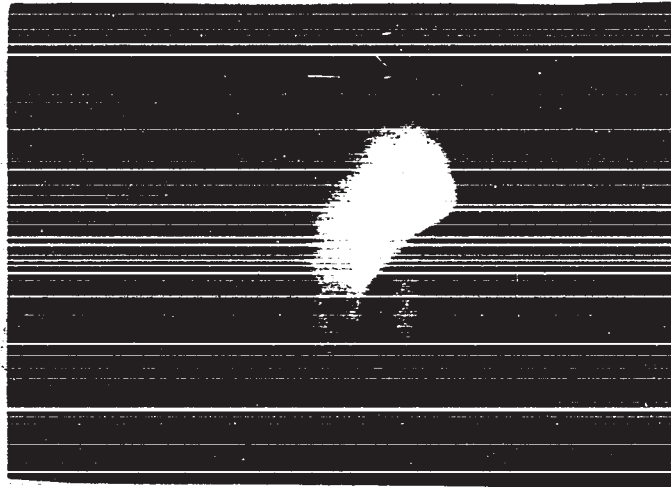
magnetic field
into paper

direction
of
plasma
flow
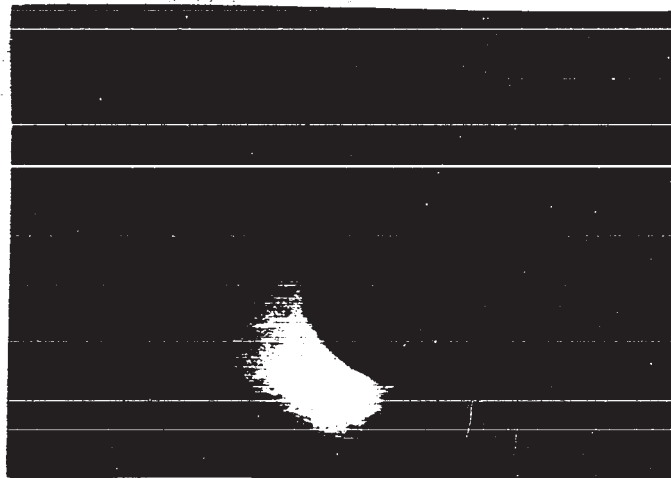
magnetic field
out of paper

zero magnetic
field

FIG. 3-5: HIGH SPEED PHOTOGRAPHS

(taken 35 microseconds after firing of plasma gun)
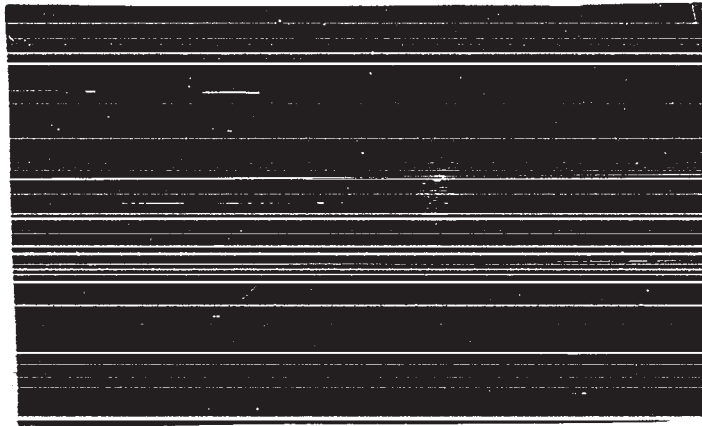
magnetic field
into paper

direction
of
→
plasma
flow
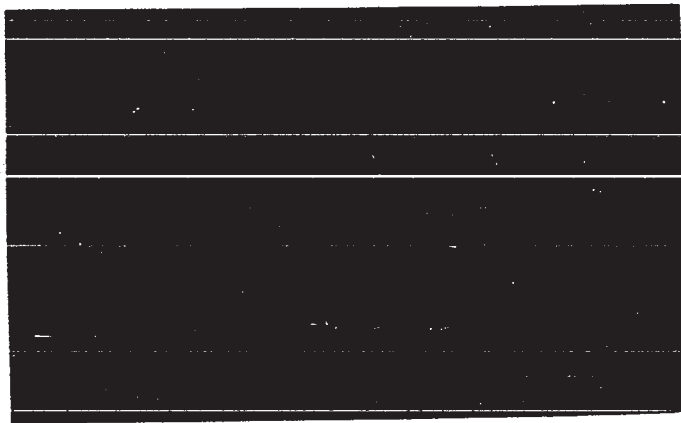
magnetic field
out of paper

zero magnetic
field

FIG. 3-5k   HIGH SPEED PHOTOGRAPHS
(taken 45 microseconds after firing of plasma gun)

CHAPTER 4

THEORETICAL ANALYSIS

It was noted with interest that, although the interaction parameters were subject to inestimable variation from shot to shot, nevertheless, the gross characteristics of the magnetic field-dependent asymmetry remained, even though the magnetic perturbation records were compiled over a series of 120 shots. Ordinarily, the solution of theoretical problems in plasma physics, either analytically or numerically, requires the simplification of the relevant equations to such a degree that interesting second-order effects are absent from the solution - for example, in the problem of magnetoaerodynamic flow past an airfoil, details of the distortion of the magnetic field are lost under the assumption of low plasma electrical conductivity (Hughes & Young, page 532).

In the problem under study, the apparent insensitivity of the asymmetry effect to gun non-reproducibility as well as the two-dimensional nature of the problem encouraged the author to view the asymmetric interaction as a first-order effect which would survive considerable simplification introduced into any proposed model.

4-1 FIELD APPROXIMATION

For use in theoretical calculations, it was necessary to obtain an analytical expression relating magnetic field variation with radial displacement from the solenoid. Previous computer calculations had shown this relationship to be of the form shown in figure 4-1a – a curve which conveniently bore a superficial resemblance to the black body radiation law of Planck. Using the analytical form of Planck's law,

$$B = \frac{A_1}{r^5 (e^{A_2/r} - 1)}$$

where B = magnetic induction per unit current

r = radial distance from solenoid

$A_1 = 5.32 \times 10^{-8}$ webers-meter^3

$A_2 = 0.3972$ meters

a curve fitting was carried out to determine the constants A_1, A_2 and the quality of the fit as shown in figure 4-1a was found to be satisfactory over the region of interest.

4-2 MAGNETOHYDRODYNAMIC MODEL

A magnetohydrodynamic model of the interaction was first considered and it became immediately obvious that this model would be inapplicable to the problem being studied. This fact is easily demonstrated from an examination of the

x Computer
  Calculation

$$- B = \frac{A_1}{r^5(e^{A_2/r} - 1)}$$

AXIAL MAGNETIC FIELD PER UNIT CURRENT
(webers/m.² - ampere x 10⁻⁴)

RADIAL DISPLACEMENT FROM CENTRE OF COIL (cm)
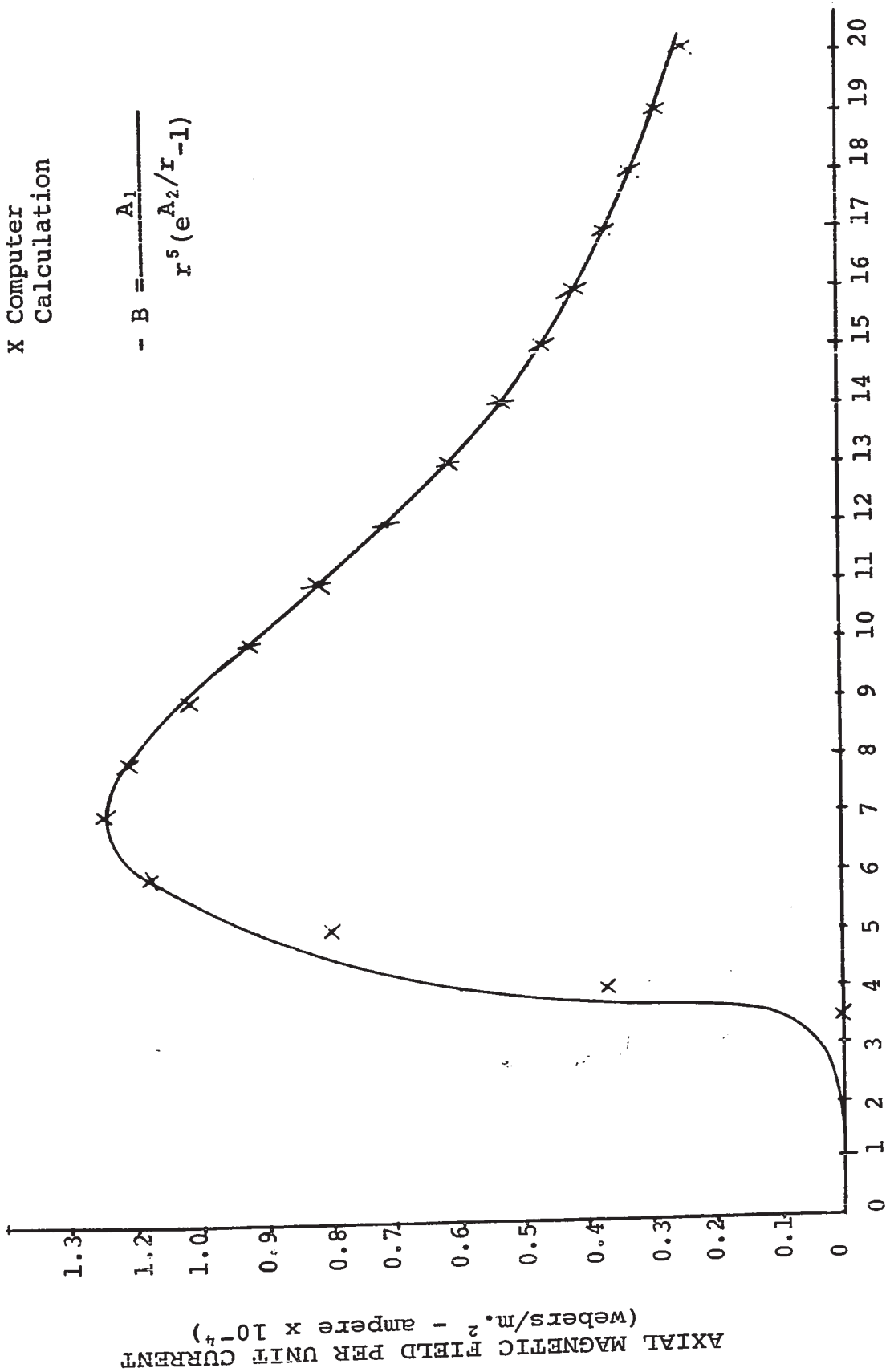
FIG. 4-1a RESULTS OF CURVE FITTING

MHD equations 4-2a and 4-2b which express the relationship between velocity and magnetic field.

$$\frac{\partial \overline{B}}{\partial t} = \nabla \times (\overline{v} \times \overline{B}) + \eta \, \nabla^2 \overline{B} \tag{4-2a}$$

$$\rho[\frac{\partial \overline{v}}{\partial t} + (\overline{v} \cdot \overline{\nabla})\overline{v}] = -\nabla P - \rho \nabla \psi + \rho \nu \nabla^2 \overline{v} + (\xi + \frac{\nu \rho}{3}) \, \nabla(\nabla \cdot \overline{v})$$

$$+ \mu_0 (\overline{H} \cdot \nabla)\overline{H} - \mu_0 \nabla(H^2/2) \tag{4-2b}$$

where

$\eta \;\; = \dfrac{1}{\sigma \mu_0}$

 = magnetic diffusivity

$\sigma \;\;$ = electrical conductivity

μ_0 = magnetic permeability

$\rho \;\;$ = fluid density

$P \;\;$ = ordinary mechanical pressure (no electromagnetic terms)

$\psi \;\;$ = gravitational potential

$\nu \;\;$ = kinematic viscosity

$\xi \;\;$ = second coefficient of viscosity

$H \;\;$ = magnetic field

Since the magnetic field appears linearly on both sides of equation 4-2a and quadratically in equation 4-2b, the solution of these equations for plasma velocity will be unaffected by a reversal of magnetic field - i.e. $B \to -B$.

The reason for the failure of this model is apparently

the fact that the equations represent the behaviour of a
fluid continuum, implying short mean free paths, high
particle densities and high particle collision rates.
These characteristics were not properties of the interaction
being studied and hence a new model was sought.

4-3   SINGLE PARTICLE MODEL

With the failure of the MHD model, a model of the
opposite extreme was examined. The incoming plasma was
pictured as an assemblage of ions and electrons of
sufficiently low particle densities that their trajectories
were essentially those of free particles. It was obvious
that such a model could not, a priori, explain the existence
of a magnetic boundary; however, it was considered to be of
interest to examine the trajectories and estimate the
distribution of light which would result from the
recombination of ions and electrons impinging on the solenoid
from these paths. The magnetic boundary was represented by
an infinitesimally thin surface across which the particles
experienced a discontinuity in magnetic field and streaming
velocity.

The familiar equations of motion in polar coordinates
(r,θ) are;

$$m (\ddot{r} - r\dot{\theta}^2) = - eBr\dot{\theta} \tag{1}$$

$$m (r\ddot{\theta} + 2\dot{r}\dot{\theta}) = (m/r)\,d/dt(r^2\dot{\theta}) = eB\dot{r} \tag{2}$$

where e = electronic charge

m = mass of particle

B = magnetic induction

and $\dot{x}$ represents differentiation of x with respect to time. The coordinate system used is defined below and the M.K.S. system of units is used throughout.
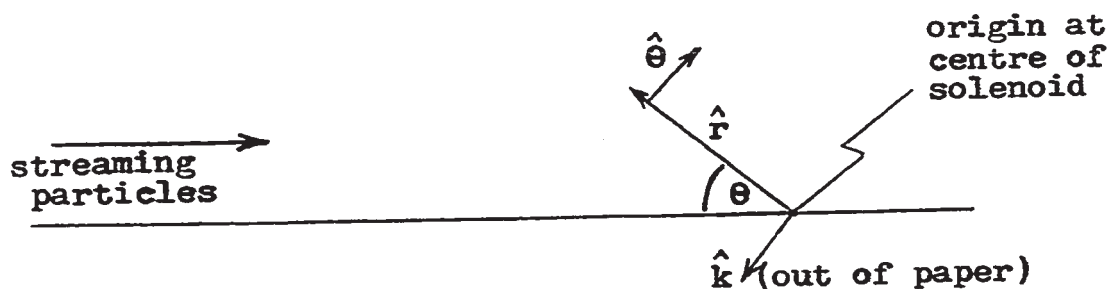
From (2),

$$r^2 \dot{\theta} = \frac{e}{m} \int Brdr$$

Inserting the analytic representation of B (with the approximation $\exp(A_2/r) - 1 \sim \exp(A_2/r)$) from section 4-1 and making the change of variable $u = A_2/r$, we obtain

$$r^2 \dot{\theta} = C \{\exp(-u)\}\{u^2 + 2u + 2\} + D \qquad (3)$$

where

$$C = \frac{eIA_1}{m \, A_2^3}$$

I = solenoid current

A_1, A_2 are the curve-shaping constants of section 4-1

and D is the integration constant which can be evaluated at the position of the particle on the magnetic boundary (discontinuity).

Equation (3) can be rewritten

$$\dot{\theta} = \frac{C}{A_2^2} \{exp(-u)\}\{u^4 + 2u^3 + 2u^2\} + \frac{Du^2}{A_2^2} \qquad (4)$$

and using the expression for $\dot{\theta}$ derived in Appendix E, the variable, time, is eliminated and the differential equation of the trajectories is found to be,

$$\frac{d^2u}{d\theta^2} - \frac{u^2}{\beta} \left(\frac{du}{d\theta}\right)^2 + \frac{u}{\beta} (\beta - u^3) = 0 \qquad (5)$$

where

$$\beta = u^2 + 2u + 2 + \frac{D\ exp(u)}{C}$$

Now let $du/d\theta = p$, then $dp/d\theta = d^2u/d\theta^2 = p(dp/du)$ and if $p = yu$, it follows

$$\frac{-y\ dy}{(y^2 + 1)} = (\frac{1}{u} - \frac{u^2}{\beta})du = (\frac{\beta - u^3}{\beta u})du$$

or

$$- \frac{1}{2} ln(y^2 + 1) = \int (\frac{\beta - u^3}{\beta u})du \qquad (6)$$

Let $\beta u = \rho$, then $d\rho = \beta du + ud\beta$ and since $d\beta = \beta - u^2$,

Then

$$\int \left(\frac{\beta - u^3}{\beta u}\right) du = \int \frac{\beta du}{\rho} - \int \frac{u^2 du}{\beta} = \int \frac{d\rho}{\rho} - \int \frac{(u d\beta + u^3) du}{\rho}$$

$$= \int \frac{d\rho}{\rho} - \int \frac{(u\beta - u^3 + u^3) du}{\beta u} = \int \frac{d\rho}{\rho} - \int du$$

and $\ln \left(\frac{1}{\sqrt{y^2 + 1}}\right) = \ln\rho - u + \ln\alpha$

where α is another constant of integration.

Rearranging, we obtain the final integral

$$\theta - \theta_0 = \int_{\theta_0}^{\Theta} d\theta = \alpha \int_{u_0}^{u} \frac{\beta \, du}{\sqrt{\exp(2u) - \alpha^2 \beta^2 u^2}}$$

where θ_0 and u_0 are the values of θ and u on the magnetic discontinuity.

A programme for the solution of this integral was written and run on an I.B.M. 7040 computer giving the numerical solution for various trajectories depending on the initial position and velocity of the particle. Typical trajectories for ions are displayed in figure 4-3a. Such trajectories were plotted for a variety of representative streaming velocities between two extreme end values - a streaming velocity so small that the particles were turned back before reaching the solenoid and a streaming velocity so large that the particles were essentially unaffected

Incident Velocity
= 2 x 10³m/sec.

B - out of paper
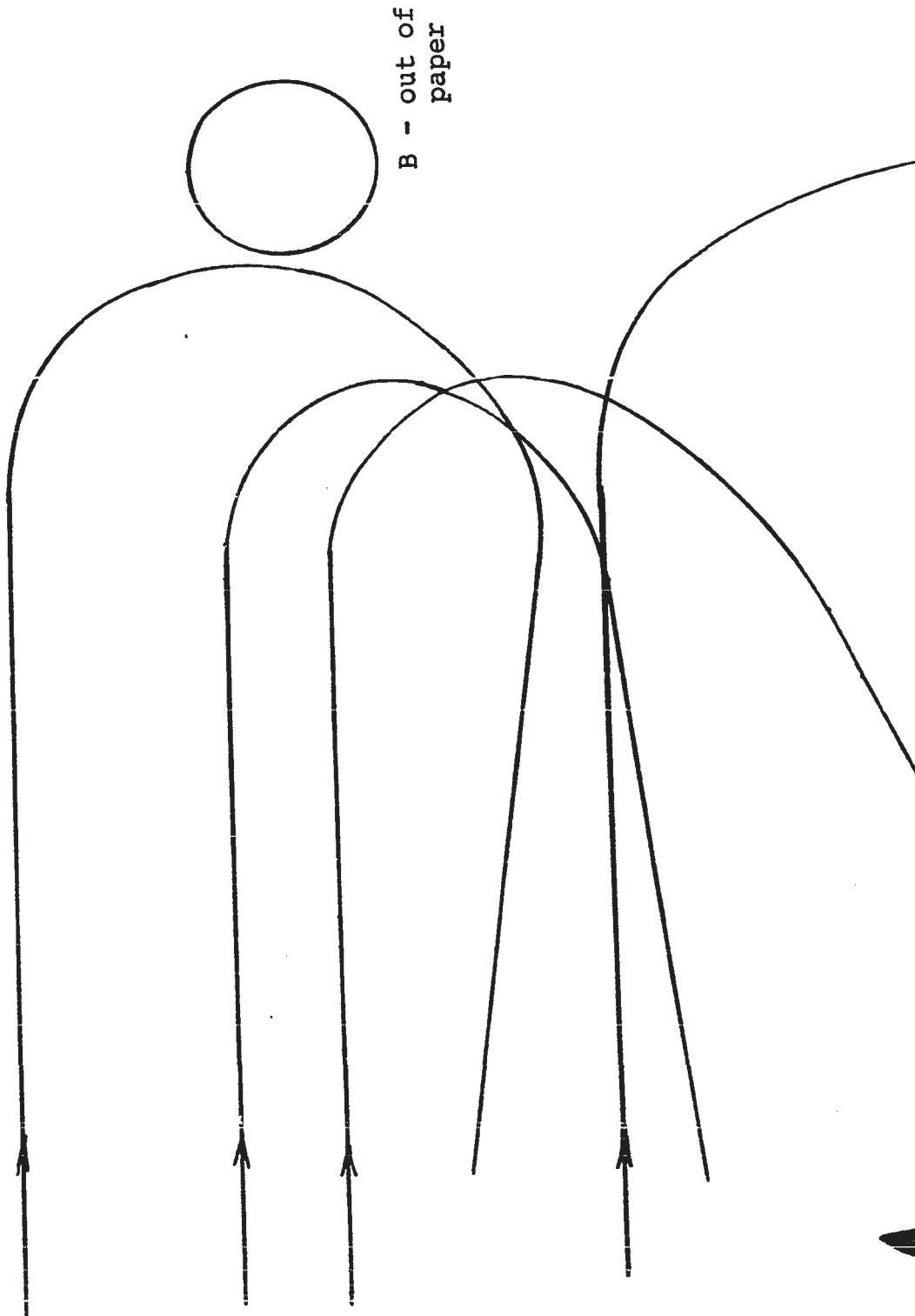
FIG. 4-3a TYPICAL PARTICLE TRAJECTORIES (½ FULL SIZE)
CALCULATED FROM SINGLE PARTICLE MODEL

by the magnetic field and simply continued in a straight line. For no value of streaming velocity did the collision points of the trajectories with the solenoid concur with the distribution of light recorded in the high-speed photographs. Clearly then, even the superposition of trajectories for various streaming velocities (simulating the effect of a velocity distribution) would not explain the photographic results.

These difficulties, in conjunction with the afore-mentioned neglect of the mechanism of establishing the magnetic boundary, showed that the independent particle model was inappropriate for this problem and that the proper model would be one in which the particles did show a collective behaviour (so that they could distort the magnetic field through the formation of currents) and yet would be quasi-free (so that their motion would be asymmetric under the influence of a magnetic field).

4-4 SELF-CONSISTENT FIELD APPROACH

The properties mentioned above are characteristic of the self-consistent field method used successfully by Beard (1960) to determine the shape of the magnetosphere on the sunlit side of the earth. From this method, the following model was proposed as representing the interaction studied in this experiment (see figure 4-4a).

Plasma Stream

(Magnetic Field → 0)

Ion Trajectory

ψ ψ

z(out of paper)

x

y

Solenoid

Boundary
(Rosenbluth Model)
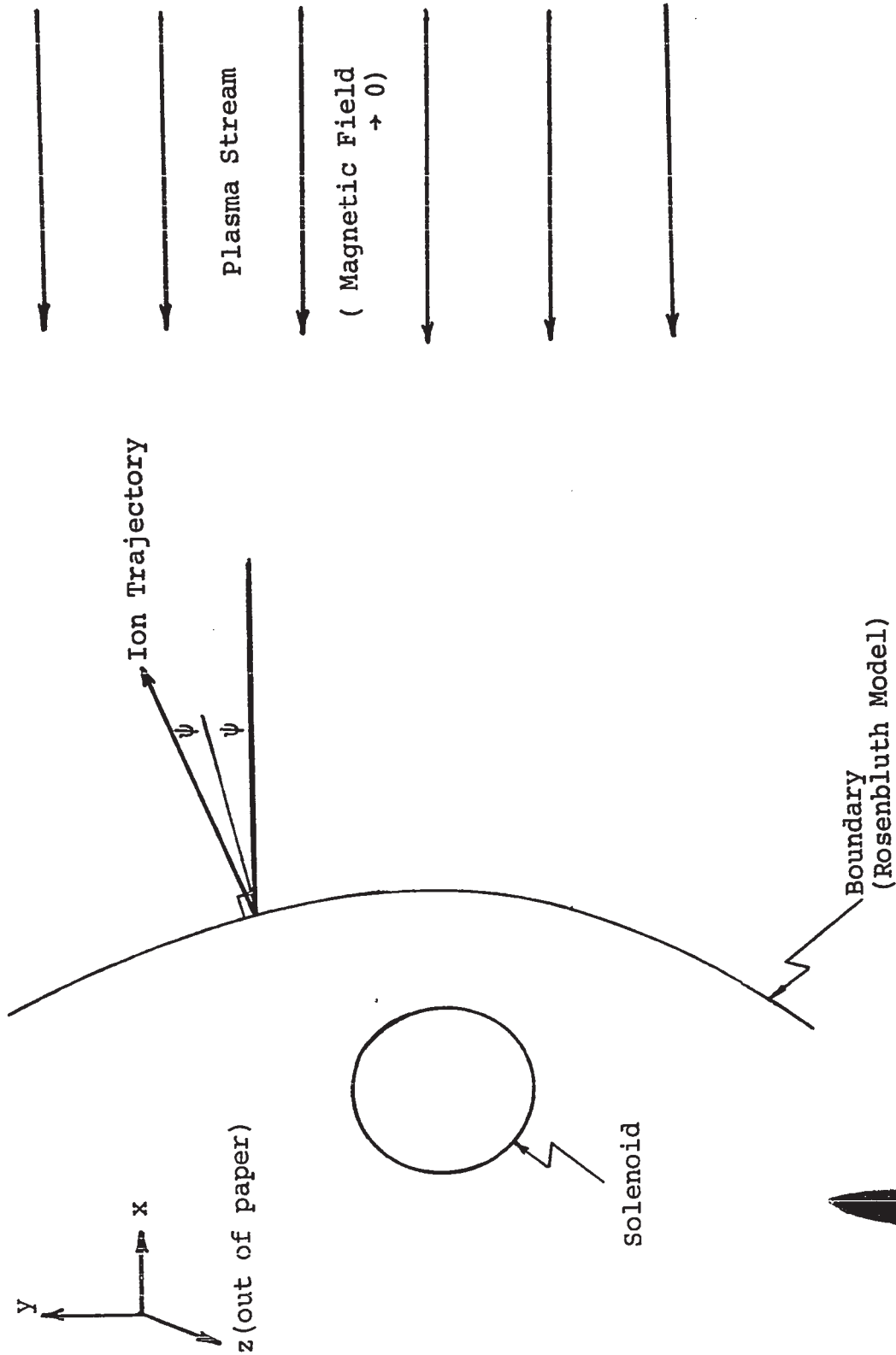
FIG. 4-4a PROPOSED MODEL OF INTERACTION

A plasma stream of infinite extent in the y direction but of finite width in the z direction streams in the -x direction towards a solenoid whose axis and magnetic field are in the z direction (over the volume encountered by the plasma stream). Because of the diamagnetic behaviour of the plasma, surface currents are induced which minimize the magnetic field inside the plasma and increase it outside the plasma surface. These currents are contained in a transition area through which the magnetic field decreases to 1/e of its free space value and the model adopted for this transition area is the boundary layer described by Rosenbluth (1954) and Shkarofsky and Johnston (1961).

If specular reflection of the particles from the boundary is assumed, an expression for particle pressure exerted on the boundary is easily obtained. A particle of mass m and velocity v, during reflection, experiences a total change in momentum equal to $2mv \cos \psi$, (see figure 4-4a). The number of particles impinging on the boundary per unit time per unit area is $Nv \cos \psi$ where N is the plasma particle density. Therefore, the total pressure perpendicular to the surface is $2mNv^2 \cos^2 \psi$ and on the boundary, this must be balanced by the opposing magnetic field pressure $B^2/2\mu_0$ where B is the total magnetic induction on the surface and μ_0 = the magnetic permeability of free space. Hence, the shape of the surface of the boundary layer is defined by the equation

$$B = \sqrt{4 \; \mu_0 mN \; v^2 \; \cos^2\psi}$$

$$= 2\sqrt{\mu_0 mN} \; v \; \cos\psi \qquad\qquad (7)$$

Let the surface be represented by the function $F(r,\theta)$ = a constant. We can, without loss of generality, write

$$F(r,\theta) = r - R(\theta) = 0$$

The unit normal to the surface is defined by

$$\hat{n} = \text{grad } F/|\text{grad } F| = \gamma \; \{\hat{r} - \hat{\theta} \; \frac{1}{r} \; \frac{dR}{d\theta}\}$$

where $\hat{r}$, $\hat{\theta}$ are the unit vectors in a polar coordinate system defined below, and γ is a normalization constant.

$$\gamma = [1 + \frac{1}{r^2} \; (\frac{dR}{d\theta})^2]^{-\frac{1}{2}}$$

$\hat{k}$ = unit vector out of paper

origin at centre of solenoid
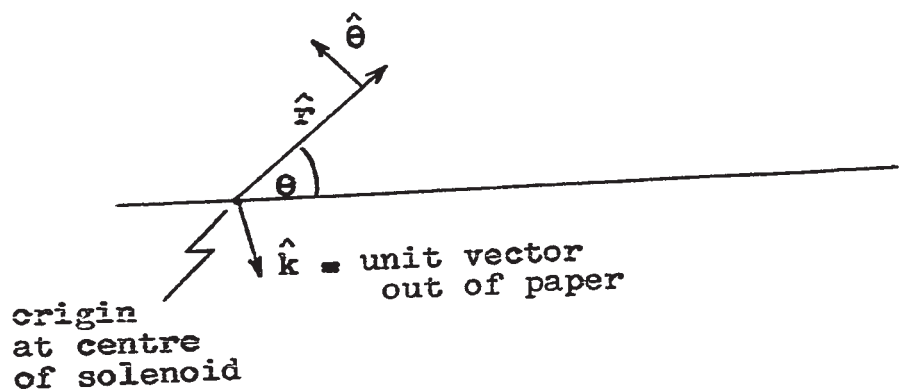
The unit **vector in** the direction of the streaming velocity is

$$\hat{v} = -\cos\theta\ \hat{r} + \sin\theta\ \hat{\theta}$$

Then, $|\cos\psi| = |\hat{n}.\hat{v}| = \gamma\{\cos\theta + \frac{\sin\theta}{r}\frac{dR}{d\theta}\}$ \hfill (8)

Substituting equation 8 into equation 7, squaring and rearranging, we obtain the differential equation describing the surface.

$$\frac{dR}{d\theta} = r\ \{\frac{\mu_0 p_0\ \sin 2\theta \pm B\ \sqrt{2\ \mu_0 p_0 - B^2}}{B^2 - 2\ \mu_0 p_0\ \sin^2\theta}\}\qquad * \qquad (9)$$

where $p_0 = 2mNv^2 = $ the kinetic energy density of the plasma

Since the value of B on the surface is not known, no further progress is possible without making an assumption. Following the method of Beard, a reasonable value for the magnetic field on the boundary was assumed and the resulting differential equation was solved numerically on the I.B.M. 7040 computer using a programme based on the Runge-Kutta method. Several other independent numerical methods such as Newton's method and Euler's method were used to compare and check the results. The boundary based on these calculations is shown in figure 4-4b.

The approximation of the magnetic field on which this solution is based is the consideration that the boundary is of negligible thickness when compared with the radius of curvature of the boundary. Then, the surface is essentially

* The minus sign is used for positive θ and the positive sign is used for negative θ.

70

Second Order Solution

First Order Solution
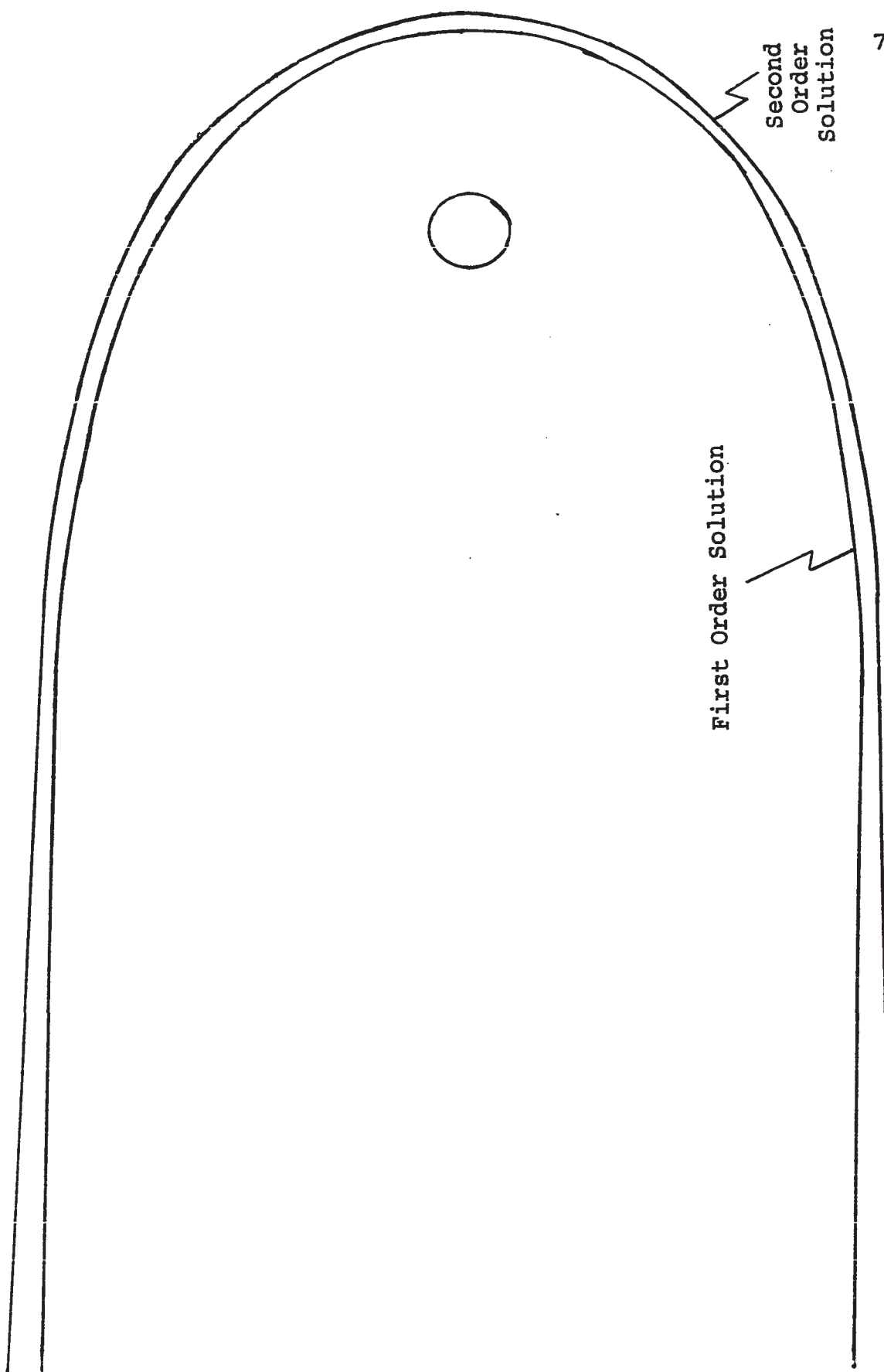
FIG. 4-4b BOUNDARIES CALCULATED FROM SELF-CONSISTENT FIELD APPROACH (¼ FULL SIZE)

a plane as far as the region surrounding a particular
point is concerned. In the case of a plane surface
separating a magnetic field region from a zero-field region,
the surface currents flowing in the plane induce equal but
opposite fields on opposite sides of the plane. Hence,
with the field zero on one side of the plane, the field
on the other side will be twice its undisturbed value.
Therefore, the approximate value of B used was double
the analytical expression for B described in section 4-1.

Having obtained a first-order solution based on the
above assumption, a second-order solution may be obtained
by improving the primary assumption concerning the magnetic
field on the surface. This improvement requires the addition
of a correction to the boundary magnetic field due to the
currents flowing in the curved boundary (which was assumed
to be planar in the first-order calculations). The value
of the correction field is given by the integral form of
the Biot-Savart law (see Jackson's "Classical Electromagnetism",
page 137, eqn. 5.14).

$$\bar{B}_C(\hat{r}_0) = \frac{\mu_0}{4\pi} \int \frac{\hat{J}(\hat{R}) \times (\hat{r}_0 - \hat{R}) \, dV}{|\hat{r}_0 - \hat{R}|^3}$$

where $\hat{r}_0$ is the radius vector to the point at which the
correction field is being evaluated, $\hat{R}$ is the radius vector
to a current element which is contributing to the field at

$\hat{r}$, and dV is the element of volume.

Expressing this integral in cylindrical polar coordinates and the current density as a Dirac delta function (since in this model, $\hat{J}$ exists only on the infinitesimally thin boundary), we obtain

$$\bar{B}_c(\hat{r}_0) = \frac{\mu_0}{4\pi} \iiint_{z\theta r} \frac{\{\hat{J}(\hat{R}) \times (\hat{r}_0 - \hat{R})\} \, R \, d\theta \, dR \, dz \, \delta(\hat{R} - \hat{R}_b)}{|\hat{r}_0 - \hat{R}|^3}$$

Where $\hat{R}_b$ is the radial vector describing the boundary,

$$= \frac{\mu_0}{4\pi} \iint_{z\theta} \frac{\{\hat{I}(\hat{R}) \times (\hat{r}_0 - \hat{R})\} \, R \, d\theta \, dz}{|\hat{r}_0 - \hat{R}|^3} \tag{10}$$

where integration has been performed over the variable R and hence, $\hat{R}$ is now exclusively on the boundary and is a function of θ only.

$\hat{I}(\hat{R})$ represents the surface current (in units of amps/ meter) and is evaluated using the well-known boundary condition (Jackson, page 236, eqn. 8.2)

$$\hat{I}(\hat{R}) = (B/\mu_0)(\hat{k} \times \hat{n}) \qquad \text{(using eqn.7)}$$

$$= \left(\frac{2p_0}{\mu_0}\right)^{\frac{1}{2}} (\hat{n}\cdot\hat{v})(\hat{k} \times \hat{n}) \tag{11}$$

where $\hat{n}$ and $\hat{k}$ are the unit vectors defined previously and B is the total magnitude of the magnetic field on the

boundary.

By expressing the vectors in their component forms, carrying out the vector operations and then simplifying the expressions (see details in Appendix F), we finally obtain from equation 10,

$$\hat{B}_c(\hat{r}_0)$$

$$= \frac{1}{2\pi} \left(\frac{p_0\mu_0}{2}\right)^{\frac{1}{2}} \hat{k} \iint_{\theta z} \frac{F(R)\ R\ d\theta\ dz}{[1+\frac{1}{R^2}(\frac{dR}{d\theta})^2][r_0{}^2+R^2-2Rr_0\cos(\theta_0-\theta)+z^2]^{3/2}} \qquad (12)$$

where $F(R) = \left(\frac{dR}{d\theta}\right)^2 \{\frac{r_0}{R^2} \sin(\theta - \theta_0)\ \sin\theta\}$

$$- \frac{dR}{d\theta} \{\sin\theta + \frac{r_0}{R} \sin(\theta_0 - 2\theta)\}$$

$$+ \cos\theta \{r_0 \cos(\theta_0 - \theta) - R\}$$

where r_0 and R are the magnitudes of $\hat{r}_0$ and $\hat{R}$ respectively and θ_0 and θ are the angles corresponding to $\hat{r}_0$ and $\hat{R}$ respectively (both variables are on the boundary).

Since the plasma stream is only of finite extent in the z direction and the z coordinate is independent of R and θ, equation 12 may be integrated over z (from -L to L, say) to give

$$\bar{B}_c(\hat{r}_0) = \frac{\hat{k}}{\pi} \left(\frac{p_0\mu_0}{2}\right)^{\frac{1}{2}} \int_\theta \frac{F(R)\ R\ d\theta}{[1+\frac{1}{R^2}(\frac{dR}{d\theta})^2][f(R)][1+f(R)/L^2]^{\frac{1}{2}}} \qquad (13)$$

where

$$f(R) = r_0^2 + R^2 - 2Rr_0 \cos(\theta_0 - \theta)$$

Prior to attempting a numerical evaluation of this integral, it was noted that an apparent singularity existed for the case where $R \rightarrow r_0$ and $\theta \rightarrow \theta_0$, that is, the contribution to the magnetic field correction from the current element immediately adjacent to the point at which the field was being calculated assumed the indeterminate form $0/0$. Further examination revealed that this element did indeed have a finite contribution and details of this examination are discussed in Appendix G.

Considering a plasma stream width of 4 cm. (i.e. 2L), equation 13 was evaluated using several numerical integration methods as accuracy checks and the results are shown in figure 4-4c. As expected, the variation of B_c was symmetric about $\theta_0 = 0$, but the results also showed that B_c experienced a local "ripple" in the neighbourhood of $\theta_0 = 0$. This was an unexpected result and, considering the magnitude of the amplitude of the ripple (about 1%), was temporarily ignored in subsequent calculations. When this correction field is added to the original approximation field, the second order surface shown in figure 4-4b was calculated and equation 13 was again evaluated. The results were similar to figure 4-4c and again showed the local field increase-decrease nature at $\theta_0 = 0$. Ignoring the anomaly once again, a third-
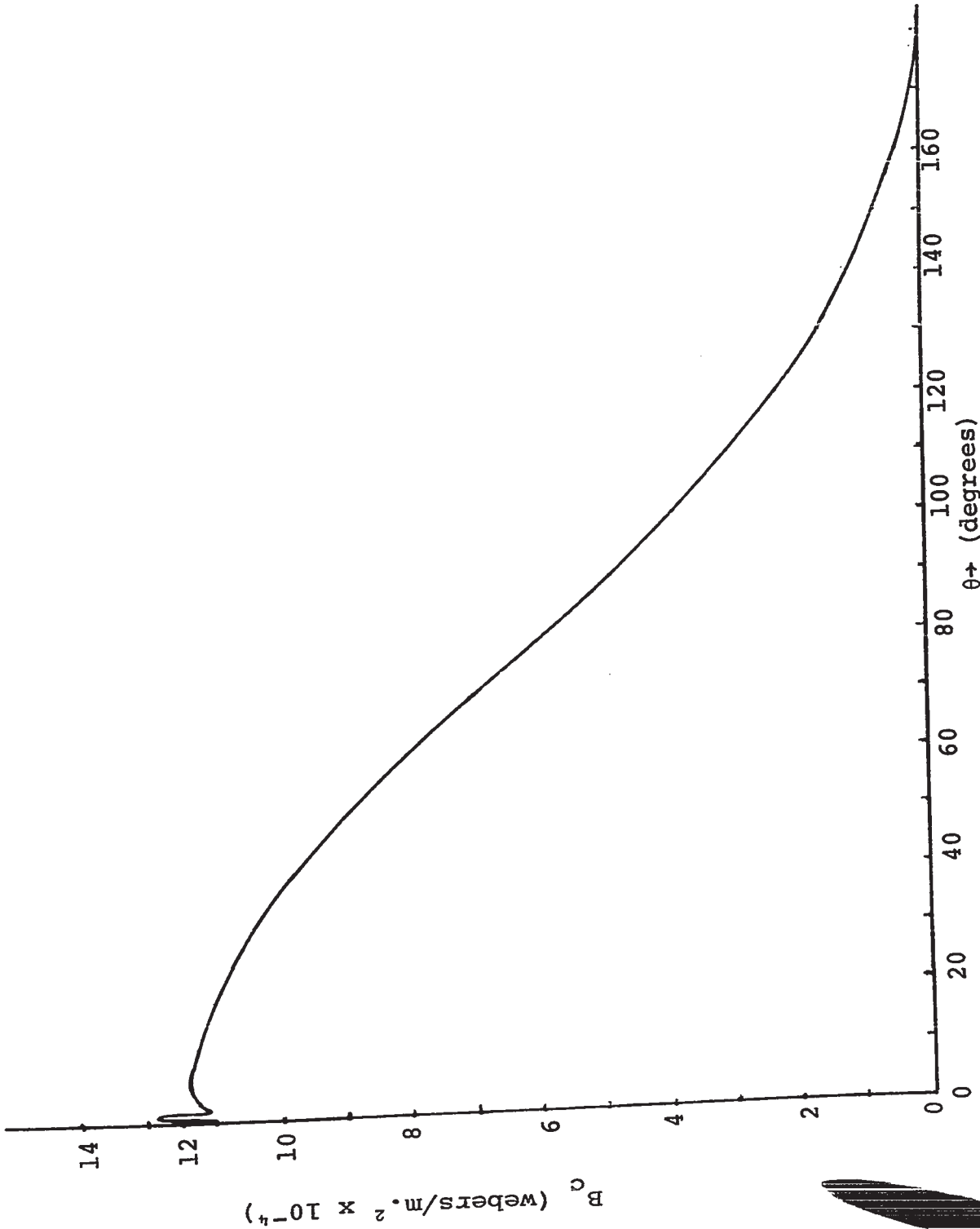
FIG. 4-4c CORRECTION FIELD CALCULATED FROM FIRST-ORDER SURFACE

order surface was found for which eqn. 13 also displayed
a correction magnetic field with a local ripple at $\theta = 0$.
Subsequent calculations of a fourth-order surface showed
no significant improvement over the third-order surface
and the solution was considered complete.

CHAPTER 5

DISCUSSION

5-1 EXPERIMENTAL DISCUSSION

In the determination of streaming velocity, the double probes were used essentially as conductivity probes and thus problems with electrode contaminants which often affect the shape of current-voltage characteristics were avoided. The velocity measurements are therefore considered to be reliable to within 25%. This uncertainty arises primarily from the non-reproducible operation of the plasma gun and to a lesser extent from recombination of the plasma stream causing a changing conductivity as it flows between the two probes.

The magnetic probe results show surprisingly good reproducibility in that the magnetic asymmetry was recorded over an experimental run of 120 gun firings. For the probe used in this experiment, the response time was found to be 5 microseconds and hence the field perturbations of duration 30 - 40 microseconds were easily studied. Moreover, due to the small physical size of the probe, there was no significant perturbation of the plasma in the interaction region and the probe provided good spatial resolution. The magnetic probe results substantiate the choice of

model to represent the interaction by indicating "magnetic compression" on the boundary where the equation

$$\frac{B^2}{2\mu_0} = 2mNv^2 \cos^2 \psi \qquad \text{(eqn. 5-1)}$$

must be satisfied. This equation represents a pressure balance between the plasma kinetic pressure and the magnetic field energy density; however, the balance point in the median plane occurs at a radial distance of about 14 cm. rather than 8 cm. as anticipated in the original solenoid calculations. Although the unperturbed field has a substantial radial component at a radius of 14 cm. (see graph 2-3b), this component is reduced under the effects of magnetic compression by the streaming plasma while the axial component is more than doubled. In this experiment, the perturbed axial field at the boundary has a value of 8.3×10^{-3} webers/meter^2 while the maximum radial component (occurring at the edge of the stream) is less than its unperturbed value of 1.0×10^{-3} webers/meter^2. Hence the relative magnitudes of the two components are

$$\frac{B_r}{B_z} = \frac{1.0}{8.3} \rightarrow 12\%$$

which represents, even in the worst possible case, an essentially transverse magnetic field.

Furthermore, if we consider the plasma to be a medium

of high electrical conductivity, both magnetic and electric
fields tend to be excluded from its interior. Therefore,
at the plasma-magnetic field interface, across which the
normal component of the magnetic induction must be continuous,
we have a further indication that the radial component is
negligibly small. Now the total axial field at 14 cm. is
8.3×10^{-3} webers/meter^2 and the streaming velocity for a
plasma gun voltage of 7 kilovolts is 9.7×10^4 meters/sec.
(see graph 3-1a). Substitution in eqn. 5-1 using m = 63.5
a.m.u. for copper ions yields an electron density of about
1.4×10^{10} /cm^3 . This value is roughly two orders of magnitude
lower than the result obtained from the triple probe
measurements. Discrepancies of this size can only be
accounted for by the effects of probe contamination.
Examination of the epoxy-cement base in which the electrodes
were mounted showed signs of deterioration under the con-
tinuous bombardment of ions and electrons. A black deposit
(possibly oxidized epoxy or a copper oxide) was observed
between the electrodes and suggested the possibility of
current leakage. Under the bombardment of plasma particles,
this deposit could become conducting and provide a low-
impedance path between the electrodes, thus displaying an
apparent current much larger than the true current flowing
within the plasma itself. As can be seen from Appendix C,
this in turn, would indicate a larger than actual value of
electron density. Furthermore, using a Maxwellian energy

distribution in developing the probe theory, the electron current is given by

$$I_e = SJ_e \exp(-\phi V)$$

where S is the probe surface area, J_e is the electron saturation current density, $\bar{V}$ is the voltage on the probe and $\phi = \dfrac{e}{kT_e}$ with e = electronic charge, k = Boltzmann's constant, and T_e = electron temperature. Suppose now that an apparent current, I'_e, is measured which due to leakage, is larger than the actual value, I_e, — then the corresponding value of ϕ would be underestimated and since $\phi \propto 1/T_e$, the value of T_e deduced from these measurements would be greater than the actual value. In an attempt to minimize such effects, the probe was carefully cleaned before each experimental run but it was impossible to ensure that it remained so between successive shots. A less important error arises at low plasma densities where the ion saturation current is no longer independent of the probe voltage (see Appendix C). The effect of such an error is to indicate values of n_e and T_e which are about 25% greater than the actual values.

The time development of the magnetically-asymmetric plasma flow pattern is revealed very clearly in the magnetic probe results. Further evidence of this asymmetry is obtained from both the high-speed photographs and the time-integrated

colour photographs. A direct comparison between the high-speed photographs and the magnetic contour maps shows the presence of light near the solenoid in a position corresponding to that of the transient, asymmetric reduction of magnetic field. In both cases, the asymmetry is dependent on the field orientation. A similar asymmetry is indicated in the time-integrated colour photographs where the blue light adjacent to the solenoid extends outward into the region of reduced magnetic field. It therefore seems reasonable to attribute this light to the recombination of copper plasma ions and electrons, since ionized copper (and copper compounds such as CuO and CuH) have abundant spectral lines in the blue-violet wavelength range.

It is also evident from the colour photographs that the bulk of this blue light emanates from a symmetrical region adjacent to the solenoid. This suggests that some incident plasma flows symmetrically around the solenoid and is not noticeably affected by the direction of the magnetic field. This is presumed to be the fast-moving component of the incident stream with velocities (greater than 10^5 meters/sec.) sufficient to penetrate the magnetic field. The magnetic boundary formed at a radius of 14 cm. is therefore not a total particle boundary. Since this plasma is not deflected by the field, its flow does not take part in the compression mechanism or subsequent distortion of the magnetic field.

The red light prominent in the time-integrated photographs was examined using an f 1.8 diffraction grating spectrograph and type 103AF spectrographic film and was identified as the H_α line (6563 Å) of atomic hydrogen. This apparently is present as a background gas originating from the dissociation of water vapour and possibly diffusion pump oil. The red light is not observed in the high speed and time-integrated black and white photographs since Polaroid film is sensitive to the blue portion of the spectrum rather than the red. Hence, these photographs presumably indicate the presence of ionized copper plasma. The time-integrated photographs show evidence of a partial particle boundary and an overall asymmetry in the plasma flow around the solenoid. Details of the asymmetry are not clear since the black and white film has poor colour sensitivity.

5-2 THEORETICAL DISCUSSION

a) ROSENBLUTH MODEL OF BOUNDARY

Rosenbluth (1954) first described the boundary between a plasma and a magnetic field in terms of a charge separation layer. The electrons and ions entering the magnetic field region are forced to gyrate. The heavier ions normally have a much larger gyro-radius than the electrons and are therefore carried farther into the magnetic field. This enforced charge separation gives rise to an electric field perpendicular to the boundary which tends to accelerate

and decelerate incoming electrons and ions respectively.
The actual gyro-radius of the ions is therefore substantially
reduced while the electrons experience a large lateral
displacement as they traverse the boundary. Typical
trajectories are illustrated in figure 5-1 for plasma
flow both normal and oblique to the boundary surface.

For an ion entering the boundary, the lateral
displacement of the ion (as it is decelerated and turned
around by the electric field in the boundary) is given by

$$y_i = 2\sqrt{2} \; (m/M) \; (c/\omega_\rho) \qquad \text{(Shkarofsky \& Johnston, 1961)}$$

where

m = electronic mass

M = ionic mass

c = speed of light

ω_ρ = plasma frequency = $(\frac{Ne^2}{\varepsilon_0 m})^{\frac{1}{2}}$

N = particle density

ε_0 = permittivity of free space

which in this experiment yields

$$y_i = 0.5 \text{ mm.}$$

Hence, on the scale of the interaction region, the ions
are specularly reflected at the boundary and the pressure
balance equation (5-1) is applicable.

For an electron entering the boundary, the lateral
displacement of the electron is given by

$$y_e = M/m \; (y_i) \qquad \text{(Shkarofsky \& Johnston, 1961)}$$
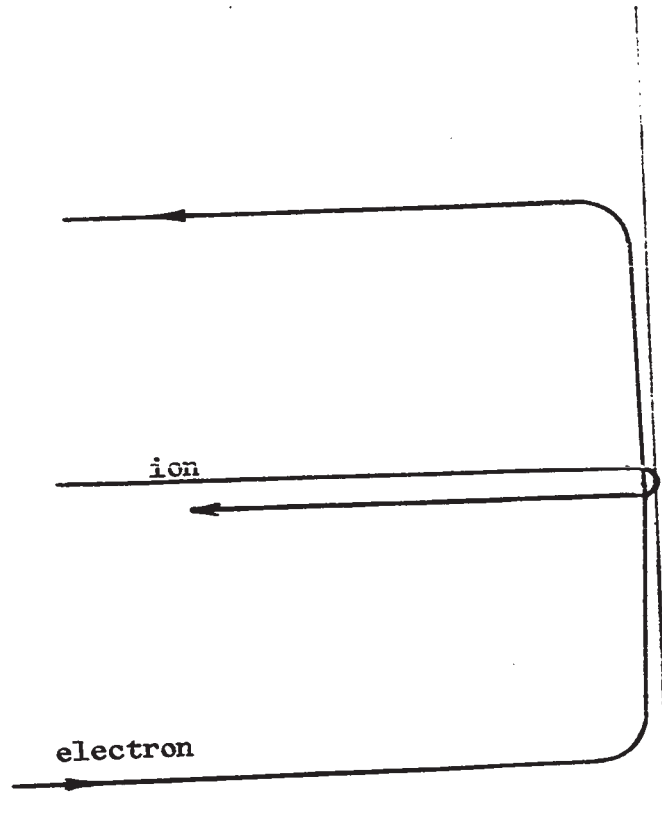
PERPENDICULAR FLOW
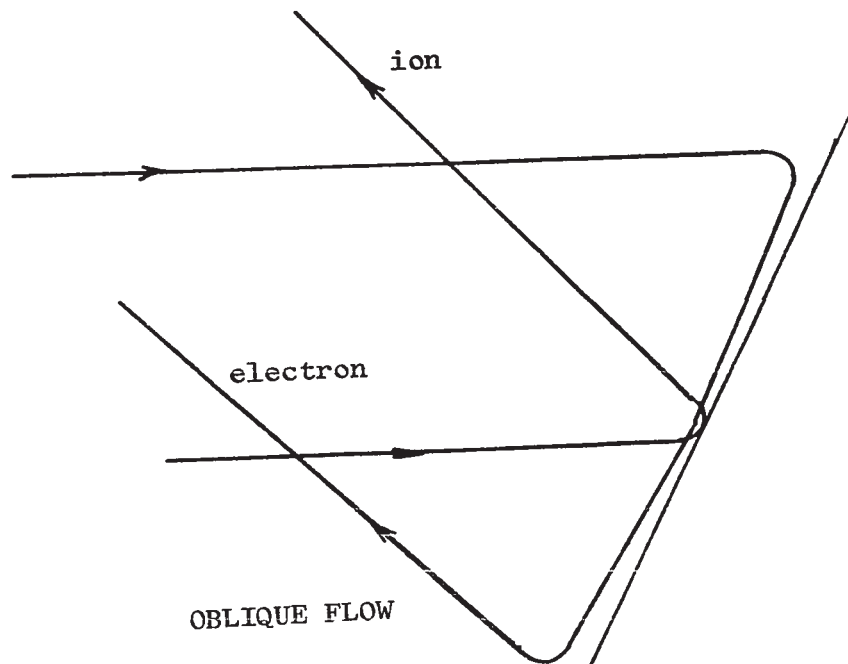
OBLIQUE FLOW

FIG. 5-1 ION AND ELECTRON TRAJECTORIES INSIDE
THE ROSENBLUTH SHEATH

$$= 45 \text{ metres,}$$

and the time spent in boundary is given by

$$10(c/v\omega_p) \qquad \qquad \text{(Shkarofsky \& Johnston, 1961)}$$

$$= 20 \text{ microseconds}$$

where v is the streaming velocity

Since the duration of the interaction is 50 - 60 microseconds, the electrons clearly have sufficient time to establish the boundary conditions and are indeed responsible for current flow within the boundary.

The Debye length is given by

$$\lambda_D = (\frac{\varepsilon_0 kT_e}{Ne^2})^{\frac{1}{2}} \qquad \text{(Kucherawy, 1966)}$$

where

ε_0 = permittivity of free space

k = Boltzmann's constant

In this experiment, λ_D has a value of 0.11 mm. (assuming $T_e \sim 30,000^\circ K$). The number of particles contained in a sphere of radius equal to the Debye length is

$$N_D = \frac{4}{3}\pi\lambda_D^3 N = 6 \times 10^4 \gg 1$$

The fact that the number of particles in the Debye sphere is much greater than unity verifies that collective behaviour will be in evidence and single particle analysis is inappropriate.

If the ions are singly-charged, the electron-ion collision frequency is given by

$$\left(\frac{2}{\pi}\right)^{\frac{1}{2}} \omega_\rho \frac{\ln\Lambda}{\Lambda} \qquad \text{where } \Lambda = 9N_D$$

(Spitzer)

$= 10^5$ collisions/sec.

$\cong$ 1 collision/ 10 microseconds.

Thus, over the time of interaction (50 - 60 microseconds), there are typically 5 electron-ion collisions and hence, the interaction is essentially collisionless.

In the Rosenbluth sheath model, the magnetic field decays exponentially into the body of the plasma as

$$B = B_0 \, e^{-x/\delta}$$

where B_0 is the boundary value of the field,

   x is the distance of penetration into the plasma,

and $\delta = \left(\frac{\varepsilon_0 mc^2}{2Ne^2}\right)^{\frac{1}{2}}$ is the e-folding width.

Magnetic probing of the boundary layer showed the magnetic profile to be exponentially decaying in good agreement with the Rosenbluth model with $\delta \sim 1.8$ cm. Using the above expression for δ, the electron density had a corresponding value of 4.3×10^{10}/cm^3. - a value which supported that calculated from the pressure balance equation 5-1, $(1.4 \times 10^{10}$/cm^3.).

b) <u>INSTABILITY</u>

As mentioned in Chapter 4, the magnetic correction field calculated from the first order surface showed a local variation in magnitude in the vicinity of $\theta = 0$ and this result recurred in the correction fields calculated from subsequent corrected surfaces even when the variations were ignored. Use of different numerical methods showed that the variation was not simply an accumulation of numerical error and hence, the problem was investigated analytically.

From section 4-4, we have the differential equation of the boundary expressed in polar coordinates,

$$\frac{dR}{d\theta} = r \left\{ \frac{\mu_0 p_0 \sin 2\theta - B\sqrt{2 \mu_0 p_0 - B^2}}{B^2 - 2\mu_0 p_0 \sin^2 \theta} \right\}$$

It follows that $\frac{dR}{d\theta} = 0$ for $\theta = 0$ (i.e. on the plasma gun-solenoid line) and also approaches zero for an angle given by

$$\theta_c = \pm \frac{1}{2} \sin^{-1} \left[\frac{B\sqrt{2\mu_0 p_0 - B^2}}{\mu_0 p_0} \right]$$

which has been calculated to be about $\frac{1}{2}$ degree. Hence, in the vicinity of $\theta = 0$, the surface has the approximate shape shown in the following figure, with the points on the boundary defined by θ_c and $-\theta_c$ having a local curvature greater than the surrounding points. As argued previously in connection with the calculation of
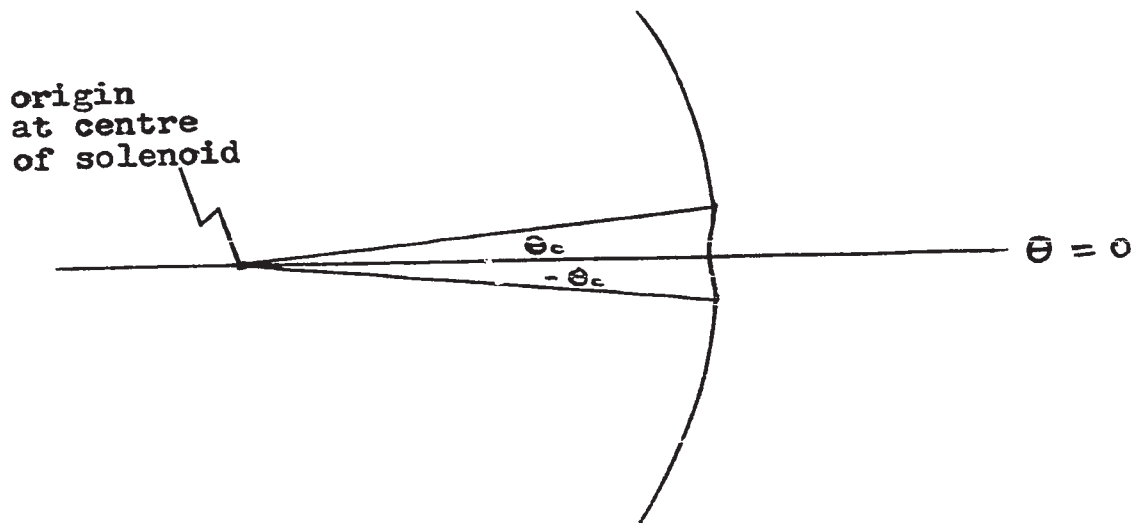
the correction field due to a curved surface, a current element which is curved induces a greater magnetic field in its interior than a corresponding planar (or less curved) element. Applying these considerations to the diagram, we would thus expect a correction field with a local minimum at $\theta_o = 0$ and two maxima at $\theta_o = \pm\theta_c$ in agreement with the numerical results (see figure 4-4c).

If the first correction field with a local minimum at $\theta_o = 0$ is added to twice the solenoid field and used to calculate the second order boundary, this will clearly produce a "depression" in the boundary around $\theta = 0$ since the magnetic pressure will experience a local minimum at this point. This produces a situation analogous to the familiar "kink" type instability and any current flowing in the boundary around this depression will produce local magnetic fields which enlarge it and hence break up the surface. Thus, although the boundary can initially be

established, the resulting currents which flow in its surface cause it to become unstable and break up with the origin of the instability at $\theta = 0$.

With the break-up of the surface, the slower, late-arriving plasma is now able to enter the cavity at $\theta = 0$, and because of relatively lower particle densities and streaming velocities, the flow pattern is likely to be dominated by the ion trajectories within the magnetic field. More specifically, these trajectories will resemble those shown in figure 4-3a (as calculated for the single particle model) with approximations to allow for the retarding effects of the gyrating electrons. The plasma flow will therefore display a field-dependent asymmetry. Indeed, there is some evidence of striations at $\theta = 0$ and an asymmetric flow of plasma in the time-integrated photographs (see figure 3-5a,b). From simple cyclotron theory, the electron gyro-period is given by

$$T = \frac{2\pi m}{eB} = 4.5 \times 10^{-9} \text{ seconds under}$$

the conditions of this experiment.

The electrons, therefore, have ample time to gyrate and reduce the field locally (according to Lenz's Law) during the penetration. The plasma which will be most effective in producing this adiabatic behaviour is that associated with the late-arriving ions with velocities low enough

that they do not impinge on the solenoid. This presumably accounts for the time lag between the appearance of illumination on the solenoid (at 35 microseconds as recorded by the high-speed camera) and the appearance of the magnetic asymmetry (at 45 - 50 microseconds as recorded by the magnetic probe).

c) CONCLUSIONS

In this experiment, a low-density plasma stream was allowed to interact with an essentially transverse field, the geometry of which was simplified to allow meaningful analytic study. A magnetic boundary was established but it was inherently unstable and quickly broke up, thus allowing plasma to penetrate the field in a flow pattern which depended on the orientation of the transverse magnetic field. The experimental conditions were found to justify the use of a Rosenbluth sheath as a model for the interaction and calculations based on this model successfully predicted the shape and position of the boundary and the origin of its instability. Comparison of these results with those for a three-dimensional dipole magnetic field suggests that this instability is due to the geometry of the magnetic field - specifically, the lack of curvature in the axial direction. The self-consistent field approach including calculations of the correction field has been applied to the 3-dimensional problem of the magnetospheric surface yielding a stable, converging solution. In this work,

calculations to investigate the effect of extension of the plasma stream to infinite axial extent showed even this situation to be unstable and, hence it is evident that field curvature must be a critical factor.

d) SUGGESTIONS FOR FUTURE WORK

In view of the previous comments, a theoretical investigation of stability-curvature criteria as applicable to this problem would be a desirable sequel to the work presented in this thesis.

Much of the experimental work was plagued by the non-reproducible nature of the coaxial plasma gun and with the recent development of gas injection plasma guns (see for example, Gore (1969)), it is hoped that a more accurate study may be carried out on the boundary layer and the nature of the fields in its interior. The use of plasma ions of lighter mass such as helium will allow the establishment of a particle boundary as well as a magnetic boundary and will be a useful test of the proposed theory of asymmetry. It would be particularly interesting to study the boundary layer behind the solenoid where the angle of incidence of the plasma stream would be grazing and thermal effects would be important.

APPENDIX A

SOLENOID CALCULATIONS

The calculation of magnetic fields due to solenoidal
current distributions has been discussed by several authors
in various regions of applicability. For example, Smythe
has obtained an analytic solution for the internal axial
field of a solenoid while Brick and Snyder (1965) have
obtained series solutions for the median-plane field
exterior to a long, thin solenoid - a) near the surface
and b) at large radial distances from the solenoid.

For the purposes of this project, such solutions were
of limited quantitative value since it was necessary to
calculate fields off the median plane; however, they did
suggest the solenoid configuration required to attain the
desired field geometry.

A cylindrical polar coordinate system was used as
defined in figure a-1.

From equations developed by Jones (1898) and applied
by Fraser & Romanowski (1955), the magnetic field at point
P (r,θ,0) due to the solenoid of length (L/2) placed with
one end at z = 0 is given by,

92

$$B_r = \frac{\mu_0 I}{2\pi\rho} \sqrt{a/r} \, \{(k - 2/k) \, F + (2/k)E\}$$

$$B_z = \frac{\mu_0 Ic}{8\pi a r\rho} \{\frac{kL}{2}\} \, \{(a + r)F + (a - r)\pi\}$$

where

I = solenoid current

a = solenoid radius

$$k^2 = \frac{4ar}{(a + r)^2 + (L/2)^2}$$

$$c^2 = \frac{4ar}{(a + r)^2}$$

ρ = wire diameter

$$F = \int_0^{\pi/2} \frac{d\phi}{(1 - c^2 \sin^2\phi)^{\frac{1}{2}}}$$

$$E = \int_0^{\pi/2} (1 - c^2 \sin^2\phi)^{\frac{1}{2}} \, d\phi$$

$$\pi = \int_0^{\pi/2} \frac{d\phi}{(1 - c^2 \sin^2\phi) \sqrt{1 - k^2 \sin^2\phi}}$$

Using these basic equations, the magnetic field for a single layer solenoid was found by adding the contributions of the left and right portions of the solenoid. Variation of the field in the direction parallel to the axis of the solenoid (z direction) was found by continuously adding the contributions of two solenoids of

different individual lengths but whose total length was L.

Starting from a conveniently sized one-layer solenoid, layers were added until the external field reached the desired magnitude at the expected boundary position. Subsequently, end turns (which serve to shape the field) were added in various configurations and the radial and axial field components were computed and compared in each case. This was done on the I.B.M. 7040 computer using a programme based on a convenient numerical method for evaluating elliptic integrals (Bartky, 1938). The specified criterion of "flatness" (ie. lack of field curvature) was that the radial component of the magnetic field be less than 5 % of the corresponding axial component over an axial length of approximately 5 cm.

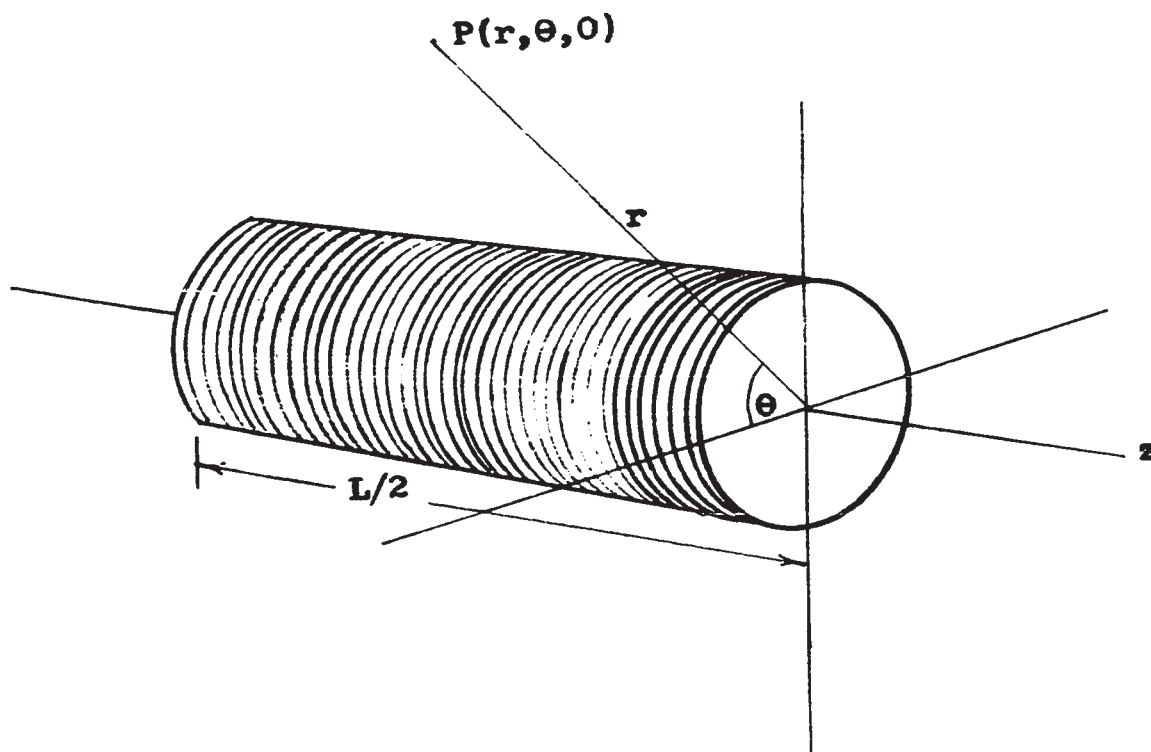The final design satisfying these criteria is described in section 2-3.

figure a-1

DEFINITION OF COORDINATE SYSTEM

APPENDIX B

NON-INDUCTIVE CURRENT LOOP

A convenient method for measuring current involves
measuring the voltage drop across a precisely known
resistance when the current under observation flows
through it. The magnitude of the resistance must be
small so that it does not affect the circuit into which
it is inserted and so that voltages across it are of
convenient size. Since the currents to be measured are
often rapidly changing, care must be taken to ensure that
the inductive reactance does not become comparable in
magnitude to the resistance. This was accomplished by
the configuration of figure b-1. The material used was
brass with dimensions 0.025 x 1.5 x 11.2 cm. and the
resistance of the final configuration was measured with
a milliohmmeter and found to be 2.5 milliohms. Hence,
for current of the order of 200 amperes, the output
voltage would be 0.5 volts - a convenient figure. Mylar
insulation was inserted between the arms of the loop and
the entire configuration was clamped securely between two
plexiglass plates to prevent separation due to the magnetic
forces of large currents.

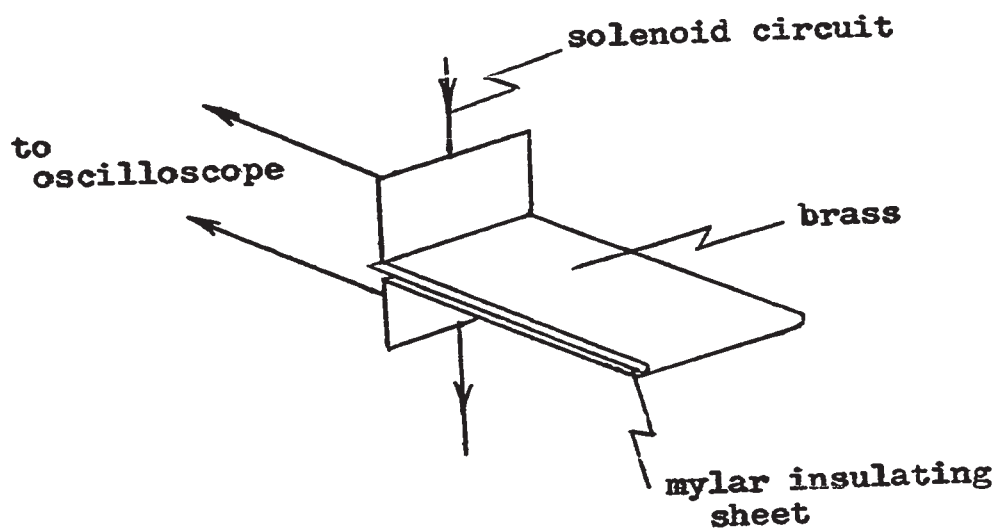This unit was inserted into the solenoid circuit to measure solenoid current (and hence, magnetic field).

FIG. b-1

NON-INDUCTIVE CURRENT LOOP

APPENDIX C

THEORY OF TRIPLE PROBE

Consider the three probes, P_1, P_2, and P_3, immersed in the plasma with dc bias potentials inserted between them as shown in figure c-1.

If the bias potentials (V_{d2} and V_{d3}) are set to zero, then all three probes collect an excess of electrons (since the electrons in the plasma are more mobile than the ions) during the formation of the plasma sheath and their electrical potential is lowered from the free space potential (= 0, say) to some value denoted as the floating potential V_f. See figure c-2. Since the probes are equipotential bodies, no net currents flow between them.

The application of the dc bias potentials (V_{d2} and V_{d3}) causes the potentials of the probes to readjust themselves to a new (electrical) potential configuration as shown in figure c-2. P_2 and P_3, are forced to a potential lower than P_1, which is also less than V_f and therefore collect mainly positive ion current. P_1 on the other hand is raised above V_f in potential, and collects mainly electron current. Using the current directions defined in figure c-1, we may write

PLASMA

P_2 P_1 P_3

I_2 $\bar{I}_1$ I_3

$-$ $+$ $+$ $-$

V_{d2} V_{d3}
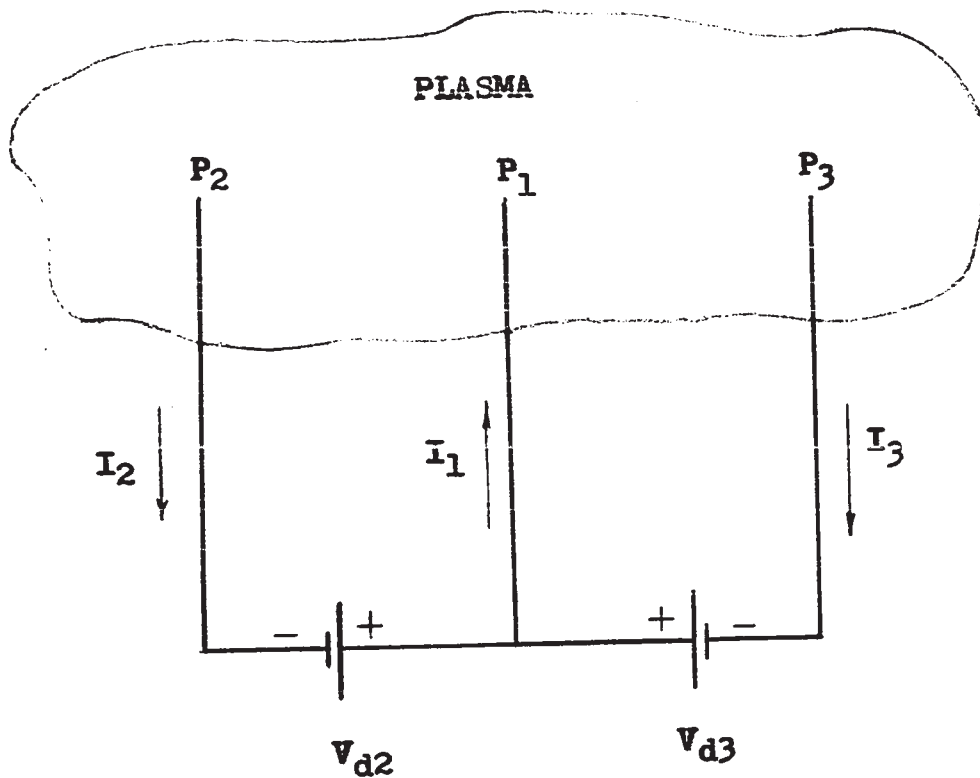
figure c-1

TRIPLE PROBE SCHEMATIC DIAGRAM

$V_s = 0$
(space
   potential)

V_1

V_2 V_3

V_{d2} V_f (floating
           potential)

V_{d3}

$\triangle V_d$

$\bar{V}$

P_2 $\bar{P}_1$ P_3
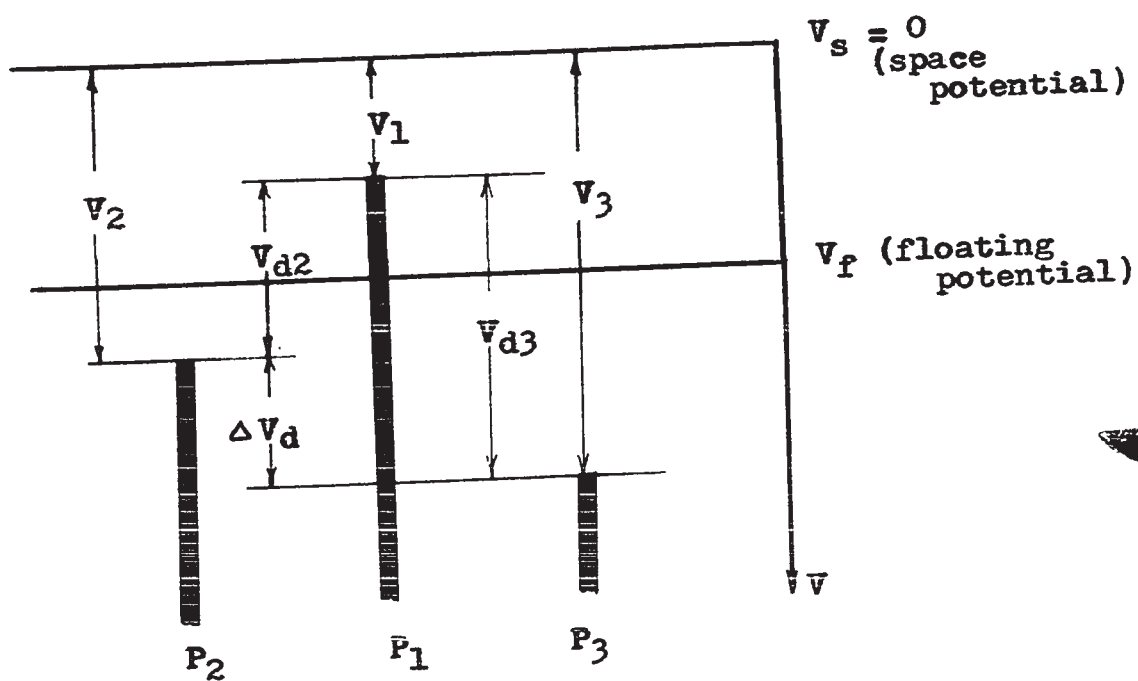
figure c-2

ELECTRICAL POTENTIAL CONFIGURATION OF TRIPLE PROBE

$$I_1 = I_2 + I_3 \tag{1}$$

$$V_2 - V_1 = V_{d2} \tag{2}$$

$$V_3 - V_1 = V_{d3} \tag{3}$$

It is common practice in probe theory to make the following assumptions:

1. The electrons in the plasma have a Maxwellian energy distribution,

2. The mean free path of the electrons is much larger than both the thickness of the plasma sheath established around each probe and the probe radius,

3. The plasma sheath thickness is less than the individual probe separation distances; therefore, mutual perturbation effects among the probes is negligible.

Under these assumptions, we may write

$$I_1 = S(J_e \exp(-\phi V_1) - J_i(V_1)) \tag{4}$$

$$I_2 = - S(J_e \exp(-\phi V_2) - J_i(V_2)) \tag{5}$$

$$I_3 = - S(J_e \exp(-\phi V_3) - J_i(V_3)) \tag{6}$$

where $\phi = e/kT_e$ and $J_e = n_e e(kT_e/2\pi m_e)^{\frac{1}{2}}$ = electron saturation current density caused by thermal electron diffusion to the probes, $J_i(V)$ is the ion saturation current density and is assumed to be practically independent of V, S is the surface

area of a probe, k is Boltzmann's constant, e and m_e are the electronic charge and mass respectively, and n_e is the electron density.

From (2), (3), (4), (5), and (6), it follows that

$$\frac{I_1 + I_2}{I_1 + I_3} = \frac{1 - \exp(-\phi V_{d2})}{1 - \exp(-\phi V_{d3})} \tag{7}$$

If the external voltage source V_{d2} is now removed and probe P_2 is forced to remain at the floating potential, $I_2 = 0$, and $I_1 = I_3$, then from (7)

$$\frac{1 - \exp(-\phi V_{d2})}{1 - \exp(-\phi V_{d3})} = \frac{1}{2} \tag{8}$$

Since V_{d3} is an externally applied voltage (= 9 V. dc), the measurement of V_{d2} allows the determination of ϕ and therefore T_e, the electron temperature.

Further, from equations (5) and (6),

$$J_i = \frac{1}{S} \left\{ \frac{I_3 - I_2 \exp(\phi(V_{d2} - V_{d3}))}{1 - \exp(\phi(V_{d2} - V_{d3}))} \right\} \tag{9}$$

and for $I_2 = 0$ and $I_3 = I_1 = I$,

$$J_i = (I/S)/(1 - \exp \phi(V_{d2} - V_{d3}))$$
$$= (I/S)/(\exp \phi(V_{d2}) - 1) \tag{10}$$

using eqn. (8)

Chen and Sekiguchi, assuming a Maxwellian energy distribution for the electrons, deduced the expression:

$$J_i = \exp(-1/2) \; e \; n_e (kT_e/m_i)^{\frac{1}{2}} \qquad (11)$$

Combining (10) and (11), we obtain

$$n_e = (\frac{m_i^{\frac{1}{2}} I}{S}) \; \frac{\exp(\frac{1}{2})}{e(kT_e)^{\frac{1}{2}}(\exp(\phi V_{d2}) - 1)} \qquad (12)$$

Thus, by measuring the current flowing from probe 1 to probe 3, (I), and using the value of electron temperature, T_e, determined from eqn. (8), a value for n_e can be calculated.

APPENDIX D

THEORY OF MAGNETIC PROBE

Desirable features of a magnetic probe are;

1. Good sensitivity to provide a reasonable
    signal to noise ratio, especially in experiments
    involving (noisy) impulsive discharges such as
    the one described herein.

2. Appropriate frequency response characteristic
    to allow observation of the rapid fluctuations
    of the magnetic field.

3. Small size to ensure that the physical presence
    of the probe does not significantly perturb the
    phenomena being studied.

A conflict arises in attempts to design a probe which
possesses all of these features.

The probe output is given by

$$V = nA \; dB/dt$$

where V is the output voltage (volts), n is the number of
turns, A is the cross-sectional area of the coil (meter^2)
and dB/dt is the time rate of change of magnetic flux
density (webers/meter^2 -sec.). A large V is desirable to
satisfy feature #1 and a reasonably small A is desirable to

103

satisfy feature #3 and hence, it would appear that n should be made large. Herein lies the conflict.

For a coil of inductance L with resistance R across its ends, the time constant $\tau = L/R$ represents the shortest field-fluctuation time to which the coil will respond with adequate sensitivity. The inductance of a multi-layer solenoid is given by

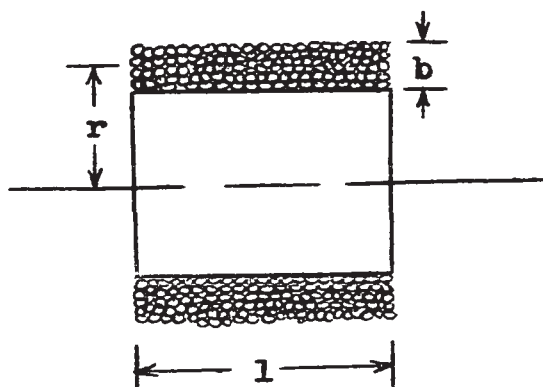$$L = \frac{0.8\ r\ n^2}{6 + 9(1/r) + 10(b/r)} \qquad \#$$

where

r = mean radius of the coil (inches)

n = total no. of turns

L = self inductance (microhenries)

l = length of coil (inches)

b = depth of coil (inches

Since a large output with small time constant is desired, a figure of merit may be defined for any coil in

ALLIED RADIO CORPORATION ELECTRONICS DATA HANDBOOK

the form

$$V/L = F(nA/rn^2) (6 + 9(l/r) + 10(b/r)) \quad \text{where } F = \text{constant}$$

Thus

$$V/L \; \alpha \; (r/n)(6 + 9(l/r) + 10(b/r)) = (6r/n + 9l/n + 10b/n)$$

According to this figure of merit, it is desirable to have a large coil with few turns - a result incompatible with the previous consideration and hence a compromise must be sought.

The resulting compromise design is described in section 2-5.

APPENDIX E

DERIVATION OF EXPRESSION FOR $\dot{\theta}$

By the derivative chain rule, we have

$$\dot{r} = (dr/d\theta)\,(d\theta/dt) = (\dot{\theta})(dr/d\theta), \text{ and thus}$$

$$\ddot{r} = \dot{\theta}^2 d^2r/d\theta^2 + \dot{\theta}\,(dr/d\theta)(d\dot{\theta}/d\theta) \qquad (e-1)$$

but the radial equation of motion (1) from section 4-3 is

$$m(\ddot{r} - r\dot{\theta}^2) = -eBr\dot{\theta}$$

and combining this with (e-1)

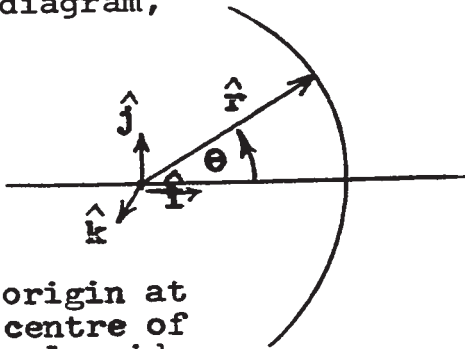$$\dot{\theta}\,(\dot{\theta}(d^2r/d\theta^2 - r) + eBr/m + (dr/d\theta)(d\dot{\theta}/d\theta)) = 0$$

The solution $\dot{\theta} = 0$ or $\theta = $ constant is spurious and so

$$\dot{\theta} = \frac{\dfrac{eBr}{m} + \dfrac{dr}{d\theta}\dfrac{d\dot{\theta}}{d\theta}}{\{r - \dfrac{d^2r}{d\theta^2}\}}$$

DERIVATION OF EXPRESSION

FOR CORRECTION MAGNETIC FIELD

Introducing Cartesian unit vectors as defined in the

diagram,

$$\hat{r} = \cos\theta\,\hat{i} + \sin\theta\,\hat{j}$$

$$\hat{\theta} = -\sin\theta\,\hat{i} + \cos\theta\,\hat{j}$$

origin at
centre of
solenoid

the position vectors may be written

$$\hat{r}_0 = (r_0\cos\theta_0)\,\hat{i} + (r_0\sin\theta_0)\,\hat{j} + z_0\hat{k}$$

$$\hat{R} = (R\cos\theta)\,\hat{i} + (R\sin\theta)\,\hat{j} + z\hat{k}$$

Then

$$|\hat{r}_0 - \hat{R}|^3 = \{(r_0\cos\theta_0 - R\cos\theta)^2 + (r_0\sin\theta_0 - R\sin\theta)^2$$

$$+ (z - z_0)^2\}^{3/2}$$

$$= \{r_0^2 + R^2 - 2Rr_0\cos(\theta_0 - \theta) + (z - z_0)^2\}^{3/2} \qquad \text{(f-1)}$$

Combining equations 8 and 11 of section 4-4

$$\hat{I}(\hat{R}) = (\frac{2p_0}{\mu_0})^{\frac{1}{2}} \gamma \{\cos\theta + \frac{\sin\theta}{R} \frac{dR}{d\theta}\}\{\hat{k} \times \hat{n}\}$$

$$= [\frac{2p_0}{\mu_0}]^{\frac{1}{2}} \gamma^2 \{\cos\theta + \frac{\sin\theta}{R} \frac{dR}{d\theta}\}\{\hat{\theta} + \frac{1}{R} \frac{dR}{d\theta} \hat{r}\}$$

$$= I_0 \{[\frac{\cos\theta}{R} \frac{dR}{d\theta} - \sin\theta]\hat{i} + [\cos\theta + \frac{\sin\theta}{R} \frac{dR}{d\theta}]\hat{j}\} \quad (f-2)$$

where

$$I_0 = [\frac{2p_0}{\mu_0}]^{\frac{1}{2}} \gamma^2 \{\cos\theta + \frac{\sin\theta}{R} \frac{dR}{d\theta}\}$$

Now $\hat{I}(\hat{R}) \times (\hat{r}_0 - \hat{R})$

$$= I_0 \{[\frac{\cos\theta}{R} \frac{dR}{d\theta} - \sin\theta]\hat{i} + [\cos\theta + \frac{\sin\theta}{R} \frac{dR}{d\theta}]\hat{j}\} \times$$

$$\{[r_0\cos\theta_0 - R\cos\theta]\hat{i} + [r_0\sin\theta_0 - R\sin\theta]\hat{j}$$

$$+ (z - z_0) \hat{k}\}$$

$$= I_0\{\beta(z - z_0)\hat{i} - \alpha[z - z_0]\hat{j} + [r_0\cos(\theta_0 - \theta)$$

$$- \frac{r_0}{R} \frac{dR}{d\theta} \sin(\theta_0 - \theta) - R]\hat{k}\} \quad (f-3)$$

where $\beta = (\cos\theta + \frac{1}{R} \frac{dR}{d\theta} \sin\theta)$

$$\alpha = (\frac{\cos\theta}{R} \frac{dR}{d\theta} - \sin\theta)$$

Now, substituting f-1 and f-3 into equation 10 of section 4-4, we obtain

$$\hat{B}_C(\hat{r}_0)$$

$$= \frac{\mu_0}{4\pi} \Big\{ \Big[\iint_{\theta z} \frac{R\beta(z - z_0) I_0 \, d\theta \, dz}{\{r_0{}^2 + R^2 - 2Rr_0\cos(\theta_0 - \theta) + (z - z_0)^2\}^{3/2}} \Big] \hat{i}$$

$$- \hat{j} \Big[\iint_{\theta z} \frac{R\alpha I_0(z - z_0) \, d\theta \, dz}{\{r_0{}^2 + R^2 - 2Rr_0\cos(\theta_0 - \theta) + (z - z_0)^2\}^{3/2}} \Big]$$

$$+ \Big[\iint_{\theta z} \frac{RI_0(r_0\cos(\theta_0 - \theta) - \frac{r_0}{R}\frac{dr}{d\theta}\sin(\theta_0 - \theta) - R) \, d\theta \, dz}{\{r_0{}^2 + R^2 - 2Rr_0\cos(\theta_0 - \theta) + (z - z_0)^2\}^{3/2}} \Big] \hat{k} \Big\}$$

We can, without loss of generality, select the median plane to be $z = 0$ and integrate the expression with respect to z from $z = -L$ to $z = L$.

In both the $\hat{i}$ and $\hat{j}$ component terms, the integrands are odd functions of z and, hence, these terms are zero.

Substituting the value of I_0 (f-2) into the $\hat{k}$ component term, there remains

$$\hat{B}_C(\hat{r}_0)$$

$$= \frac{1}{2\pi} \Big(\frac{p_0 \mu_0}{2}\Big)^{\frac{1}{2}} \hat{k} \iint_{\theta z} \frac{F(R) \, R \, d\theta \, dz}{[1 + \frac{1}{R^2}(\frac{dR}{d\theta})^2][r_0{}^2 + R^2 - 2Rr_0\cos(\theta_0 - \theta) + z^2]^{3/2}}$$

where

$$F(R) = \left(\frac{dR}{d\theta}\right)^2 \left\{\frac{r_0}{R^2} \sin(\theta - \theta_0) \sin\theta\right\}$$

$$- \frac{dR}{d\theta} \left\{\sin\theta + \frac{r_0}{R} \sin(\theta_0 - 2\theta)\right\}$$

$$+ \cos\theta \left\{r_0\cos(\theta_0 - \theta) - R\right\}$$

which is equation 12 of section 4-4.

APPENDIX G

CONSIDERATION OF SINGULARITY IN

CORRECTION MAGNETIC FIELD INTEGRAL

The integrand of equation 13, section 4-4 is

$$\frac{R \, F(R)}{[1 + \frac{1}{R^2} (\frac{dR}{d\theta})^2][f(R)][1 + f(R)/L^2]^{\frac{1}{2}}}$$

where

$$F(R) = (\frac{dR}{d\theta})^2 \{\frac{r_0}{R^2} \sin(\theta - \theta_0) \sin\theta\}$$

$$- \frac{dR}{d\theta} \{\sin\theta + \frac{r_0}{R} \sin(\theta_0 - 2\theta)\}$$

$$+ \cos\theta \{r_0\cos(\theta_0 - \theta) - R\}$$

and

$$f(R) = r_0^2 + R^2 - 2Rr_0\cos(\theta_0 - \theta)$$

Clearly, as $\theta \to \theta_0$ and $R \to r_0$, ie. the point of observation is approached, the integrand tends to the indeterminate form 0/0 since $F(R) \to 0$ and $f(R) \to 0$. To determine the contribution of the current element at the point of observation, it is necessary to determine the limiting value of the integrand.

By the application of L'Hôpital's rule, we find

$$\lim_{\substack{R \to r_0 \\ \theta \to \theta_0}} \frac{R\ F(R)}{[1 + \frac{1}{R^2} (\frac{dR}{d\theta})^2][f(R)][1 + f(R)/L^2]^{\frac{1}{2}}}$$

$$= \frac{[\sin\theta_0 \frac{dR}{d\theta} + r_0\cos\theta_0][\frac{1}{r_0} \frac{d^2R}{d\theta^2} - 1 - \frac{2}{r_0^2} (\frac{dR}{d\theta})^2]}{2r_0 [1 + \frac{1}{r_0^2} (\frac{dR}{d\theta})^2]}$$

where differentiation of the numerator and denominator must be carried out twice to attain a finite limit.

Variation of the integrand with θ is shown in figure g-1 for different positions of observation.

Incorporated into the correction field calculations was a special sub-programme, written to take into account the results described in this appendix.
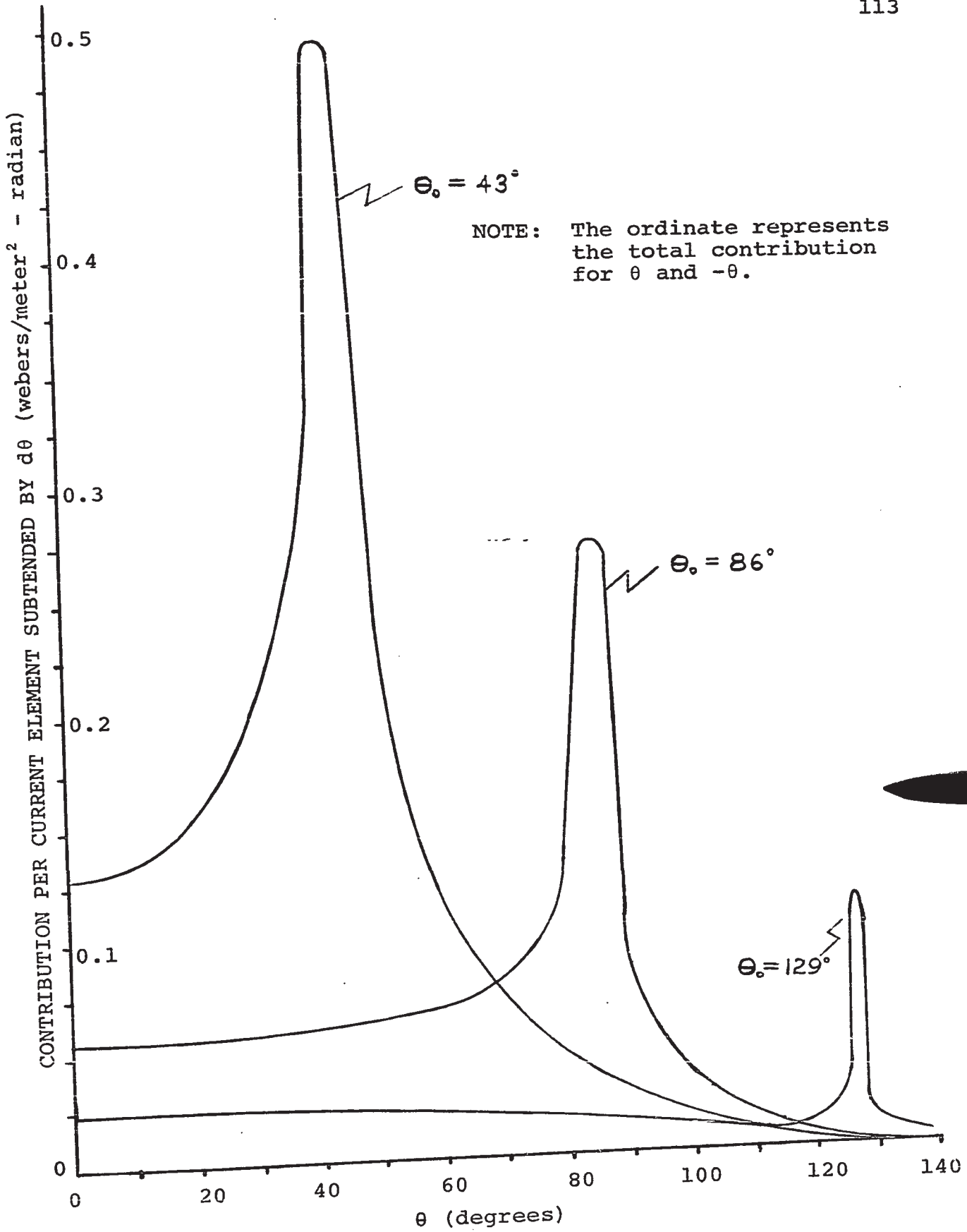
FIG. 9-1 CONTRIBUTION TO CORRECTION FIELD ALONG BOUNDARY

BIBLIOGRAPHY

Aisenberg, S., Journal of Applied Physics, Vol. 35, p. 130, (1964).

Alfven, H., L. Danielson, C.G. Falthammar, and L. Lindberg, On the penetration of Interplanetary Plasma into the Magnetosphere – presented at Plasma Space Science Symposium, Catholic University, Washington, D.C., June 11-14, 1963.

Allied Radio Corp. Electronics Data Handbook, 2nd edition, Allied Radio Corp., Chicago 80, Illinois.

Bartky, W., Numerical Calculation of a Generalized Complete Elliptic Integral, Reviews of Modern Physics, Vol. 10, October, 1938.

Beard, D.B., The Interaction of the Terrestrial Magnetic Field with the Solar Corpuscular Radiation, Journal of Geophysical Research, Vol. 65, p. 3559-3568, 1960.

Beard, D.B., The Solar Wind-Geomagnetic Field Boundary, Reviews of Geophysics, Vol. 2, May, 1964.

Bennett, W.H., Self-Focusing Streams, The Physical Review, Vol. 98, p. 1584-1593, 1955.

Bennett, W.H., Auroral and Magnetic-Storm Theory, The Astrophysical Journal, Vol. 127, May, 1958.

Bennett, W.H., Solar Proton Stream Forms with a Laboratory Model, The Review of Scientific Instruments, Vol. 30, p. 63-69, February, 1959.

Bennett, W.H., Stormer Orbits, Proceedings of Symposia
in Applied Mathematics, IX, Orbit Theory,
p. 19-28, 1959.

Bernstein, W., R.W. Fredericks and F.L. Scarf, A Model
for a Broad Disordered Transition between the
Solar Wind and the Magnetosphere, J. Geophys. Res-
earch, Vol. 69, p. 1201, 1964.

Biermann, L., Kometenschweife und solare korpuscular
strahlung, Z. Astrophys., Vol. 29, p. 274-289, 1951.

Birkeland, K., Expedition Norvegienne de 1899-1900 pour
l'etude des aurores boreales, Vid. Selsk. Skr.
Math. Nat. Kl., No. 1 (1901).

Block, L., Scaling Considerations for Magnetospheric Model
Experiments, Planet. Space Sci., Vol. 15, p. 1479,
(1967).

Bostick, W.H., H. Byfield and M. Brettschneider, Plasma
Flow around a 3-dimensional Dipole, J. Geophys.
Res., Vol. 68, p. 5315, (1963).

Brick, D.B., and A.W. Snyder, External D.C. Field of a Long
Solenoid, Amer. J. Physics, Vol. 33, p. 905-9,
November, 1965.

Chapman, S., and V.C.A. Ferraro, A New Theory of Magnetic
Storms, Terr. Mag. Atmos. Elect., Vol. 36, p. 77,
p. 171, (1931); Vol. 37, p. 147 (1932); Vol. 38,
p. 79, (1933).

Chen, S.L., and T. Sekiguchi, Instantaneous Direct-Display
System of Plasma Parameters by Means of Triple
Probe, J. Applied Physics, Vol. 36, No. 8, (1965).

Clauser, F.H., Symposium of Plasma Dynamics, Addison-Wesley,
Reading, Massachusetts, U.S.A. (1960).

Colgate, S.A., Ionization in Crossed Electric and Magnetic
Fields, Collisionless Shocks, Collision Broadening
of a Strong Shock Layer, Collision Broadening of
a Weak Shock Layer, presented at the Symposium
on Electromagnetics and Fluid Dynamics of
Gaseous Plasma, Polytechnic Institute of Brooklyn,
April 4, 5, 6, 1961.

Fraser, P.A., and M. Romanowski, Considerations on the
Primary Winding of the Campbell Standard Inductor,
Canadian Journal of Physics, Vol. 33, p. 871-885,
1955.

Gore, J.V., A Study of the Boundary between a Flowing
Plasma and a Dipole Magnetic Field, Lab. Report
No. 7-801-79, R.C.A. Research Laboratories,
Montreal 207, Quebec, (1969).

Grad, H., Boundary Layer Between A Plasma and A Magnetic
Field, Physics of Fluids, Vol. 4, p. 1366-75,
(1961).

Hamming, R.W., Numerical Methods for Scientists and Engineers,
McGraw-Hill Publishing Co., New York, 1962.

Huddlestone, R.H., Plasma Diagnostic Techniques, Academic
Press, New York, U.S.A. 1965.

Hughes, W.F., and F.J. Young, The Electrodynamics of Fluids,
John Wiley & Sons, New York, U.S.A. 1966.

Hurley, J., Interaction of a Streaming Plasma with the
Magnetic Field of a Two-Dimensional Dipole, The
Physics of Fluids, Vol. 4, No. 7, p. 854, 1961.

Jackson, J.D., Classical Electrodynamics, John Wiley &
Sons, New York, U.S.A. 1962.

Johnson, E.O., and L. Malter, A Floating Double Probe
Method for Measurements in Gas Discharges, Physical
Review, Vol. 80, No. 1, p. 58, 1950.

Jones, J.V., On the Calculation of the Coefficient of
Mutual Induction of a Circle and a Coaxial Helix,
and of the Electromagnetic Force Between a Helical
Current and a Uniform Coaxial Circular Cylindrical
Current Sheet, Roy. Soc. Proc. 63, p. 192-205, 1898.

Kucherawy, M.D., The Boundary between a Streaming Plasma
and a Transverse Magnetic Field, a literature-
survey report, Dept. of Physics, University of
Western Ontario, London, Canada, (1966).

Langmuir, I., and H.M. Mott-Smith, Gen. Elec. Rev. 27,
449, 538, 616, 762, 810 (1924).

Lehnert, B., Dynamics of Charged Particles, Amsterdam,
North-Holland Publishing Co., 1964.

Midgley, J.E., and L. Davis, Computations of the Bounding
Surface of a Dipole Field in a Plasma by a Moment
Technique, J. Geophys. Res., Vol. 67, p. 499-504,
1962.

Osborne, F.J.F., M.P. Bachynski and J.V. Gore, Laboratory
Studies of the Variation of the Magnetosphere with
Solar Wind Properties, J. Geophys. Res., Vol. 69,
p. 4441, (1964).

Pai, Shih-I, Magnetogasdynamics and Plasma Dynamics,
Prentice-Hall Inc., Englewood Cliffs, New Jersey,
(1962).

Parker, E.N., Dynamics of the Interplanetary Gas and Magnetic
Fields, Astrophys. J., Vol. 128, p. 667-676, 1958.

Pearse, R.W.B., and A.G. Gaydon, The Identification of
Molecular Spectra, third edition, Chapman and
Hall, (1963).

Pfirsch, D., Zeitschrift fur Physik, Vol. 190, p. 238-252,
1966.

Rosenbluth, M., Surface Layer Model in the Limit of No
Collisions, Los Alamos Report No. LA-1850, 1954.

Sellen, J.H., and W. Bernstein, Interaction of Collisionless
Plasma Streams with Transverse Magnetic Fields,
Physics of Fluids, Vol. 7, p. 977-981, 1964.

Sestero, A., Charge Separation Effects in the Ferraro-
Rosenbluth Cold Plasma Sheath Model, Physics of
Fluids, Vol. 8, p. 739-744, 1965.

Shkarofsky, I.P., and T.W. Johnston, Equilibrium Solutions and Instabilities in Inhomogeneous Plasma Sheaths, Lab. Report No. 7-801-13, R.C.A. Research Laboratories, Montreal 207, Quebec, 1961.

Shkarofsky, I.P., T.W. Johnston and M.P. Bachynski, The Particle Kinetics of Plasmas, Addison-Wesley, Don Mills, Ontario, 1966.

Slutz, R.J., The Shape of the Geomagnetic Field Boundary under Uniform External Pressure, J. Geophys. Res., Vol. 67, p. 505-513, 1962.

Spitzer, L., Physics of Fully-Ionized Gases, Interscience Publishers, New York, 1956.

Spreiter, J.R., and B.R. Briggs, Theoretical Determination of the form of the Boundary of the Solar Corpuscular Stream produced by the Interaction with the Magnetic Dipole Field of the Earth, J. Geophys. Research, Vol. 67, p. 37-51, 1962.

Stormer, C., The Polar Aurora, Oxford University Press, London, 1955.